# IMPLANTABLE ELECTROMAGNETIC FIELD PROBES IN FINITE BIOLOGICAL BODIES

Dissertation for the Degree of Ph. D.
MICHIGAN STATE UNIVERSITY
SEYED HOSSEIN MOUSAVINEZHAD
1977



This is to certify that the

thesis entitled

# IMPLANTABLE ELECTROMAGNETIC FIELD PROBES IN FINITE BIOLOGICAL BODIES

presented by

Seyed Hossein Mousavinezhad

has been accepted towards fulfillment of the requirements for

Ph.D. degree in Electrical Engineering and Systems Science

Major professor

Date <u>March 9, 1977</u>

**O**-7639

66/39/92 153

#### ABSTRACT

# IMPLANTABLE ELECTROMAGNETIC FIELD PROBES IN FINITE BIOLOGICAL BODIES

Ву

## Seyed Hossein Mousavinezhad

This thesis presents some theoretical and experimental results on the study of a dielectrically coated, small spherical probe used to measure the induced EM fields in conducting (biological) bodies of finite extent. The receiving and radiating characteristics of the insulated probe are determined as functions of the electrical parameters and geometry of a spherical conducting body.

First, a general theory for a wire probe in a volume conductor is presented and the relation between the output of the probe and the induced electric field in the body is derived. The receiving properties of an insulated spherical probe immersed in a uniform electric field inside a conducting body are then discussed. An expression for the effective diameter of the probe is also derived.

The expression for the input impedance of a dielectrically coated spherical antenna imbedded in a

Seyed Hossein Mousavinezhad finite conducting body is formulated based both on the matrix equation method and transmission line theory.

Finally, experimental results on the input impedance of insulated spherical probes and the measurements of the induced electric field inside conducting bodies are presented.

The convergence problem of the theoretical input admittance and the computation of Hankel functions are also included in two Appendices.

# IMPLANTABLE ELECTROMAGNETIC FIELD PROBES IN FINITE BIOLOGICAL BODIES

Ву

Seyed Hossein Mousavinezhad

#### A DISSERTATION

Submitted to
Michigan State University
in partial fulfillment of the requirements
for the degree of

DOCTOR OF PHILOSOPHY

Department of Electrical Engineering and Systems Science

This thesis is dedicated to my wife, Susan, and our children Jamshid, Mehri,...?

•

#### **ACKNOWLEDGEMENTS**

The author wishes to offer his sincere gratitude to his major professor, Dr. Kun Mu Chen, for his assistance and encouragement throughout the course of this work and also for his editorial assistance in the preparation of the manuscript.

He also would like to thank Dr. D.P. Nyquist, a member of the guidance committee, for his many helpful suggestions and comments. I also want to thank Dr. Bong Ho and Dr. C.Y. Lo, other members of the committee for their time and efforts. Special thanks also to Mrs. Noralee Burkhardt for her skillful typing of the manuscript.

This research was supported by U.S. Army Research Office under Grant DAAG 29-76-G-0201. I would like to express my appreciation for this support.

Finally, I would like to thank my family for their patience and cooperation.

## TABLE OF CONTENTS

Chapter		Page
I	INTRODUCTION	1
II	GENERAL THEORY FOR AN IMPLANTABLE ELECTROMAGNETIC FIELD PROBE IMMERSED IN A FINITE VOLUME CONDUCTOR	4
	2.1 A Wire Probe in a Finite	_
	Conducting Body 2.2 Spherical Antenna as a Probe	4 9
III	AN INSULATED SPHERICAL PROBE IN A CONDUCTING BODY	11
	3.1 Statement of the Problem and the Superposition Principle	11
	3.2 Scattering from a Dielectrically Coated Sphere	14
	3.3 Equivalent Circuit of an Insulated Spherical Probe in a Conducting Body 3.4 Some Theoretical Results on the Normalized Effective Diameter	21
	of the Spherical Probe	24
IV	DIELECTRICALLY COATED SPHERICAL ANTENNA IN A FINITE CONDUCTING BODY	31
	4.1 Geometry of the Problem	32
	4.2 Electromagnetic Field Solutions	34
	4.3 Applications of Boundary Conditions	40
	4.4 Matrix Equation Formulation of the	4.0
	Input Impedance Expression 4.5 Transmission Line Approach	46 55
	4.5 Transmission Line Approach 4.6 Some Theoretical Results of the	55
	Input Impedance Computations	64
	4.7 Radial Transmission Lines	81
	4.8 Apparent Antenna Impedance and	-
	Capacitive End Correction	88

Chapter		Page
V	SOME EXPERIMENTAL RESULTS	94
	<ul><li>5.1 V-I (or E-H) Probe Impedance Measuring Techniques</li><li>5.2 Experimental Setup for the Measurement of the Input Impedance</li></ul>	95
	of a Dielectrically Coated Spherical Antenna in a Finite Conducting Body 5.3 Comparison of Theory and Experiment 5.4 Field Measurements using Insulated Spherical Probes	114 118 129
VI	SUMMARY AND CONCLUSIONS	144
	APPENDICES	
	A. Higher Order Modes and the Convergence of the Input Admittance	
	Expression  B. Computation of Hankel Functions	146 158
	REFERENCES	166

## LIST OF TABLES

Table		Page
3.1	Complex Normalized Effective Diameter of Small Spherical Antenna in Free Space (f = 600 MHz; $\lambda_0 = 50$ cm.)	26
4.1	Values of Hankel Functions $H_{n+1/2}^{(2)}(k_i^a)$ when $a = 1$ cm, $f = 600$ MHz $(a/\lambda_0 = 0.02;$ $\lambda_0$ is free space wavelength) and $\epsilon_i = 2.1 \; \epsilon_0; \; \epsilon_0$ is free space	
	permittivity	52
4.2	Values of Hankel Function with Complex Argument, $H_{n+1/2}^{(2)}(kb)$ , when $b=1.5$ cm, $f=600$ MHz $(a/\lambda_0=0.03)$ , $k=\omega\sqrt{\mu_0\xi}$ ; $\xi=\epsilon-j\frac{\sigma}{\omega}$ ; $\epsilon=70$ $\epsilon_0$ , $\sigma=1\frac{\mho}{m}$	53
5.1	Theoretical and Experimental Values of the Input Impedance of a Coated Hemispherical Antenna in a Finite External Medium. (a = 1.1 cm., b = 1.21 cm., c = 5.5 cm., f = 600 MHz, $\varepsilon_{ir} \doteq 3.0$ ) (T = 20°c)	122
5.2	Theoretical and Experimental Values of the Input Impedance of a Coated Hemispherical Antenna in a Finite External Medium. (a = 1.1 cm., b = 1.5 cm., c = 5.5 cm., f = 600 MHz, $\epsilon_{ir} = 3.0$ ) (T = 20°c)	123
5.3	Theoretical and Experimental Values of the Input Impedance of a Dielectrically Coated Hemispherical Antenna in a Finite External Medium. (a = 1.1 cm., b = 3.1 cm., c = 5.5 cm., f = 600 MHz, $\epsilon_{ir} \doteq 3.0$ ) (T = 20°c)	125

Table Page 5.4 Experimental Input Impedance of a Dielectrically Coated Hemispherical Antenna at Different Locations in a Finite Conducting Body (a = 1.1 cm,  $b = 1.2 \text{ cm.}, c = 5.5 \text{ cm.}, \epsilon_{ir} = 3.0,$  $\varepsilon_r = 77.898$ ,  $\sigma = 0.925$  mho/m, f = 600 MHz; d is the Distance from the Center of the Antenna to the Center of the Conducting Body) 127 5.5 Experimental Input Impedance of a Dielectrically Coated Hemispherical Antenna at Different Locations in a Finite Conducting Body (a = 1.1 cm.,  $b = 1.6 \text{ cm.}, c = 5.5 \text{ cm.}, \epsilon_{ir} = 3.0,$  $\varepsilon_{r} = 77.898$ ,  $\sigma = 0.925$  mho/m, f = 600 MHz; is the Distance from the Center of the Antenna to the Center of the 128 Conducting Body) 5.6 Experimental Input Impedance of a Dielectrically Coated Hemispherical Antenna at Different Locations in a Finite Conducting Body (a = 1.1 cm.,  $b = 2.2 \text{ cm.}, c = 5.5 \text{ cm.}, \epsilon_{ir} = 3.0,$  $\varepsilon_r = 77.898, \sigma = 0.925 \text{ g/m}, f = 600 \text{ MHz};$ is the Distance from the Center of the Antenna to the Center of the 130 Conducting Body) Illustrating the Convergence of the A.1 Input Admittance Series. (a = 1.0 cm., b = 1.5 cm., c = 5.5 cm., f = 600 MHz;  $a/\lambda_0 = 0.02$ ,  $\epsilon_{ir} = 2.1$ ,  $\epsilon_r = 77.9$ ,  $\sigma = 0.925 \text{ U/m}, 2\theta_0$  is the total angular width, in degrees, of the gap) 156 B.1 Spherical Bessel Functions of Order 0, 1 and 2. These Results are Computed by using the Routine "COMBES" 164

## LIST OF FIGURES

Figure		Page
2.1	Configuration of Probe in a Finite Heterogeneous Volume Conductor	5
2.2	Equivalent Circuit for Probe in a Finite Heterogeneous Volume Conductor	5
2.3	Insulated Spherical Probe in a Con- ducting Body Irradiated by an Incident EM Wave	10
3.1	Dielectrically Coated Small Spherical Probe in a Uniform Incident Electric Field Inside a Biological Body	12
3.2	Illustrating the Superposition Principle	12
3.3	The Scattering from a Dielectrically Coated Sphere when Irradiated by a Uniform Incident Electric Field in the z Direction, Inside a Conducting Body	15
3.4	Equivalent Circuit of the Dielectrically Coated Spherical Probe in a Homogeneous Biological Body	23
3.5	Magnitude of the Normalized Effective Diameter of a Dielectrically Coated Spherical Probe Imbedded in Biological Body with Relative Dielectric Constant $^{\varepsilon}\mathbf{r}$	28
3.6	Normalized Effective Diameter of a Dielectrically Coated Spherical Probe as a Function of the Relative Dielectric Constant of the Conducting Body	30
4.1	Dielectrically Coated Small Spherical Antenna in a Finite Biological Body. A Generator Maintains a Voltage V Across a Narrow Equatorial Gap of the Conducting Sphere. Spherical Coordinate Ssystem is also Shown	33

Figure		Page
4.2	Enlarged View of the Gap Region of the Spherical Antenna. A Coaxial Line Connected to a R.F. Source, Maintains a Voltage V Across the Narrow Gap. Input Current I is Shown at the Edge where $\theta = \pi/2 - \theta_0$ ( $2\theta_0$ is the Angular Width of the Gap)	41
4.3	Input Conductance (or Radiation Conductance) of a Spherical Antenna in Free Space as a Function of $k_0$ a, where a is the Radius of Sphere and $k_0 = \omega \sqrt{\mu_0 \epsilon_0}$ is the Free Space Wavenumber	66
4.4	Input Reactance of a Small Spherical Probe as a Function of the Radius of the Conducting Sphere	67
4.5	Theoretical and Experimental Values of the Dissipated Power due to $E_{X}$ , $\sigma/2 E_{X} ^2$ , as a Function of Y along $x = 0.5$ cm. Freq. = 2.45 GH, $\sigma = 5.934$ $v/m$ , $\varepsilon = 68.487$ $\varepsilon_{0}$ . Salt Concentration = 0.5 normal	70
4.6	Theoretical and Experimental Values of the Dissipated Power due to $E_X$ , $\sigma/2 E_X ^2$ , as a Function of Y along X = 0.5. Freq. = 2.45 GHz, $\sigma$ = 5.934 $\Im$ /m, $\varepsilon$ = 68.487 $\varepsilon$ <sub>0</sub> . Salt concentration = 0.5 normal	, 71
4.7a	Input Reactance of a Small Spherical Probe as a Function of the Permittivity of the Conducting Sphere	73
4.7b	Input Reactance of a Small Spherical Probe as a Function of the Permittivity of the Conducting Body; b/a = 1.1,,3.0	75
4.8	Input Impedance of a Dielectrically Coated Spherical Antenna as a Function of the Conductivity of the Conducting Body	76

Figure		Page
<b>4.</b> 9a	Input Reactance of a Small Spherical Probe as a Function of the Relative Dielectric Constant of the Conducting Body	78
<b>4.</b> 9b	Input Reactance of a Small Spherical Probe as a Function of the Relative Dielectric Constant of the Conducting Body. The Parameters are Relative Dielectric Constants of the Insulating Dielectric Shell	80
4.10	The Geometry of Radial Transmission Line. $\mathbf{Z}_{L}$ is the "edge" Impedance of the Spherical Antenna. The Gap Corresponds to the Medium Between the Conducting Plates	82
4.11	(a) is the Junction Equivalent Circuit of the Spherical Antenna with an Edge Input Admittance of Y <sub>IN</sub> . (b) is the Configuration of the Circular Parallel Plates of Area A which Approximates the Gap of the Antenna	89
5.1	Cross-sectional (a) and Longitudinal (b) Views of the Cylindrical Coaxial Transmission Line. A Generator Maintains a Voltage (or Potential Difference) V Between the Inner and Outer Conductors	96
5.2	Block Diagram for E-H (or V-I) Probe Impedance Measuring Device. All the Lines Shown are Standard GR 50 $\Omega$ Coaxial Transmission Lines	102
5.3	Test Line Together with E-H Block which Supports the Voltage and Current Probes	103
5.4	Cross-sectional View of the V-I Probe Assembly, Electric Probe (b), and Magnetic Probe (c)	105
5.5	The Calibration of the Phase Meter Used in the Vector Voltmeter Measurements. For the Configuration Shown the Phase Meter Should Read "Zero".	107

Figure		Page
5.6	Experimental Setup for Measuring the Input Impedance of a Dielectrically Coated Hemisphere in a Finite Conducting Body	116
5.7	Theoretical and Experimental Input Re- actance of a Dielectrically Coated Hemisphere in Free Space as a Function of Frequency	120
5.8	Configuration of the Dielectrically Coated Spherical Probe Loaded with a Microwave Detector. (Free Space Incident Plane Wave is also Shown.)	131
5.9	Dielectrically Coated Spherical Probe in the Upper Half Side of a TEM Trans- mission Cell. (Note: not drawn to scale.) Calibration Curve of the Probe is also Shown	133
5.10	The Intensity of the Square of Electric Field Inside the TEM Cell. The Spherical Probe was Located 6 cm Above the Center Conductor of the Cell. f = 320 MHz	135
5.11	The Output of the Dielectrically Coated Spherical Probe Inside a Finite Body Containing the 0.0 N Solution. The Frequency is f = 320 MHz	136
5.12	(a): Three Dimensional View of Tapered Anechoic Chamber. (b): Conducting Body Illuminated by Incident EM Wave	138
5.13	The Distribution of the Square of Electrifield Induced in a 16 cm × 12 cm × 4 cm Distilled Water Body as a Function of Z Along Different Depths Indicated by the Parameter "%"	ic 140
5.14	Distribution of the Square of the Induced Electric Field 0.5 cm Above the Center of a Finite Conducting Body Containing 0.1 N Saline Solution (f = 500 MHz; $\varepsilon_r$ = 77.92, $\sigma$ = .897 mho/m)	143
		747

#### CHAPTER I

#### INTRODUCTION

In recent years, many researchers have investigated the problem of Electromagnetic Radiation effects on biological systems and related potential health hazards. In order to understand the nature of the problem and to determine whether the radiation-induced effect is thermal or non-thermal, one needs to know the actual intensities of the induced electromagnetic fields inside the irradiated biological bodies. Experimentally, implantable EM field probes can be inserted into these bodies to measure the field intensities. In order not to perturb the actual field distribution in the body and to have a good resolution of the measurement, the probes are required to be electrically small.

In this thesis, we present a study on an implantable EM field probe which can be used to measure the induced EM field in a finite conducting (biological) body. Recent studies on the characteristics of some conventional probes used in conducting bodies have been reported [1], [2], [3]. In almost all these works, an infinite conducting body was assumed which neglected the effect of

the boundary of the medium on the characteristics of the probe. In the present study, we consider a coated spherical probe in a finite conducting body, taking into account the boundary effects.

In Chapter 2, we discuss some general properties of the probe in a volume conductor. We derive the relationship between the output of the probe and the induced electric field intensity in the irradiated body. The receiving characteristics of an insulated spherical probe is investigated in Chapter 3. A relation is derived for the effective diameter of the probe immersed in a uniform incident electric field inside a conducting body.

In Chapter 4 we formulate the expression for the input impedance (acting as a radiating element) of a dielectrically coated spherical probe located at the center of a spherical conducting body. Two different approaches are discussed to obtain the series expression for the input admittance and some numerical results are presented. The end effects of the probe are also discussed.

Finally, in Chapter 5, we present some experimental results obtained in measuring the input impedance of the spherical probe in which a relatively new method of impedance measurement is introduced. A few examples of the measurement of the induced electric field in finite conducting bodies containing saline solution is

also shown and compared to the theory. Two appendices, at the end of the thesis, discuss the convergence problem of the series expression obtained in Chapter 4 and the numerical computation of Hankel functions used in the computer program.

#### CHAPTER II

# GENERAL THEORY FOR AN IMPLANTABLE ELECTROMAGNETIC FIELD PROBE IMMERSED IN A FINITE VOLUME CONDUCTOR

In order to measure electromagnetic field intensities induced in finite conducting bodies, appropriate field probes may be inserted in these bodies. In this chapter, we derive the relationship between the output of a wire probe and the intensity of the electric field at the location of the probe inside a volume conductor which is irradiated by an incident electromagnetic wave. After this, a simple spherical probe is proposed for further study because, an exact analytical solution exists for such a probe.

### 2.1. A Wire Probe in a Finite Conducting Body

Consider a conducting body of volume V with electrical parameters  $\varepsilon(\vec{r})$ ,  $\sigma(\vec{r})$  and  $\mu_0$  irradiated by a non-uniform EM wave with an electric field intensity  $\vec{E}^i(\vec{r})$ , as shown in Figure 2.1. The induced electric field  $\vec{E}(\vec{r})$  inside the body, in the absence of the probe, can be theoretically obtained based on the Tensor Integral Equation method developed originally by Livesay and Chen [4].

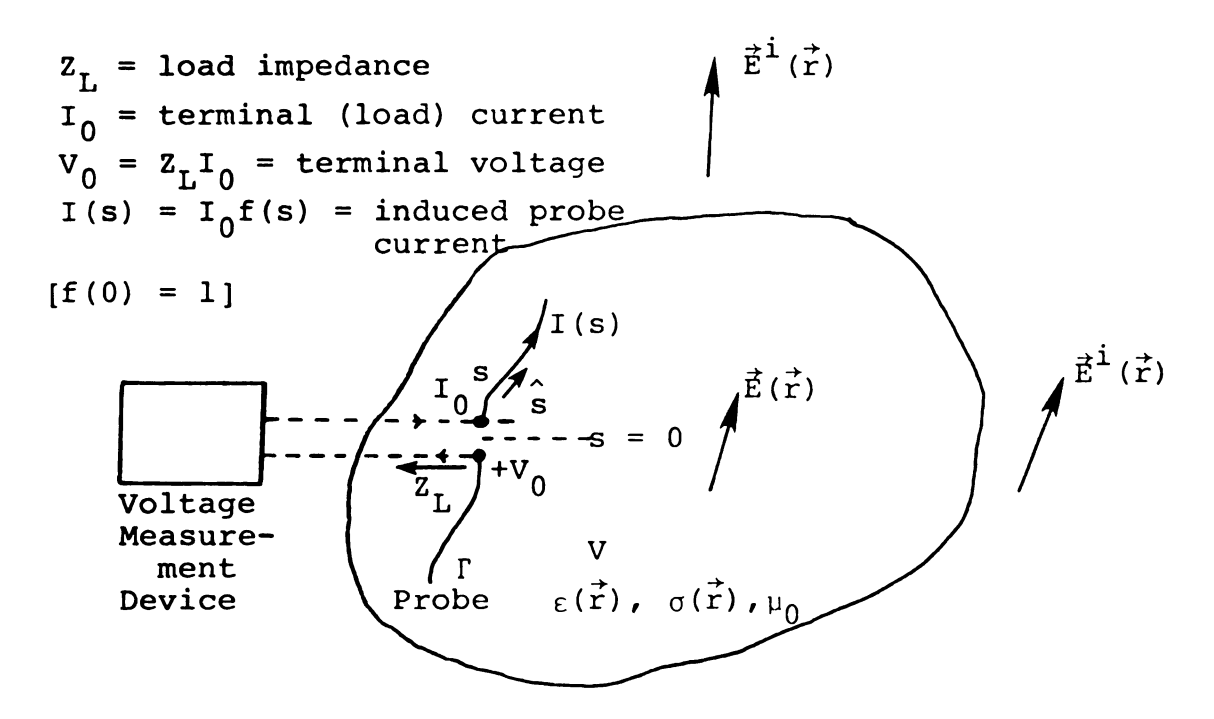


Figure 2.1. Configuration of Probe in a Finite, Heterogeneous Volume Conductor.

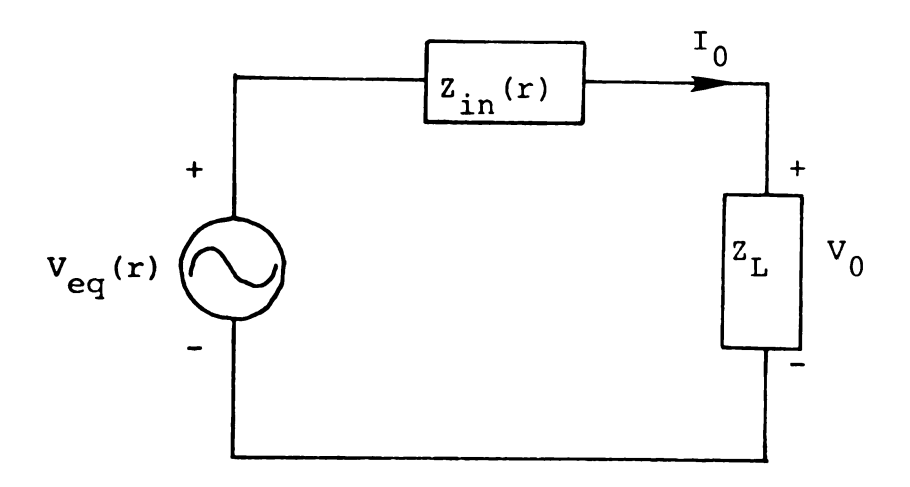


Figure 2.2. Equivalent Circuit for Probe in a Finite Heterogeneous Volume Conductor.

When a probe is introduced into the body,  $\vec{E}(\vec{r})$  induces a current I(s) on the probe. (s measures the distance along the contour  $\Gamma$  of the thin probe as shown in Figure 2.1.) This current maintains its own secondary field  $\vec{E}_{D}(\vec{r})$  at any point in the body.

Assuming the linearity, the total electric field at any point can be expressed as

$$\vec{E}_{t}(\vec{r}) = \vec{E}(\vec{r}) + \vec{E}_{p}(\vec{r}). \qquad (2.1)$$

We aim to find the relation between output voltage of the probe  $V_0(\vec{r})$  and the induced field  $\vec{E}(\vec{r})$  at the probe location.

Using the boundary condition that the tangential electric field vanishes at any point on the surface of the perfectly conducting probe, one can write,

$$\hat{\mathbf{S}} \cdot \hat{\mathbf{E}}_{\mathsf{t}}(\mathbf{s}) = \mathbf{V}_{\mathsf{0}}(\mathbf{s}) \, \delta(\mathbf{s}) = \mathbf{Z}_{\mathsf{L}} \mathbf{I}_{\mathsf{0}} \delta(\mathbf{s}) \tag{2.2}$$

where  $\mathbf{Z}_{\mathbf{L}}$  is the load impedance and  $\hat{\mathbf{S}}$  is a unit vector along the contour  $\Gamma$ . Assuming that  $\mathbf{I}(\mathbf{s}) = \mathbf{I}_0 \mathbf{f}(\mathbf{s})$  as the induced current on the surface of the probe, we can multiply both sides of Eq. (2.2) by  $\mathbf{f}(\mathbf{s})$  and then integrate along  $\Gamma$  to get

$$\int_{\Gamma} f(s) \hat{s} \cdot \vec{E}(s) ds + \int_{\Gamma} f(s) \hat{s} \cdot \vec{E}_{p}(s) ds = Z_{L} I_{0}$$
 (2.3)

(note that f(0) = 1). The second integral on the left hand side is proportional to input current  $I_0$  and we

can define the internal impedance of the probe as

$$z_{in} = -\frac{1}{I_0} \int_{\Gamma} f(s) \hat{s} \cdot \vec{E}_{p}(s) ds \qquad (2.4)$$

This is equal to the input impedance to the probe when it is used as a radiating element. Substituting (2.4) in (2.3), we have

$$V_0(\vec{r}) = \frac{z_L}{z_{in}(\vec{r}) + z_L} \int_{\Gamma} f(s) \hat{s} \cdot \vec{E}(s) ds \qquad (2.5)$$

where the relation  $V_0 = Z_L I_0$  has been used. Equation (2.5) is the general relation between the output voltage of the probe  $V_0(\vec{r})$  and the electric field at the probe location in the conducting body. If we define

$$V_{eq}(\vec{r}) = \int_{\Gamma} f(s) \hat{s} \cdot \vec{E}(s) ds$$
 (2.6)

as an equivalent voltage source for the probe, and noting that  $\frac{v_0}{z_L} = I_0$ , Eq. (2.5) can be rewritten as

$$I_0 Z_{in}(\vec{r}) + I_0 Z_L = V_{eq}(\vec{r})$$
 (2.7)

Equation (2.7) suggests an equivalent circuit for the probe in the conducting body as shown in Figure 2.2.

In practice, we are interested in electrically small probes such that internal electric field at probe location is uniform. Thus Eq. (2.5) can be written as

$$V_0(\vec{r}) \doteq \left[ \frac{z_L}{z_{in}(\vec{r}) + z_L} \int_{\Gamma} f(s) \hat{s} ds \right] \cdot \vec{E}(\vec{r}) . \qquad (2.8)$$

This is the desired relation which shows that the output of the probe is proportional to the electric field at the probe's location in the absence of the probe. shows that the proportionality factor is a strong function of the location of the probe in the body (i.e.  $\overrightarrow{r}$ ) and also of electrical parameters of the medium (i.e.  $\epsilon(\vec{r})$ ,  $\sigma(\vec{r})$  and  $\mu_0$ ) at the probe location. We note that the current distribution function f(s) is, in general, a function of the parameters of the medium. At the same time, input impedance of the probe when used as a radiating element  $Z_{in}(\overset{\rightarrow}{r})$  is a function of not only location  $\vec{r}$  but of electrical parameters  $\epsilon$ ,  $\sigma$  and  $\mu_0$ . It is obvious that in order to measure the field intensity inside, say, a biological body, we need to have a location - and local parameter - independent probe. In other words, the equivalent circuit shown in Figure 2.2 differs from the conventional circuits for a receiving antenna, in which  $z_{in}$  is a strong function of location and local parameters. Also as hidden in  $V_{eq}(\vec{r})$ , the current distribution function f(s) is not constant as one moves the probe around in a heterogeneous body.

The solution of the input impedance of a dipole or a loop type probe is not easily obtainable in a finite conducting body. Therefore, a simple spherical probe will be treated rigorously throughout this study because, an exact analytical solution is possible for this model.

## 2.2. Spherical Antenna as a Probe

The problem which will be examined in the next few chapters deals with an insulated spherical antenna as an implantable probe in a finite conducting body. The problem is schematically shown in Figure 2.3. It will be shown that when the coated spherical probe is located in the center of a spherical homogeneous conducting body, a closed form analytical solution can be obtained. After this, we will study the receiving and radiating characteristics of a dielectrically coated spherical antenna imbedded in a finite biological body.

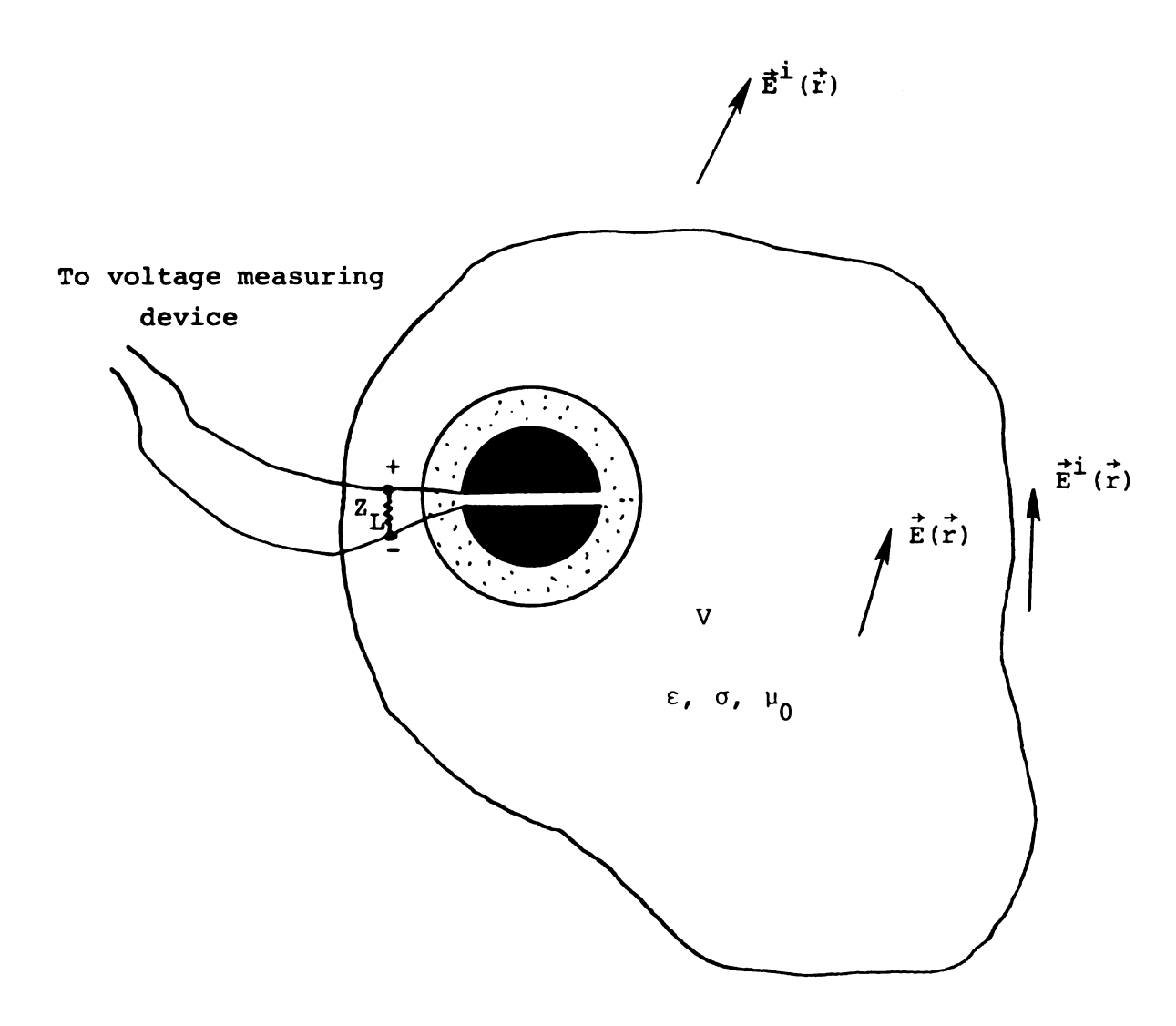


Figure 2.3. Insulated Spherical Probe in a Conducting Body Irradiated by an Incident EM Wave.

#### CHAPTER III

# AN INSULATED SPHERICAL PROBE IN A CONDUCTING BODY

As was mentioned in the previous chapter, a dielectrically coated spherical antenna may be used as a probe in a conducting body. In this chapter, we consider the receiving characteristics of an insulated spherical probe when illuminated by a uniform electric field inside a biological body. An expression will be derived for the effective diameter of the probe and some theoretical results will be presented for the normalized effective diameter as a function of relative dielectric constant and conductivity of the conducting body.

It should be noted, however, that the results of this chapter are partly based on the results of the input impedance of a coated spherical probe when used as a radiating element in a finite body. The latter results are developed thoroughly in the next chapter.

3.1. Statement of the Problem and the Superposition Principle

As shown in Figure 3.1, an electrically small sphere of diameter 2a, coated by a dielectric shell of

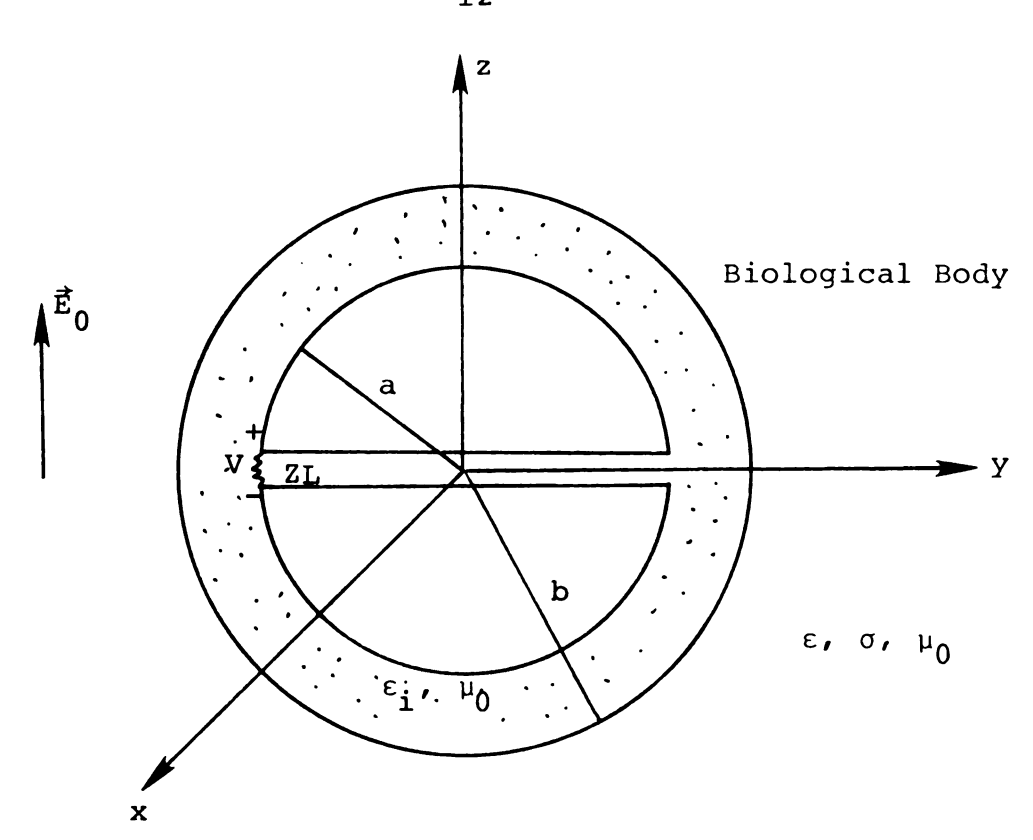


Figure 3.1. Dielectrically Coated Small Spherical Probe in a Uniform Incident Electric Field Inside a Biological Body

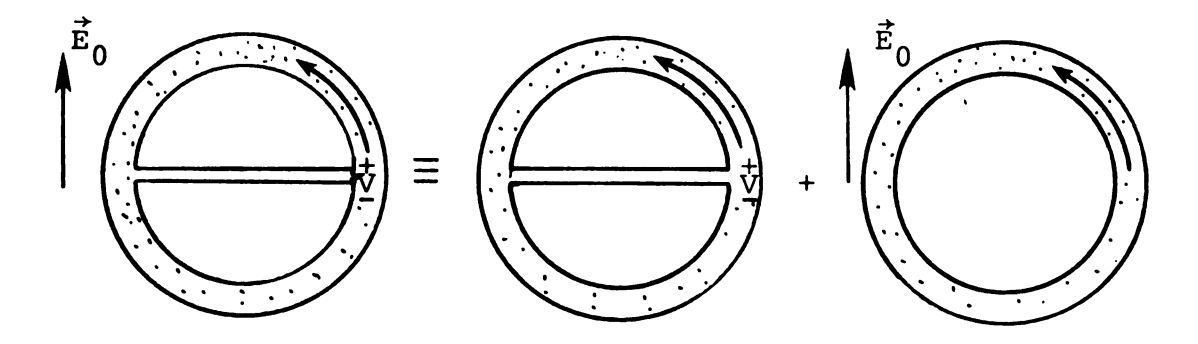


Figure 3.2. Illustrating the Superposition Principle

.

ε

t

۶

ŧ

'n

3

20

S

3

...

\$. 15. radius b is imbedded in a biological body. Assume that an electric field  $\vec{E}_0$  exists at the probe location and this  $\vec{E}_0$  is uniform over the probe when the probe is small. There is an impedance  $Z_L$  across a narrow gap of the probe and we aim to derive a relation between the induced voltage across  $Z_L$  and the impressed electric field  $\vec{E}_0$ . The dielectric coating has a permittivity  $\epsilon_i$  and permeability  $\mu_0$ . The electrical parameters of the body are  $\epsilon$ ,  $\sigma$  and  $\mu_0$ . The spherical probe is located such that the z axis of the rectangular coordinate system is perpendicular to the plane of the narrow gap and the impressed electric field is in the z direction.

Since the biological body is assumed to be linear, we can apply the superposition principle. This principle states that the total electromagnetic field present at any point outside the spherical probe is the sum of the scattered fields from the shorted probe (a coated solid sphere) illuminated by the impressed electric field, plus the field radiated by the coated spherical antenna driven by a voltage which is equal to the voltage drop across the load impedance at the narrow gap. This is illustrated in Figure 3.2 where arrows on the spheres show the directions of currents.

The radiating antenna will be analyzed in the next chapter and its input impedance will be formulated. In this chapter, we will solve the scattering problem.

#### 3.2. Scattering from a Dielectrically Coated Sphere

An insulated solid sphere together with the spherical coordinate system is shown in Figure 3.3. The incident electric field at the sphere is expressed as

$$\vec{E}_0 = E_0 \hat{z} = E_0 \cos \theta \hat{r} - E_0 \sin \theta \hat{\theta}$$
 (3.1)

based on the approximation of the field being uniform over a small sphere. Time harmonic dependence of the form  $\exp(j\omega t)$  is implied but not shown in the analysis.

From the incident field of equation (3.1), we can see that there exists only the r- and  $\theta$ - components of the electric field in dielectric region and the conducting body. Furthermore, all fields are independent of azimuthal angle  $\varphi$  due to the rotational symmetry. The magnetic field associated with this uniform electric field can be shown, via Maxwell's curl equation, to be identically zero. This implies that the effect of the magnetic field will be neglected at this stage. The following relations are true under the stated approximations.

$$\frac{\partial}{\partial \varphi} = 0$$
,  $E_{\varphi} = 0$  and  $H_{r} = H_{\theta} = 0$ . (3.2)

Of course, there is a scattered magnetic field maintained by the current induced on the sphere by the uniform incident electric field.

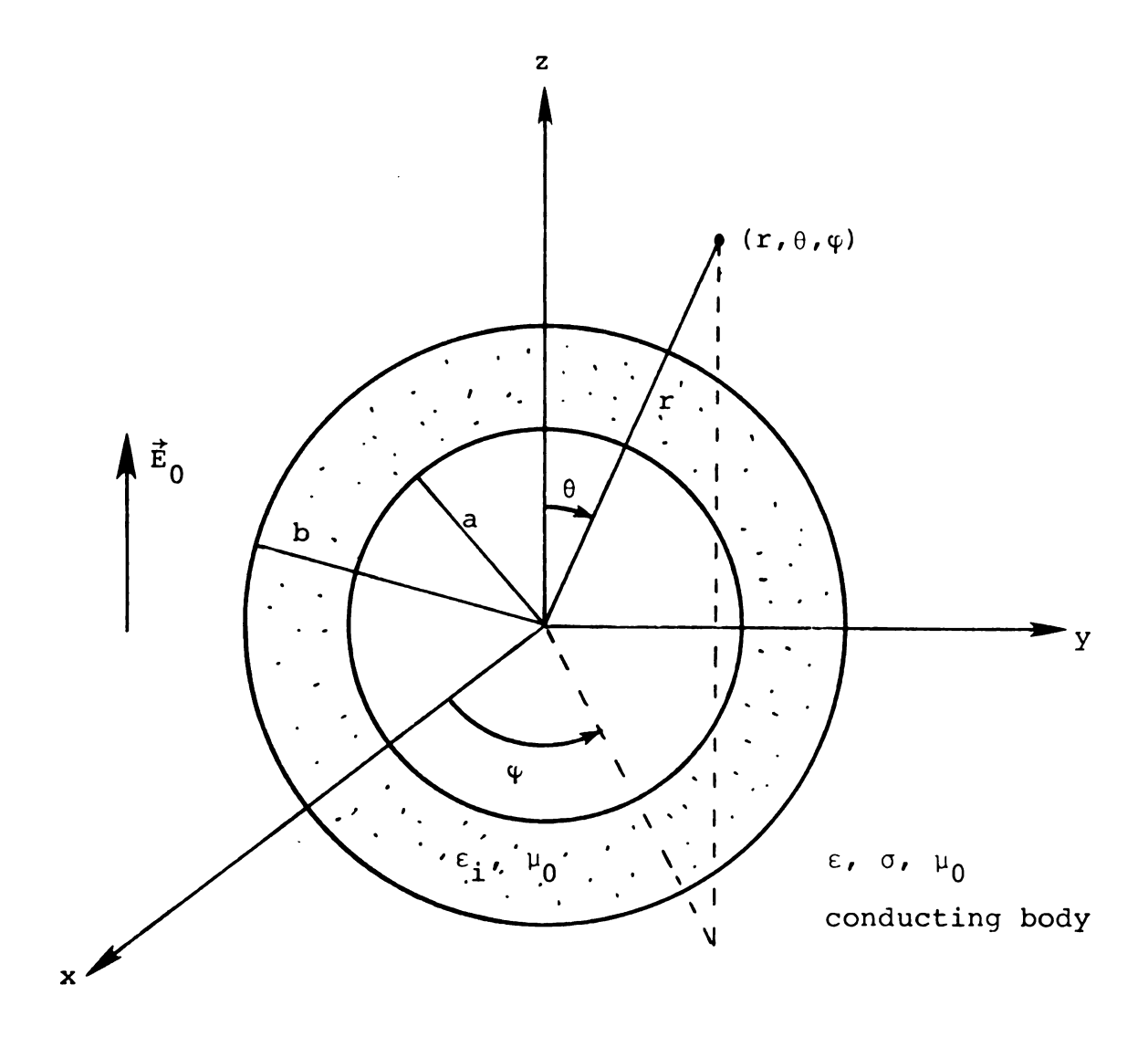


Figure 3.3. The Scattering from a Dielectrically Coated Sphere when Irradiated by a Uniform Incident Electric Field in the z Direction, Inside a Conducting Body.

There are two regions where we have to find expressions for the total EM field components. To do this, we can start from the Maxwell's equations and derive the Helmholtz Wave equation. The solution to this equation will be considered in more detail in the next chapter. Here, we just write down the tangential components of  $\vec{E}$  and  $\vec{H}$  fields in the two regions:

For  $r \geq b$ , the scattered fields by the coated sphere are

$$H_{\varphi n}^{s}(r,\theta) = P_{n}^{l}(\cos \theta)H_{\varphi n}^{s+}(r)$$
 (3.3)

$$E_{\theta n}^{s}(r,\theta) = P_{n}^{1}(\cos \theta) Z_{sn}^{+}(r) H_{\phi n}^{s+}(r)$$
 (3.4)

where

$$\begin{cases} H_{\varphi n}^{s+}(r) = \frac{A_{n}H_{n+\frac{1}{2}}^{(2)}(kr)}{\sqrt{kr}}, & k^{2} = \omega^{2}\mu_{0}\xi \\ \xi = \varepsilon - j\frac{\sigma}{\omega}, & \eta = \sqrt{\frac{\mu_{0}}{\xi}} \end{cases}$$

$$Z_{sn}^{+}(r) = j\eta \left[ \frac{H_{n-\frac{1}{2}}^{(2)}(kr)}{H_{n+\frac{1}{2}}^{(2)}(kr)} - \frac{n}{kr} \right]$$
(3.5)

 $H^{(1)}$  and  $H^{(2)}$  are Hankel functions of the first and second kind, respectively.  $\xi$  is the complex permittivity of the conducting body and  $Z_{sn}^+(r)$  is the TM mode wave impedance in this region.  $A_n$ , for integer n, is an unknown coefficient to be determined later from the boundary conditions. In Equations (3.3) and (3.4), only the

out-going waves are considered. This approximation neglects the reflection of the waves at the outer surface of the conducting body. This may be valid because of the losses in the medium.

For  $a \le r \le b$ , the total fields in this region can be expressed as

$$H_{\varphi n}(r,\theta) = P_n^1(\cos \theta) \left[ H_{\varphi n}^-(r) + H_{\varphi n}^+(r) \right]$$
 (3.6)

$$E_{\theta n}(r,\theta) = P_n^1(\cos \theta) [Z_n^+(r)H_{\psi n}^+(r) - Z_n^-(r)H_{\psi n}^-(r)]$$
 (3.7)

where

$$\begin{cases} H_{\phi n}^{-}(r) = \frac{B_{n}H_{n+\frac{1}{2}}^{(1)}(k_{i}r)}{\sqrt{k_{i}r}}, H_{\phi n}^{+}(r) = \frac{C_{n}H_{n+\frac{1}{2}}^{(2)}(k_{i}r)}{\sqrt{k_{i}r}} \\ k_{i}^{2} = \omega^{2}\mu_{0}\epsilon_{i}, \eta_{i} = \sqrt{\frac{\mu_{0}}{\epsilon_{i}}} \\ Z_{n}^{+}(r) = j\eta_{i} \left[ \frac{H_{n-\frac{1}{2}}^{(2)}(k_{i}r)}{H_{n+\frac{1}{2}}^{(2)}(k_{i}r)} - \frac{n}{k_{i}r} \right] \\ Z_{n}^{-}(r) = -j\eta_{i} \left[ \frac{H_{n-\frac{1}{2}}^{(1)}(k_{i}r)}{H_{n+\frac{1}{2}}^{(1)}(k_{i}r)} - \frac{n}{k_{i}r} \right] . \end{cases}$$

$$(3.8)$$

Note that since this is a finite region, there exist both out-going spherical wave,  $H_{\phi n}^+(r)$ , and incoming spherical wave,  $H_{\phi n}^-(r)$ .  $B_n$  and  $C_n$  are two other unknowns to be determined later.

Since there is a solution for each n, the actual  $\vec{E}$  and  $\vec{H}$  fields are infinite sums of fields given by equations (3.3), (3.4) and (3.6), (3.7), i.e.;

$$H_{\varphi}(r,\theta) = \sum_{n=1}^{\infty} H_{\varphi n}(r,\theta)$$
 (3.9)

where  $H_{\phi n}(r,\theta)$  is as given by (3.6). Similar expressions can be written for other field components.

Up to this point, we have introduced three un-known coefficients  $A_n$ ,  $B_n$  and  $C_n$ . To solve for these unknowns, we use the Boundary Conditions.

The first boundary condition is that the tangential electric field vanishes at any point on the perfect conducting metallic sphere, i.e.

$$E_{\theta n}(a,\theta) = P_n^1(\cos \theta) [Z_n^+(a)H_{\psi n}^+(a) - Z_n^-(a)H_{\psi n}^-(a)] = 0$$
 (3.10)

which is valid for all n and  $\theta$ .

The second boundary condition states that the tangential  $\vec{E}$  and  $\vec{H}$  field components are continuous at r=b, or

$$H_{\varphi n}^{-}(b) + H_{\varphi n}^{+}(b) = H_{\varphi n}^{s+}(b)$$
 (3.11)

$$z_n^+(b)H_{\varphi n}^+(b) - z_n^-(b)H_{\varphi n}^-(b) = z_{sn}^+(b)H_{\varphi n}^{s+}(b) - E_0\delta_{1n}$$
 (3.12)

Note that in writing the continuity of  $\vec{E}$  field, the uniform incident electric field  $E_0$  in the conducting body is included in the right hand side of equation (3.12).

The notation associated with  $E_0$ , i.e.

$$\delta_{1n} = \begin{cases} 1 & n = 1 \\ 0 & n \neq 1 \end{cases}$$
 (3.13)

is the Kronecker delta.

The three unknown coefficients are the solutions of the following system:

$$Y_n X_n = F_n \tag{3.14}$$

where

$$Y_{n} = \begin{bmatrix} A_{n} \\ B_{n} \\ C_{n} \end{bmatrix}, \quad F_{n} = \begin{bmatrix} E_{0} \delta_{1n} \\ 0 \\ 0 \end{bmatrix}$$

$$Y_{n} = \begin{bmatrix} \frac{H_{n+1/2}^{(2)}(kb)}{\sqrt{kb}} z_{sn}^{+}(b) & \frac{H_{n+1/2}^{(1)}(k_{1}b)}{\sqrt{k_{1}b}} & z_{n}^{-}(b) & \frac{H_{n+1/2}^{(2)}(k_{1}b)}{\sqrt{k_{1}b}} & z_{n}^{+}(b) \\ \frac{H_{n+1/2}^{(2)}(kb)}{\sqrt{kb}} & \frac{-H_{n+1/2}^{(1)}(k_{1}b)}{\sqrt{k_{1}b}} & \frac{H_{n+1/2}^{(2)}(k_{1}b)}{\sqrt{k_{1}b}} \\ 0 & H_{n+\frac{1}{2}}^{(1)}(k_{1}a) z_{n}^{-}(a) & H_{n+\frac{1}{2}}^{(2)}(k_{1}a) \end{bmatrix}$$

$$(3.15)$$

The matrix equation (3.14) gives us non-zero solutions for  $A_n$ ,  $B_n$  and  $C_n$  only when n=1. That means there is only one term in the infinite series of equation (3.9). This simply is due to the fact that the incident electric field was assumed to be uniform. If, for example, the incident field was assumed to be a plane wave, the

solution would be quite involved and there would be infinite terms in the series solution of Equation (3.9).

We can now define

$$a_1 = \frac{A_1}{E_0}$$
,  $b_1 = \frac{B_1}{E_0}$  and  $c_1 = \frac{C_1}{E_0}$  (3.16)

such that the expression for the tangential H field on the surface of sphere, as given in equation (3.6), can be expressed as

$$H_{\varphi}(a,\theta) = \sin \theta \left[ \frac{H_{3/2}^{(1)}(k_i a)}{\sqrt{k_i a}} b_1 + \frac{H_{3/2}^{(2)}(k_i a)}{\sqrt{k_i a}} c_1 \right] E_0$$
 (3.17)

Note that  $P_1^1(\cos \theta) = \sin \theta$ . The unknowns  $b_1$  and  $c_1$  are solved from equations (3.16) and (3.15) as

$$\begin{cases} b_1 = \frac{\sqrt{k_i b}}{\left[z_{s1}^+(b) + z_1^-(b)\right] H_{3/2}^{(1)}(k_i b) + \left[z_{s1}^+(b) - z_1^+(b)\right] \alpha(a) H_{3/2}^{(2)}(k_i b)} \\ c_1 = \alpha(a) b_1 \\ \alpha(a) = \frac{z_1^-(a) H_{3/2}^{(1)}(k_i a)}{z_1^+(a) H_{3/2}^{(2)}(k_i a)} \end{cases}$$
(3.18)

Up to now, the magnetic field on the sphere is completely known.

We are interested in the current on the sphere.

The surface current on the surface of the sphere is given by

$$\vec{K}(\theta) = \hat{n} \times \vec{H} = \hat{r} \times H_{\psi}(a,\theta) \hat{\psi} = -H_{\psi}(a,\theta) \hat{\theta}$$
 (3.19)

where  $H_{\phi}(a,\theta)$  is as given by equation (3.17). This current is proportional to  $E_0$  and can be written as

$$K_{\theta}(\theta) = -H_{\varphi}(a, \theta) = Y(\theta)E_{0}$$
 (3.20)

where

$$Y(\theta) = -\left[\frac{H_{3/2}^{(1)}(k_{i}a)}{\sqrt{k_{i}a}} b_{1} + \frac{H_{3/2}^{(2)}(k_{i}a)}{\sqrt{k_{i}a}} c_{1}\right] \sin \theta$$
 (3.21)

with  $b_1$  and  $c_1$  as given by equation (3.18). Note that  $Y(\theta)$  has the dimensions of an admittance.

3.3. Equivalent Circuit of an Insulated Spherical Probe in a Conducting Body

Referring back to superposition principle as depicted in Figure 3.2, the total surface current on the insulated sphere of Figure 3.1 is given by

$$K_{+\theta}(\theta) = K_{\theta}(\theta) + K_{\theta}^{\bullet}(\theta)$$
 (3.22)

where  $K_{\theta}(\theta)$  is found in the previous section and is given by equation (3.20),  $K_{\theta}^{\bullet}(\theta)$  is the surface current on the spherical probe when it is driven by a voltage generator. The radiating problem will be solved in the next chapter. At this point, we write  $K_{\theta}^{\bullet}$  at the probe gap or  $\theta = 90^{\circ}$  simply as

$$K_{\theta}^{\bullet}(\theta = 90^{\circ}) = \frac{V}{2\pi a Z_{in}}$$
 (3.23)

where V is the induced voltage (or the voltage drop) across the load impedance of the spherical probe, and  $Z_{in}$  is the input impedance of the coated sphere when used as a radiating antenna in the same conducting body. The general expression for this input impedance  $Z_{in}$  will be derived in the next chapter.

The induced voltage across the load impedance is given by

$$V = -Z_L I = -2\pi a K_{t \theta} (\theta = 90^\circ) Z_L$$
 (3.24)

Note the polarity of this voltage drop as shown in Figure 3.1. Substituting equations (3.23) and (3.24) into the equation (3.22), one gets;

$$- \frac{V}{2\pi a Z_{T}} = \frac{V}{2\pi a Z_{in}} + Y(\theta = 90^{\circ}) E_{0}.$$

After rearranging, it becomes

$$V(Z_{in} + Z_{L})/Z_{L} = -2 a\pi Z_{in}Y(\theta = 90^{\circ})E_{0}$$
 (3.25)

where  $Y(\theta)$  is given in equation (3.21).

Equation (3.25) suggests an equivalent circuit for the insulated spherical probe in a conducting body as shown in Figure 3.4. The equivalent driving voltage for the probe in Figure 3.4 is,

$$V_{eq} = -2\pi a Z_{in}Y(\theta = 90^{\circ})E_{0}$$
 (3.26)

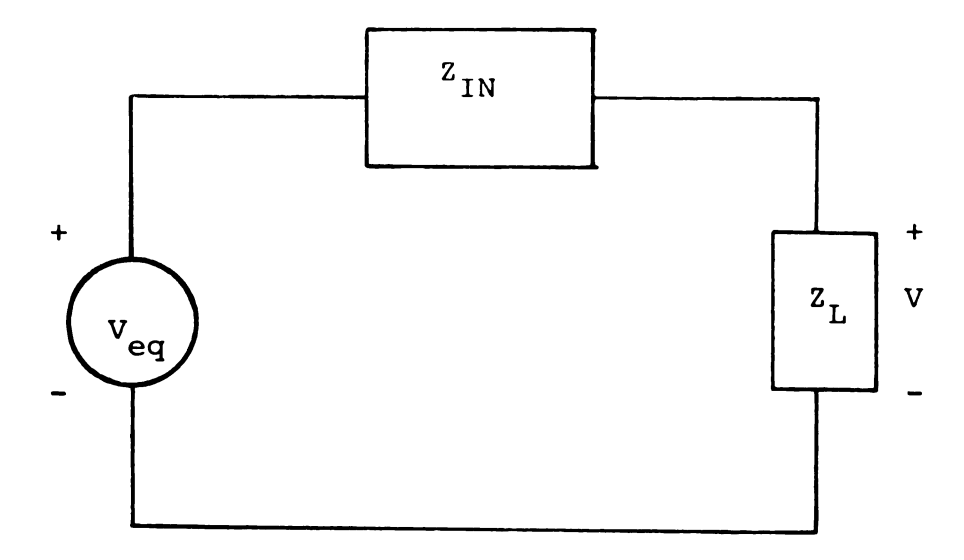


Figure 3.4. Equivalent Circuit of the Dielectrically Coated Spherical Probe in a Homogeneous Biological Body.

Note that Figure 3.4 is similar to Figure 2.2 of Chapter 2 which is the equivalent circuit of a wire probe.

In analogy with a wire probe, we can define an "effective" diameter of the probe as

$$D_{eff} = V_{eq}/E_0 = -2\pi a Z_{in}Y(\theta = 90^\circ)$$
 (3.27)

Furthermore, this can be normalized to the physical diameter of the sphere, 2a, to give dimensionless normalized effective diameter as

$$d_{eff} = D_{eff}/2a = -\pi Z_{in}Y(\theta = 90^{\circ})$$
 (3.28)

Finally, before ending this section, we note that  $V_{\rm eq}$  is the voltage developed across the load impedance when  $Z_{\rm L}$   $^{+}$   $^{\infty}$ . Therefore, useful information can be obtained from the effective diameter of the probe. Some theoretical results of this parameter are shown in the next section.

3.4. Some Theoretical Results on the Normalized Effective Diameter of the Spherical Probe

The expression for the normalized effective diameter of the spherical probe was derived and expressed in equation (3.28) of the last section. The results of this section are also based on the results of the input impedance of the spherical probe acting as a radiating element  $Z_{in}$ , which will be analyzed in the next chapter.

First, in order to compare the receiving characteristics of the spherical antenna to the other conventional probes (such as dipoles and loops), the effective diameter of a small sphere in free space is calculated. In Table 3.1, the real and imaginary parts (or magnitude and phase) of the normalized effective diameter for a small spherical probe in the free-space are shown. The frequency is assumed to be 600 megahertz which corresponds to the free space wavelength of 50 cm. The spherical probes considered are all electrically small.

As can be seen from Table 3.1, for small spherical receiving antennas,

$$D_{eff}/2a = 1/2$$
 (3.29)

is a good approximation. This means that

$$D_{eff} \doteq a \tag{3.30}$$

which is the physical radius of the sphere. This is similar to small dipole type probes, where the effective length is one half of the total physical length. The theory for the dipole antenna as a receiving element, can be found in King's book [5].

Several examples were worked out for the insulated spherical probe of Figure 3.1. It was found that the effective diameter, in general, is a strong function of the relative dielectric constant of the conducting body.

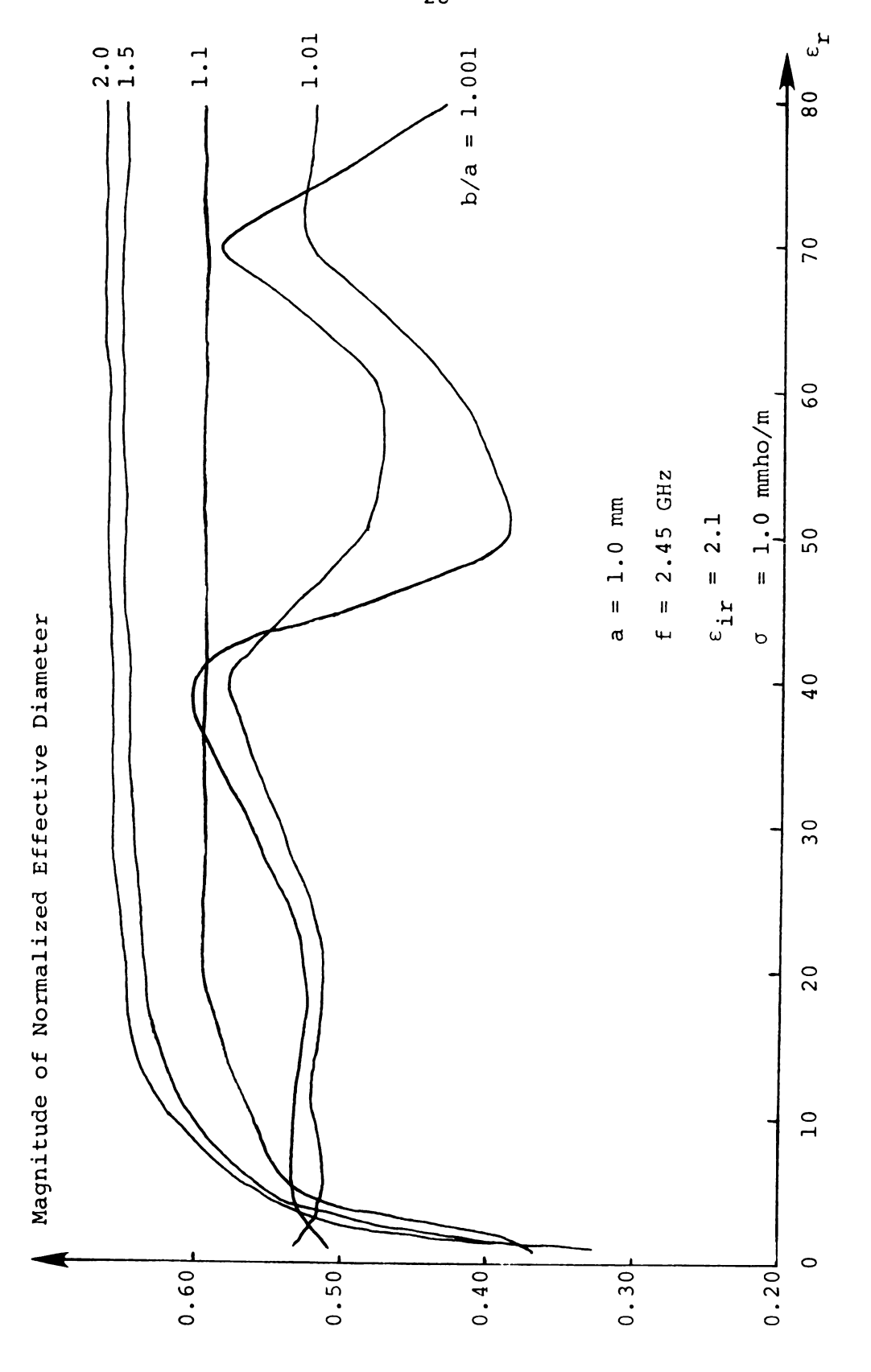
Table 3.1. Complex Normalized Effective Diameter of Small Spherical Antenna in Free Space (f = 600 MHz;  $\lambda_0$  = 50 cm.)

a (cm)	D <sub>eff</sub> /2a		
(Citt)	MAGNITUDE	PHASE (DEGREES)	
0.5	0.44738	-0.00478	
1.0	0.44805	-0.03796	
1.5	0.45078	-0.12655	
2.0	0.45448	-0.29493	
2.5	0.45902	-0.56393	
3.0	0.46428	-0.95012	
3.5	0.47010	-1.46559	
4.0	0.47630	-2.11801	
4.5	0.48270	-2.91084	
5.0	0.48913	-3.84390	
5.5	0.49541	-4.91383	
6.0	0.50137	-6.11478	
6.5	0.50685	-7.43891	
7.0	0.51170	-8.87698	
7.5	0.51579	-10.41877	
8.0	0.51902	-12.05351	
8.5	0.52127	-13.77013	
9.0	0.52247	-15.55751	
9.5	0.52254	-17.40459	
10.0	0.52144	-19.30041	

Of course, it is also a function of the thickness of the coating (or b). The example shown in Figure 3.5 illustrates the magnitude of normalized effective diameter for a small, coated spherical probe. The frequency is f=2.45 GHz (corresponding to the free space wavelength of  $\lambda_0=12.24$  cm) and the radius of the sphere is a=1.0 mm. The sphere is coated with a dielectric of dielectric constant  $\epsilon_{ir}=2.1$  (Teflon). The conductivity of the body is  $\sigma=1$  mmho/m. The curves are plotted for different thicknesses of the coating as a parameter. The independent variable is the relative dielectric constant of the conducting body. It is to be noted that although the effective diameter is a complex quantity, the imaginary part is usually small compared with the real part.

As can be seen from Figure 3.5, for smaller values of b/a (i.e. for thin coatings), there is a considerable variation in the effective diameter as the relative dielectric constant is changed. But for higher values of b/a (i.e. for thicker coatings), there is almost no variation in the effective diameter of the probe as the  $\varepsilon_{r}$  is varied. This is not true, however, for lower values of  $\varepsilon_{r}$ , say,  $\varepsilon_{r}$  < 10. Fortunately, for most cases of interest in biological bodies,  $\varepsilon_{r}$  is greater than 10.

The results obtained in this chapter are based on the geometry of a conducting body of infinite extent.



Magnitude of the Normalized Effective Diameter of a Dielectrically Coated Spherical Probe Imbedded in Biological Body with Relative Dielectric Constant  $\epsilon_{\rm r}$ Figure 3.5.

:::

::

:-:

...

71.

:...

::

...

·::

.

: 1.

•

::

:

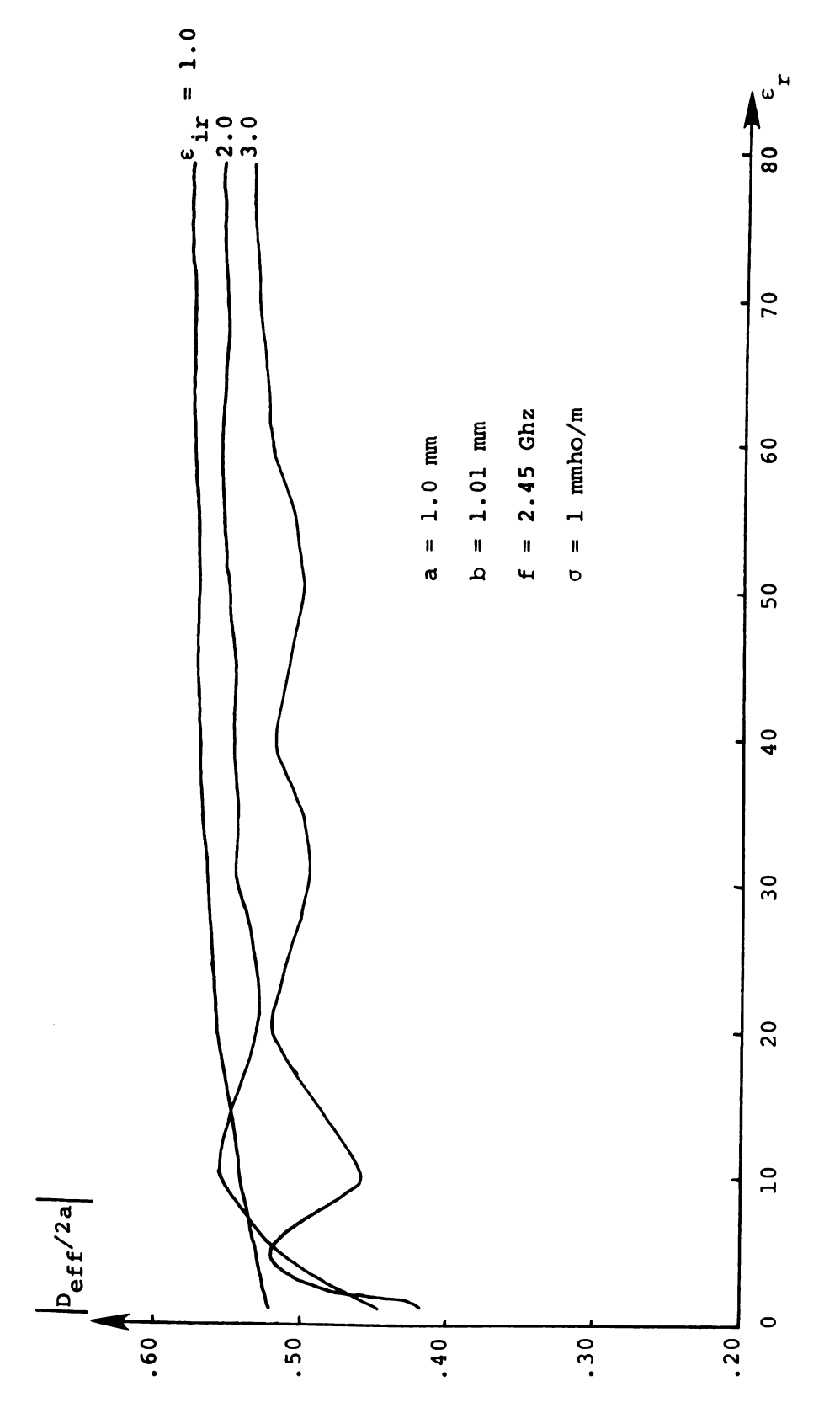
::

:

However, as we will see later, the input impedance of the probe is quite independent of the electrical parameters of the conducting body and the probe location. When the dielectric coating is sufficiently thick, the effective diameter expression derived in this chapter may also be valid for an insulated spherical probe immersed in a finite body.

Finally, in Figure 3.6, the normalized effective diameter of the probe is shown as a function of the dielectric constant of the conducting body for different values of the relative dielectric constant of the coating,  $\epsilon_{\rm ir}$ . It is seen in this figure that for lower values of  $\epsilon_{\rm ir}$ , the effective diameter remains almost constant for a wide range of relative dielectric constants of the conducting medium.

Therefore, as far as the receiving characteristics of the insulated spherical probe are concerned, in order to have the output of the probe to be independent of the electrical parameters of the conducting body, a thick coating with low dielectric constant materials is appropriate. In the next chapter, the radiating characteristics of the coated spherical probe will be studied as functions of the electrical parameters of the medium and the probe location in a conducting body.



Normalized Effective Diameter of a Dielectrically Coated Spherical Probe as a Function of the Relative Dielectric Constant of the Conducting Body. Figure 3.6.

#### CHAPTER IV

# DIELECTRICALLY COATED SPHERICAL ANTENNA IN A FINITE CONDUCTING BODY

As was seen in Chapter 2, the output of an EM field probe immersed in a finite conducting body is, in general, a strong function of its Input Impedance when used as a radiating element. Furthermore in Chapter 3, the expression for the effective diameter of a dielectrically coated spherical probe was found to be dependent on the input impedance of the radiating spherical antenna.

It is evident that to understand the performance of an EM field probe in a biological body, the input impedance of the probe acting as a radiating element must be determined. In this chapter the expression for the input impedance of the probe is determined as a function of the parameters of the body and the relative probe location inside the body.

The theoretical results for the input impedance of a coated spherical probe in a finite conducting body were computed numerically with a digital computer and are shown in figures. In the next chapter, the accuracy of these results is verified by experiments.

It is noted that the major difference between the problem studied here and the ones considered by other workers and available in the literature is the fact that the conducting body in the present study is finite. The selection of a finite conducting body increases the degree of difficulty in the theoretical analysis. However, with the geometries of a spherical conducting body and a spherical probe, an exact solution is obtainable by the method of boundary value problem. In the course of solving the problem, the matrix inversion method was first applied without success. Later, a transmission line approach was employed to find the solution successfully.

# 4.1. Geometry of the Problem

Figure 4.1 shows the geometry of the problem to be considered in this chapter. An electrically small sphere of radius a is driven by a voltage generator which maintains a potential difference V across a narrow equatorial gap. The spherical antenna is coated by a dielectric shell of outer radius b and dielectric constant  $\varepsilon_i$ . This dielectric coating region is assumed to be almost lossless, i.e.  $\varepsilon_i$  is a real quantity. The coated antenna is then imbedded in the center of a conducting body of radius c. The electrical parameters of the conducting body are  $\varepsilon$  (permittivity) and  $\sigma$ 

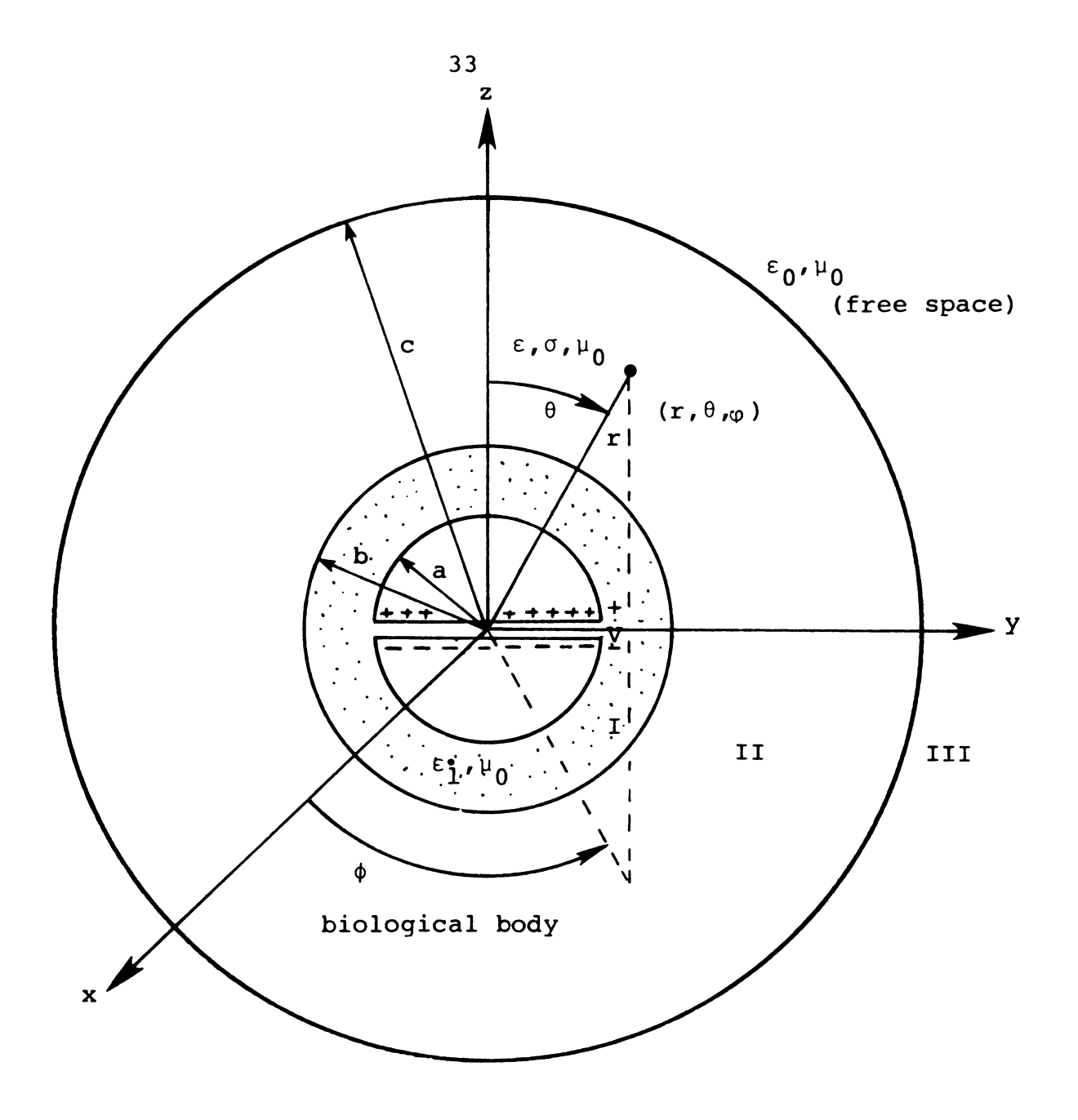


Figure 4.1. Dielectrically Coated Small Spherical Antenna in a Finite Biological Body. A Generator Maintains a Voltage V Across a Narrow Equatorial Gap of the Conducting Sphere. Spherical Coordinate System is Also Shown.

(conductivity). It is noted that for an exact solution to exist, the insulated sphere should be located at the center of the conducting body.

We aim to find an expression for the input impedance of a radiating, insulated spherical antenna, which is electrically small and can be used as a probe, imbedded in the center of a spherical biological body. This input impedance will be shown to be a function of all parameters involved, namely, a, b, c,  $\epsilon_i$ ,  $\epsilon$ ,  $\sigma$  and the frequency of the oscillating source, f.

## 4.2. Electromagnetic Field Solutions

Due to the geometry of the problem, the usual spherical coordinate system  $(r,\theta,\phi)$  is used as shown in Figure 4.1. There are three regions in which electric and magnetic fields are to be determined from the Maxwell's Equations. The two curl equations are:

$$\nabla \times \vec{E} = -j\omega\mu_0 \vec{H}$$
 (4.1)

$$\nabla \times \vec{H} = j\omega_{\underline{\varepsilon}}\vec{E}$$
 (4.2)

in which  $\underline{\varepsilon}$  is, in general, a complex permittivity. The time dependence of  $\exp(j_\omega t)$  is understood. Due to the rotational symmetry, all field quantities are independent of  $\phi$ , i.e.

$$\frac{\partial}{\partial \rho}$$
 ( )  $\equiv$  0 (4.3)

Also, due to the uniform excitation of the antenna around the gap, it is true that

$$E_{\varphi} = 0 \tag{4.4}$$

It implies that there is no  $_{\phi}$  component of the electric field in any region. With conditions (4.3) and (4.4), it can be shown that the magnetic field has only the  $\psi$  component. From Equation (4.1),

$$\nabla \times \vec{E} = \left(\frac{1}{r} \frac{\partial}{\partial r} (rE_{\theta}) - \frac{1}{r} \frac{\partial E_{r}}{\partial \theta}\right) \hat{\phi} = -j\omega\mu_{0} \vec{H}$$
 (4.5)

Equation (4.5) shows that  $\vec{H} = H_{\hat{p}}$ , i.e. there is only  $\hat{p}$  component of  $\vec{H}$  field at any point outside the spherical antenna.

Taking curl of Equation (4.2) one gets

$$\nabla \times \nabla \times \vec{H} = j\omega_{\vec{E}} \nabla \times \vec{E}$$
 (4.6)

in which the complex permittivity  $\underline{\varepsilon}$  is assumed to be independent of the location. Using Equation (4.1) in (4.6), one has

$$\nabla \times \nabla \times \vec{H} = \omega^2 \mu_0 \underline{\varepsilon} \vec{H}$$
 (4.7)

Since  $\vec{H} = \hat{\phi}H_{\phi}$ , Equation (4.7) can be rewritten as

$$\frac{\partial^{2}}{\partial r^{2}} (rH_{\varphi}) + \frac{1}{r^{2}} \frac{\partial}{\partial \theta} \left[ \frac{1}{\sin \theta} \frac{\partial}{\partial \theta} (rH_{\varphi} \sin \theta) \right] + \omega^{2} \mu_{0} \underline{\varepsilon} rH_{\varphi} = 0.$$
(4.8)

This partial differential equation is a key relation for the derivation of all EM field components in the different regions. It is written in a form to facilitate the solution by the usual "separation of variables" technique.

Let us now consider the 3 different regions as shown in Figure 4.1:

Region I, a  $\leq$  r  $\leq$  b or the dielectric coating region.

In this region the insulating layer has a real dielectric constant  $\epsilon_i$  and Equation (4.8) can be written as

$$\frac{\partial^{2}}{\partial r^{2}} (rH_{l_{\varphi}}) + \frac{1}{r^{2}} \frac{\partial}{\partial \theta} \left[ \frac{1}{\sin \theta} \frac{\partial}{\partial \theta} (rH_{l_{\varphi}} \sin \theta) \right] + k_{i}^{2} rH_{l_{\varphi}} = 0$$
(4.9)

where  $k_i^2 = \omega^2 \mu_0 \epsilon_i$  and  $k_i$  is the real wave number in this region. Solution to the above equation can be written as

$$rH_{l_{\varphi}}(r,\theta) = R(r)\Theta(\theta) \qquad (4.10)$$

and Equation (4.9) is rewritten;

$$\frac{r^2}{R} \frac{d^2 R}{dr^2} + \frac{1}{\Theta} \frac{d}{d\theta} \left[ \frac{1}{\sin \theta} \frac{d}{d\theta} \left( \mathcal{E} \sin \theta \right) \right] + k_i^2 r^2 = 0. \quad (4.11)$$

The above equation is true if,

$$\begin{cases} \frac{r^2}{R} \frac{d^2 R}{dr^2} + k_i^2 r^2 = K \\ \frac{1}{\Theta} \frac{d}{d\theta} \left[ \frac{1}{\sin \theta} \frac{d}{d\theta} \left( \frac{1}{\Theta} \sin \theta \right) \right] = -K \end{cases}$$
(4.12)

where K is a separation constant. However, to get well-behaved solutions to (4.12), K should be equal to n(n + 1) where  $n = 1, 2, 3, \ldots$ . The resulting ordinary differential equations are well known equations in mathematical physics [6]. With this choice of K, we can write the solutions as (details omitted and are in the reference)

$$\begin{cases} R_{n}(r) = \sqrt{r} [A_{n}H_{n+1/2}^{(2)}(k_{i}r) + B_{n}H_{n+1/2}^{(1)}(k_{i}r)] \\ g_{n}(\theta) = P_{n}^{1}(\cos \theta) \end{cases}$$
(4.13)

In the above equations,  $H^{(1)}$  and  $H^{(2)}$  are Hankel Functions of the first and second kinds, respectively. Physically, they represent in-coming and out-going waves which exist in the dielectric coating region.  $P_n^1(\cos\theta)$  is an Associated Legendre function of the first kind, order n and degree l. Furthermore,  $A_n$  and  $B_n$  are, at the present time, unknown coefficients to be determined later from boundary conditions.

From Equation (4.13), we write the expression for the tangential component of the magnetic field as

$$H_{l_{\varphi}}(r,\theta) = \frac{1}{\sqrt{r}} \sum_{n=1}^{\infty} P_{n}^{l}(\cos \theta) [A_{n}H_{n+1/2}^{(2)}(k_{i}r) + B_{n}H_{n+1/2}^{(1)}(k_{i}r)]$$
(4.14)

With the magnetic field determined, electric field is found from Maxwell equation (4.2). This gives

$$E_{1r}(r,\theta) = \frac{j}{\omega \varepsilon_{i} r \sqrt{r}} \sum_{n=1}^{\infty} n(n+1) P_{n}(\cos \theta) \left[ A_{n} H_{n+1/2}^{(2)}(k_{i}r) + B_{n} H_{n+1/2}^{(1)}(k_{i}r) \right]$$
(4.15)

and

$$E_{1\theta}(r,\theta) = -\frac{j}{\omega \varepsilon_{i} r \sqrt{r}} \sum_{n=1}^{\infty} P_{n}^{1}(\cos \theta) \{A_{n}[nH_{n+1/2}^{(2)}(k_{i}r) - k_{i}rH_{n-1/2}^{(2)}(k_{i}r)] + B_{n}[nH_{n+1/2}^{(1)}(k_{i}r) - k_{i}rH_{n-1/2}^{(1)}(k_{i}r)]\}$$

$$(4.16)$$

Note that in deriving the above equations, the following relations of Legendre and Hankel functions have been used:

$$\begin{cases} \frac{d}{d\theta} \left[ P_n^1(\cos \theta) \right] = \frac{1}{\sin \theta} \left[ n P_{n+1}^1(\cos \theta) - (n+1)\cos \theta P_n^1(\cos \theta) \right] \\ \frac{1}{\sin \theta} \left[ \cos \theta P_n^1(\cos \theta) - P_{n+1}^1(\cos \theta) \right] = (n+1) P_n(\cos \theta) \end{cases}$$

$$(4.17)$$

$$\begin{cases} \frac{d}{dr} H_{n+1/2}^{(1)}(r) = -\frac{n+1/2}{r} H_{n+1/2}^{(1)}(r) + H_{n-1/2}^{(1)}(r) \\ \frac{d}{dr} H_{n+1/2}^{(2)}(r) = -\frac{n+1/2}{r} H_{n+1/2}^{(2)}(r) + H_{n-1/2}^{(2)}(r) \end{cases}$$

$$(4.18)$$

Up to this point, we have found the complete expressions for the total EM field components in the dielectric coating region  $a \le r \le b$ . In other regions, the fields are written by inspection since the form of the wave equations is similar in all regions.

Region II, b  $\leq$  r  $\leq$  c or the biological body region.

In this region because of the losses in the conducting body, the wave number of the medium is complex and given by

$$k^2 = \omega^2 \mu_0 \xi; \quad \xi = \varepsilon - j \frac{\sigma}{\omega}$$
 (4.19)

The tangential field components in this region are,

$$H_{2_{\phi}}(r,\theta) = \frac{1}{\sqrt{r}} \sum_{n=1}^{\infty} P_{n}^{1}(\cos \theta) [C_{n}H_{n+1/2}^{(2)}(kr) + D_{n}H_{n+1/2}^{(1)}(kr)]$$
(4.20)

and

$$E_{2\theta}(r,\theta) = -\frac{j}{\omega \xi r \sqrt{r}} \sum_{n=1}^{\infty} P_n^1(\cos \theta) \{C_n[nH_{n+1/2}^{(2)}(kr)]\}$$

$$- krH_{n-1/2}^{(2)}(kr)] + D_n[nH_{n+1/2}^{(1)}(kr) - krH_{n-1/2}^{(1)}(kr)] \} (4.21)$$

Note that  $E_{2r}$  is omitted since it is not used in the determination of the unknown coefficients  $A_n$ ,  $B_n$ ,  $C_n$  and  $D_n$ .

Region III,  $r \ge c$  or the free space region. In this region, the wave number is real and given by

$$k_0^2 = \omega^2 \mu_0 \varepsilon_0 \tag{4.22}$$

and only outward traveling waves represented by  $H_n^{(2)}(k_0r) \quad \text{are present.} \quad \text{Therefore, the tangential field}$  components are given as

$$H_{3_{\varphi}}(r,\theta) = \frac{1}{\sqrt{r}} \sum_{n=1}^{\infty} E_n P_n^1(\cos \theta) H_{n+1/2}^{(2)}(k_0 r)$$
 (4.23)

and

$$E_{3\theta}(r,\theta) = -\frac{j}{\omega \epsilon_0 r \sqrt{r}} \sum_{n=1}^{\infty} E_n P_n^1(\cos \theta) [nH_{n+1/2}^{(2)}(k_0 r) - H_{n-1/2}^{(2)}(k_0 r)]$$
(4.24)

This completes the derivation of EM field components in the three regions shown in Figure 4.1. There are five unknown coefficients  $A_n$ ,  $B_n$ ,  $C_n$ ,  $D_n$  and  $E_n$  for each integer n. To find these unknowns and obtain the expression for the magnetic field on the metallic sphere (and thus the current), we use the boundary conditions on the tangential field components as outlined in the next section.

#### 4.3. Applications of Boundary Conditions

The boundary conditions state that the tangential components of electric and magnetic fields are continuous at r = b and r = c (see Figure 4.1). Moreover, on the surface of the metallic sphere (assumed to be perfectly conducting),  $E_{1\theta}(a,\theta)$  vanishes at any point except at the narrow equatorial gap. An enlarged view of the gap region and a possible feeding system is shown in Figure 4.2. The angular width of the gap is  $2\theta_0$  and is assumed to be very small (e.g.  $2\theta_0$  is of order of 10 degrees or smaller). Mathematically, we write

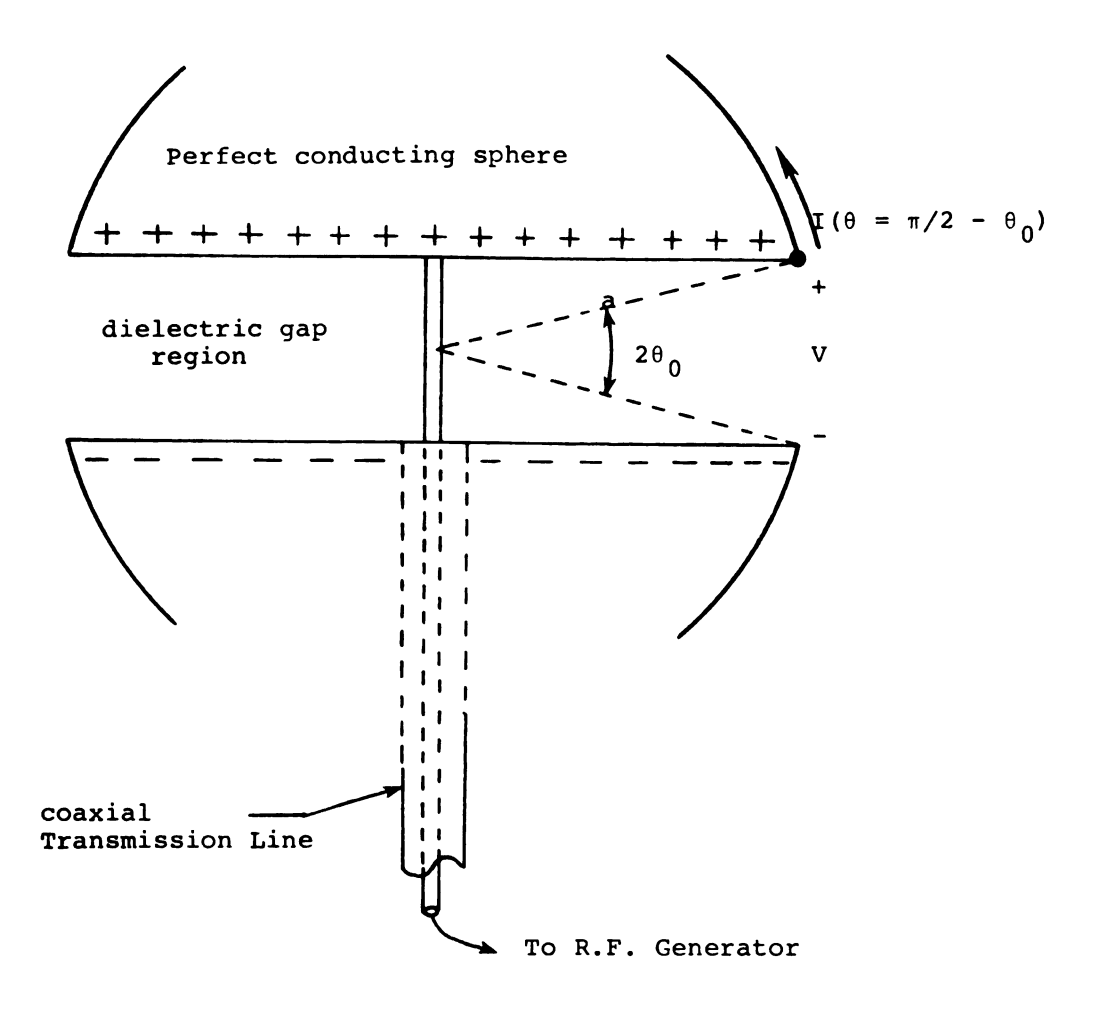


Figure 4.2. Enlarged View of the Gap Region of the Spherical Antenna. A Coaxial Line Connected to a R.F. Source, Maintains a Voltage V Across the Narrow Gap. Input Current I is Shown at the Edge where  $\theta=\pi/2-\theta_0$  (200 is the Angular Width of the Gap).

$$E_{1\theta}(a,\theta) = \frac{V}{a} \delta(\theta - \pi/2) \qquad (4.25)$$

On the other hand, from Equation (4.16) in the last section, we have

$$E_{1\theta}(a,\theta) = -\frac{j}{\omega \epsilon_i a \sqrt{a}} \sum_{n=1}^{\infty} P_n^1(\cos \theta) \{A_n[nH_{n+1/2}^{(2)}(k_i a)\}$$

$$-k_{i}aH_{n-1/2}^{(2)}(k_{i}a)$$
] +  $B_{n}[nH_{n+1/2}^{(1)}(k_{i}a) - k_{i}aH_{n-1/2}^{(1)}(k_{i}a)]$ } (4.26)

Multiply both sides of Equation (4.26) by  $"P_m^1(\text{Cos }\theta)\sin \,\theta" \quad \text{and integrate from 0 to} \quad \pi \quad \text{on} \quad \theta \quad \text{to}$  get

$$\int_{0}^{\pi} E_{1\theta}(a,\theta) P_{m}^{1}(\cos\theta) \sin\theta d\theta = -\frac{j}{\omega \epsilon_{i} a \sqrt{a}} \sum_{n=1}^{\infty} \{A_{n}[nH_{n+1/2}^{(2)}(k_{i}a)]\}$$

$$-k_{i}aH_{n-1/2}^{(2)}(k_{i}a)] + B_{n}[nH_{n+1/2}^{(1)}(k_{i}a)]$$

$$-k_{i}aH_{n-1/2}^{(1)}(k_{i}a)]\} \int_{0}^{\pi} P_{m}^{1}(\cos \theta)P_{n}^{1}(\cos \theta)\sin \theta d\theta \qquad (4.27)$$

where we interchanged the summation and integration opeations. We now use the following orthogonality relations of the Associated Legendre functions:

$$\begin{cases} \int_{0}^{\pi} P_{m}^{1}(\cos \theta) P_{n}^{1}(\cos \theta) \sin \theta d\theta = 0 ; & m \neq n \\ \int_{0}^{\pi} \left[P_{n}^{1}(\cos \theta)\right]^{2} \sin \theta d\theta = \frac{2n(n+1)}{2n+1} ; & m = n \end{cases}$$

$$(4.28)$$

Equation (4.27) then becomes,

$$\int\limits_{0}^{\pi} E_{1\theta}(a,\theta) P_{m}^{1}(\cos \theta) \sin \theta d\theta = -\frac{j}{\omega \epsilon_{i} a \sqrt{a}} \cdot \frac{2m(m+1)}{2m+1}.$$

$$\{A_{m}[mH_{m+1/2}^{(2)}(k_{i}a) - k_{i}aH_{m-1/2}^{(2)}(k_{i}a)\}$$

+ 
$$B_{m}[mH_{m+1/2}^{(1)}(k_{i}a) - k_{i}aH_{m-1/2}^{(1)}(k_{i}a)]$$
 (4.29)

Using Equation (4.25) for the tangential E field on the sphere, the left hand side of Equation (4.29) is evaluated as follows:

$$\int_{0}^{\pi} E_{1\theta}(a,\theta) P_{m}^{1}(\cos \theta) \sin \theta d\theta = \int_{0}^{\pi} \frac{V}{a} \delta(\theta - \pi/2) P_{m}^{1}(\cos \theta) \sin \theta d\theta$$
$$= \frac{V}{a} P_{m}^{1}(0). \tag{4.30}$$

Therefore, Equation (4.29) is finally written as (after some rearrangements and replacing m by n)

$$y_{1n}A_n + y_{2n}B_n = g_nV$$
 (4.31)

where

$$\begin{cases} y_{1n} = nH_{n+1/2}^{(2)}(k_{i}a) - k_{i}aH_{n-1/2}^{(2)}(k_{i}a) \\ y_{2n} = nH_{n+1/2}^{(1)}(k_{i}a) - k_{i}aH_{n-1/2}^{(1)}(k_{i}a) \\ g_{n} = j\omega\epsilon_{i}\sqrt{a} P_{n}^{1}(0) \cdot \frac{(2n+1)}{2n(n+1)} \end{cases}$$

$$(4.32)$$

Note that, since  $P_n^1(0)$  is zero for all even integers (see for example Reference 7), we have

$$n = 1, 3, 5, 7, \dots$$
 odd integers only (4.33)

Equation (4.31) is written in a form suitable for matrix solution which will be used to find the impedance expression.

The other boundary conditions are stated by the following relations:

$$\begin{cases} E_{1\theta}(b,\theta) = E_{2\theta}(b,\theta), & E_{2\theta}(c,\theta) = E_{3\theta}(c,\theta) \\ H_{1\phi}(b,\theta) = H_{2\phi}(b,\theta), & H_{2\phi}(c,\theta) = H_{3\phi}(c,\theta) \end{cases}$$
(4.34)

Note that these relations are valid for all values of the angle  $\theta$ . Using the expressions for the tangential components of fields derived in the previous section, we write down the following equations:

# at r = b;

$$y_{3n}^{A}_{n} + y_{4n}^{B}_{n} + y_{5n}^{C}_{n} + y_{6n}^{D}_{n} = 0$$
 (4.35)

and

$$y_{7n}A_n + y_{8n}B_n + y_{9n}C_n + y_{10n}D_n = 0$$
 (4.36)

where

$$\begin{cases} y_{3n} = \xi/\epsilon_{i} \left[ nH_{n+1/2}^{(2)}(k_{i}b) - k_{i}bH_{n-1/2}^{(2)}(k_{i}b) \right] \\ y_{4n} = \xi/\epsilon_{i} \left[ nH_{n+1/2}^{(1)}(k_{i}b) - k_{i}bH_{n-1/2}^{(1)}(k_{i}b) \right] \\ y_{5n} = -\left[ nH_{n+1/2}^{(2)}(kb) - kbH_{n-1/2}^{(2)}(kb) \right] \\ y_{6n} = -\left[ nH_{n+1/2}^{(1)}(kb) - kbH_{n-1/2}^{(1)}(kb) \right] \\ y_{7n} = H_{n+1/2}^{(2)}(k_{i}b) \\ y_{8n} = H_{n+1/2}^{(1)}(k_{i}b) \\ y_{9n} = H_{n+1/2}^{(2)}(kb) \\ y_{10n} = H_{n+1/2}^{(1)}(kb) \end{cases}$$

Equation (4.35) results from the continuity of  $E_{\theta}$  and Equation (4.36) from the continuity of  $H_{\rho}$ , at the boundary r=b.

## at r = c;

$$y_{11n}C_n + y_{12n}D_n + y_{13n}E_n = 0$$
 (4.38)

and

$$y_{14n}^{C_n} + y_{15n}^{D_n} + y_{16n}^{E_n} = 0$$
 (4.39)

with

$$\begin{cases} y_{11n} = -\left[nH_{n+1/2}^{(2)}(kc) - kcH_{n-1/2}^{(2)}(kc)\right] \\ y_{12n} = -\left[nH_{n+1/2}^{(1)}(kc) - kcH_{n-1/2}^{(1)}(kc)\right] \\ y_{13n} = \xi/\epsilon_0 \left[nH_{n+1/2}^{(2)}(k_0c) - k_0cH_{n-1/2}^{(2)}(k_0c)\right] \\ y_{14n} = H_{n+1/2}^{(2)}(kc) \\ y_{15n} = H_{n+1/2}^{(1)}(kc) \\ y_{16n} = -H_{n+1/2}^{(2)}(k_0c) \end{cases}$$

$$(4.40)$$

This completes the application of the boundary conditions. In the next section, we put the equations derived in this section into a more compact form.

# Matrix Equation Formulation of the Input Impedance Expression

Equations found in the last section relating the unknown amplitude coefficients A, B, C, D, and E, can be put in a matrix form as follows:

$$YX = GV (4.41)$$

where V is the (scalar) applied voltage and

$$Y = \begin{bmatrix} y_{1n} & y_{2n} & 0 & 0 & 0 \\ y_{3n} & y_{4n} & y_{5n} & y_{6n} & 0 \\ y_{7n} & y_{8n} & y_{9n} & y_{10n} & 0 \\ 0 & 0 & y_{11n} & y_{12n} & y_{13n} \\ 0 & 0 & y_{14n} & y_{15n} & y_{16n} \end{bmatrix}, \quad X = \begin{bmatrix} A_n \\ B_n \\ C_n \\ D_n \\ E_n \end{bmatrix}$$
(4.42)

The elements of the coefficient matrix Y are defined in Equations (4.32), (4.37) and (4.40) of the last section.

The column vector G has only the first non zero element and is given by

$$G = \begin{bmatrix} g_n \\ 0 \\ 0 \\ 0 \\ 0 \end{bmatrix} \tag{4.43}$$

with  $g_n$  as given in Equation (4.32).

The solution to the matrix equation (4.41) is found by inverting the known matrix Y,

$$X = Y^{-1}GV (4.44)$$

where  $YY^{-1} = I$  and I is the  $5 \times 5$  unit matrix. We are mainly interested in solving for the current which flows on the surface of the sphere. This is related to the solutions X of the equation (4.44) as is seen from the following discussion.

The surface current density at any point on the surface of the metallic sphere of radius r=a is given by

$$\vec{K}(\theta) = \hat{n} \times \vec{H}_1(a,\theta)$$
 (4.45)

where  $\hat{n}$  is the unit outward normal vector to the surface of the sphere or  $\hat{n} = \hat{r}$ ; a unit vector in r direction of the spherical coordinate system as shown previously in Figure 4.1. Based on Equation (4.45), we compute the current which flows on the surface of the antenna as

$$I(\theta) = (2\pi a \sin \theta) K_{\theta}(\theta) \quad (amp.) \tag{4.46}$$

Or, substituting for  $K_{\rho}(\theta)$  from Equation (4.45),

$$I(\theta) = -2\pi a \sin \theta H_{1_0}(a,\theta) \qquad (4.47)$$

Now, the input current, which is defined as the current flowing from the input terminal  $\theta=\pi/2-\theta_0$  toward the top of the spherical antenna (see Figure 4.2), is given by

$$I = -I(\theta = \pi/2 - \theta_0)$$
 (4.48)

which, by virtue of Equation (4.47), becomes

$$I = 2\pi a \cos \theta_0 H_{1_0} (a, \pi/2 - \theta_0)$$
 (4.49)

Or, using  $H_{\mathbf{l}_0}$   $(\mathbf{r},\theta)$  as given in Equation (4.14), we get

 $I = 2\pi\sqrt{a} \cos \theta_0 \sum_{n=1}^{\infty} P_n^1 (\sin \theta_0) [A_n^H_{n+1/2}^{(2)}(k_i^a)]$ 

+ 
$$B_n H_{n+1/2}^{(1)}(k_i a)$$
] . (4.50)

From Equation (4.41), we see that all coefficients  $\mathbf{A}_n$ ,  $\mathbf{B}_n$ ,  $\mathbf{C}_n$ ,  $\mathbf{D}_n$  and  $\mathbf{E}_n$  are proportional to the applied voltage V. Therefore defining,

$$a_n = \frac{A_n}{V}, b_n = \frac{B_n}{V}, \dots \text{ etc.}$$
 (4.51)

we write Equation (4.50) as

 $I = 2\pi\sqrt{a} \cos \theta_0 V \sum_{n=1}^{\infty} P_n^1(\sin \theta_0) \left[a_n H_{n+1/2}^{(2)}(k_i a)\right]$ 

+ 
$$b_n H_{n+1/2}^{(1)}(k_i a)$$
], (4.52)

where now  $a_n$  and  $b_n$  are solutions of

$$YX' = G (4.53)$$

with Y and G as given previously and

$$X' = \begin{bmatrix} a_n \\ b_n \\ c_n \\ d_n \\ e_n \end{bmatrix}$$

$$(4.54)$$

is our unknown column vector.

Equation (4.52) is the desired relation. From this equation, input admittance of the coated spherical

antenna in a finite conducting body shown in Figure 4.1, is found to be

$$Y_{IN} = \frac{I}{V} = 2\pi\sqrt{a} \cos \theta_0 \sum_{n=1}^{\infty} P_n^1(\sin \theta_0) [a_n H_{n+1/2}^{(2)}(k_i a) + b_n H_{n+1/2}^{(1)}(k_i a)]$$

$$(4.55)$$

One may change the index of summation by letting n = 2m+1 and let m run from 0 to  $\infty$ ;

$$Y_{IN} = 2\pi\sqrt{a} \cos \theta_0 \sum_{m=0}^{\infty} P_{2m+1}^{1} (\sin \theta_0) [a_{2m+1}^{2m+1} H_{2m+3/2}^{(2)} (k_i a)] + b_{2m+1}^{1} H_{2m+3/2}^{(1)} (k_i a)]$$
(4.56)

The input impedance is the inverse of the input admittance;

$$z_{IN} = (Y_{IN})^{-1}$$
 (4.57)

This completes the derivation of the input impedance of our spherical antenna as shown schematically in Figure 4.1. The final solution, of course, is obtained by inverting the matrix Y of Equation (4.53).

Although the solution obtained through the matrix operations is mathematically sound and rigorous, final results must be obtained with a computer which evaluates the matrix elements of the matrix Y in Equation (4.53) and inverts the matrix. A computer program was written to solve the problem and find the input impedance.

However, after some computations, it was found that it is difficult to compute the higher order modes or terms of the admittance expression, Equation (4.55). Specifically, it was found that, in some cases the solution blew up and inaccurate results were obtained through the matrix inversion. After checking all the steps involved and printing some of the matrix elements, it was discovered that the matrix Y was, in some cases, nearly singular (or the determinant was almost zero). Physically, in general, all modes are excited and there is a solution for each odd integer n. The problem may be due to the fact that since arguments of the Hankel functions involved are very small, and it is difficult for the computer to handle an operation involving these functions. For example, in Table 4.1, we show the values computed for  $H_{n+1/2}^{(2)}(k_{i}a)$  for a case where a = 1 cm, f = 600 MHZ (free space wavelength of 50 cm) and  $\epsilon_i$  = 2.1  $\epsilon_0$ ,  $\epsilon_0$ being the free space permittivity. These values are needed when we want to compute the first 20 terms of the series for input admittance. Table 4.2 shows the values  $H_{n+1/2}^{(2)}$  (kb) when  $\varepsilon_r = 70$ ,  $\sigma = 1 \text{ U/m}$  and b = 1.5In this case the arguments of the Hankel function are complex.

As can be seen from Tables 4.1 and 4.2, the Hankel functions needed for the input impedance computation are such that we are dealing with either very large numbers

Table 4.1. Values of Hankel functions  $H_{n+1/2}^{(2)}(k_i a)$  when a = 1 cm, f = 600 MHz  $(a/\lambda_0 = 0.02;$   $\lambda_0$  is free space wavelength) and  $\epsilon_i = 2.1 \; \epsilon_0; \; \epsilon_0$  is free space permittivity.

		777		
n	$H_{n+1/2}^{(2)}(k_{i}a)$			
	REAL	IMAGINARY		
1	.20625 × 10 <sup>-1</sup>	.10423 × 10 <sup>2</sup>		
3	$.19603 \times 10^{-4}$	.46462 × 10 <sup>4</sup>		
5	.65809 × 10 <sup>-8</sup>	.87992 × 10 <sup>7</sup>		
7	$.11213 \times 10^{-11}$	.37860 × 10 <sup>11</sup>		
9	$.11534 \times 10^{-15}$	.29055 × 10 <sup>15</sup>		
11	$.79330 \times 10^{-20}$	.34895 × 10 <sup>19</sup>		
13	$.39042 \times 10^{-24}$	.60397 × 10 <sup>23</sup>		
15	$.14426 \times 10^{-28}$	$.14235 \times 10^{28}$		
17	$.41491 \times 10^{-33}$	.43840 × 10 <sup>32</sup>		
19	$.95514 \times 10^{-38}$	.17090 × 10 <sup>37</sup>		
21	$.17996 \times 10^{-42}$	.82270 × 10 <sup>41</sup>		
23	$.28264 \times 10^{-47}$	.47923 × 10 <sup>46</sup>		
25	$.37570 \times 10^{-52}$	.33225 × 10 <sup>51</sup>		
27	$.42813 \times 10^{-57}$	.27036 × 10 <sup>56</sup>		
29	$.42287 \times 10^{-62}$	.25516 × 10 <sup>61</sup>		
31	$.36551 \times 10^{-67}$	.27646 × 10 <sup>66</sup>		
33	$.27880 \times 10^{-72}$	.34082 × 10 <sup>71</sup>		
35	$.18903 \times 10^{-77}$	.47434 × 10 <sup>76</sup>		
37	$.11468 \times 10^{-82}$	.74013 × 10 <sup>81</sup>		
39	.62626 × 10 <sup>-88</sup>	.12867 × 10 <sup>87</sup>		

Table 4.2. Values of Hankel function with complex argument,  $H_{n+1/2}^{(2)}(kb)$ , when b=1.5 cm, f=600 MHz  $(a/\lambda_0=0.03)$ ,  $k=\omega\sqrt{\mu_0\xi}$ ;  $\xi=\epsilon-$  j  $\frac{\sigma}{\omega}$ ;  $\epsilon=70$   $\epsilon_0$ ,  $\sigma=1$   $\frac{\upsilon}{m}$ .

n	REAL PART	IMAGINARY PART
1	.23754 × 10 <sup>0</sup>	.51620 × 10 <sup>0</sup>
3	$14714 \times 10^{1}$	$.22733 \times 10^{1}$
5	48549 × 10 <sup>2</sup>	$.27834 \times 10^{2}$
7	28124 × 10 <sup>4</sup>	.27098 × 10 <sup>3</sup>
9	24679 × 10 <sup>6</sup>	81352 × 10 <sup>5</sup>
11	28138 × 10 <sup>8</sup>	24123 × 10 <sup>8</sup>
13	33292 × 10 <sup>10</sup>	71960 × 10 <sup>10</sup>
15	59027 × 10 <sup>11</sup>	$22745 \times 10^{13}$
17	.31749 × 10 <sup>15</sup>	79329 × 10 <sup>15</sup>
19	.28798 × 10 <sup>18</sup>	28714 × 10 <sup>18</sup>
21	.22228 × 10 <sup>21</sup>	$88300 \times 10^{20}$
23	.17026 × 10 <sup>24</sup>	.46718 × 10 <sup>22</sup>
25	.13111 × 10 <sup>27</sup>	.60576 × 10 <sup>26</sup>
27	.96185 × 10 <sup>29</sup>	.10688 × 10 <sup>30</sup>
29	.53449 × 10 <sup>32</sup>	$.15724 \times 10^{33}$
31	17019 × 10 <sup>35</sup>	.21959 × 10 <sup>36</sup>
33	15418 × 10 <sup>39</sup>	.29450 × 10 <sup>39</sup>
35	43918 × 10 <sup>42</sup>	.35780 × 10 <sup>42</sup>
37	10406 × 10 <sup>46</sup>	.29790 × 10 <sup>45</sup>
39	22865 × 10 <sup>49</sup>	28955 × 10 <sup>48</sup>

or very small ones. Now, due to the fact that the computer carries only a finite number of significant figures (e.g. in CDC 6500 system 30 for double precision arithmetic), this will lead to errors in evaluating the matrix elements of the matrix Y because of the roundoffs. In fact, after printing some of the elements out, it is found that, for example, two rows of the matrix are identical while theoretically they are always different. This computational error makes the matrix nearly singular and therefore, the results obtainable from this method were inaccurate.

It is true that for small antennas only the first few terms are needed for the real part of the input admittance (i.e. the conductance). In fact the infinite series of the real part of  $Y_{IN}$  in Equation (4.63) converges while the series for the imaginary part (the reactance) converges only for the assumption of finite gap (i.e.  $\theta_0 \neq 0^{\circ}$ ). This is shown more carefully in Appendix A.

To solve the problem of computational error, we used a different approach in solving for the unknown amplitudes of the EM fields components in the three different regions. This method uses the formulation used in the transmission line theory and is described in the next section.

## 4.5. Transmission Line Approach

The method discussed in this section, employs the definitions of the reflection and transmission coefficients as used in the transmission line theory.

Following Stratton [8], we write the solutions of field components in the three regions as

Region I (a  $\leq$  r  $\leq$  b);

$$H_{\omega_1}(r,\theta) = \sum_{n=1}^{\infty} P_n^1(\cos \theta) [H_{\omega_{1n}}^+(r) + H_{\omega_{1n}}^-(r)]$$
 (4.58)

where

$$H_{\varphi}^{-}(r) = \frac{A_{n}H_{n+1/2}^{(1)}(k_{i}r)}{\sqrt{k_{i}r}},$$

$$H_{\varphi}^{+}(r) = \frac{B_{n}H_{n+1/2}^{(2)}(k_{i}r)}{\sqrt{k_{i}r}}$$
(4.59)

 $\mathbf{A}_{\mathbf{n}}$  and  $\mathbf{B}_{\mathbf{n}}$  are the two new unknown amplitude coefficients (note that they are different from those used in the previous section). Other notations have been introduced in the previous sections.

Physically  $H_{\phi}^{\dagger}$  (r) and  $H_{\phi}^{\dagger}$  (n) represent, respectively, outgoing and inward spherical waves which are present in this region. The tangential component of the  $\vec{E}$  field is written as

$$E_{\theta 1}(r,\theta) = \sum_{n=1}^{\infty} P_{n}^{1}(\cos \theta) [Z_{1n}^{+}(r)H_{\varphi 1n}^{+}(r) - Z_{1n}^{-}(r)H_{\varphi 1n}^{-}(r)]$$
(4.60)

where TM mode wave impedances are defined by

$$\begin{cases} z_{1n}^{+}(r) = j\eta_{1} \left[ \frac{H_{n-1/2}^{(2)}(k_{i}r)}{H_{n+1/2}^{(2)}(k_{i}r)} - \frac{n}{k_{i}r} \right] \\ z_{1n}^{-}(r) = -j\eta_{1} \left[ \frac{H_{n-1/2}^{(1)}(k_{i}r)}{H_{n+1/2}^{(1)}(k_{i}r)} - \frac{n}{k_{i}r} \right] \end{cases}$$

$$(4.61)$$

with  $\eta_1 = \sqrt{\frac{\mu_0}{\epsilon_i}}$  being intrinsic impedance of the dielectric coating medium.

Region II (b  $\leq$  r  $\leq$  c): In this region the wave-number is complex and tangential field components can be written similar to that in region I as

$$H_{\varphi_{2}}(r,\theta) = \sum_{n=1}^{\infty} P_{n}^{1}(\cos \theta) [H_{\varphi_{2n}}^{+}(r) + H_{\varphi_{2n}}^{-}(r)]$$
 (4.62)

and

$$E_{\theta 2}(r,\theta) = \sum_{n=1}^{\infty} P_{n}^{1}(\cos \theta) [Z_{2n}^{+}(r)H_{\varphi 2n}^{+}(r) - Z_{2n}^{-}(r)H_{\varphi 2n}^{-}(r)]$$

$$(4.63)$$

where

$$H_{\varphi}^{-}(r) \equiv \frac{C_{n}H_{n+1/2}^{(1)}(kr)}{\sqrt{kr}}, H_{\varphi}^{+}(r) \equiv \frac{D_{n}H_{n+1/2}^{(2)}(kr)}{\sqrt{kr}}$$
(4.64)

$$\begin{cases}
z_{2n}^{+}(r) = j\eta_{2} \left[ \frac{H_{n-1/2}^{(2)}(kr)}{H_{n+1/2}^{(2)}(kr)} - \frac{n}{kr} \right] \\
z_{2n}^{-}(r) = -j\eta_{2} \left[ \frac{H_{n-1/2}^{(1)}(kr)}{H_{n+1/2}^{(1)}(kr)} - \frac{n}{kr} \right]
\end{cases} (4.65)$$

where TM mode wave impedances are defined by

$$\begin{cases} z_{1n}^{+}(r) = j\eta_{1} \left[ \frac{H_{n-1/2}^{(2)}(k_{i}r)}{H_{n+1/2}^{(2)}(k_{i}r)} - \frac{n}{k_{i}r} \right] \\ z_{1n}^{-}(r) = -j\eta_{1} \left[ \frac{H_{n-1/2}^{(1)}(k_{i}r)}{H_{n+1/2}^{(1)}(k_{i}r)} - \frac{n}{k_{i}r} \right] \end{cases}$$

$$(4.61)$$

with  $\eta_1 = \sqrt{\frac{\mu_0}{\epsilon_i}}$  being intrinsic impedance of the dielectric coating medium.

Region II (b  $\leq$  r  $\leq$  c): In this region the wave-number is complex and tangential field components can be written similar to that in region I as

$$H_{\varphi_2}(r,\theta) = \sum_{n=1}^{\infty} P_n^1(\cos\theta) [H_{\varphi_{2n}}^+(r) + H_{\varphi_{2n}}^-(r)]$$
 (4.62)

and

$$E_{\theta 2}(r,\theta) = \sum_{n=1}^{\infty} P_n^1(\cos \theta) [Z_{2n}^+(r)H_{\phi 2n}^+(r) - Z_{2n}^-(r)H_{\omega 2n}^-(r)]$$
(4.63)

where

$$H_{\varphi}^{-}(r) \equiv \frac{C_n H_{n+1/2}^{(1)}(kr)}{\sqrt{kr}}, H_{\varphi}^{+}(r) \equiv \frac{D_n H_{n+1/2}^{(2)}(kr)}{\sqrt{kr}}$$
 (4.64)

$$\begin{cases} z_{2n}^{+}(r) = j\eta_{2} \left[ \frac{H_{n-1/2}^{(2)}(kr)}{H_{n+1/2}^{(2)}(kr)} - \frac{n}{kr} \right] \\ z_{2n}^{-}(r) = -j\eta_{2} \left[ \frac{H_{n-1/2}^{(1)}(kr)}{H_{n+1/2}^{(1)}(kr)} - \frac{n}{kr} \right] \end{cases}$$
(4.65)

 $\eta_2=\sqrt{\frac{\mu_0}{\xi}}$  is the complex intrinsic impedance of the conducting body.  $k^2=\omega^2\mu_0\xi;~\xi=\epsilon-j\frac{\sigma}{\omega}$  were defined previously.  $C_n$  and  $D_n$  are two more unknown amplitude coefficients.

Region III  $(r \ge c)$ : In this free space region we can write the field components as

$$H_{\omega 3}(r,\theta) = \sum_{n=1}^{\infty} P_n^1(\cos \theta) H_{\omega 3n}^+(r)$$
 (4.66)

and

$$E_{\theta 3}(r,\theta) = \sum_{n=1}^{\infty} P_n^1(\cos \theta) Z_{3n}^+(r) H_{\phi 3n}^+(r)$$
 (4.67)

Note that in this region only an outgoing wave is expected, and

$$H_{\varphi}^{+}_{3n}(r) \equiv \frac{E_{n}^{H(2)}_{n+1/2}(k_{0}r)}{\sqrt{k_{0}r}}$$
 (4.68)

The wave impedance is

$$z_{3n}^{+}(r) = j\eta_{0} \left[ \frac{H_{n-1/2}^{(2)}(k_{0}r)}{H_{n+1/2}^{(2)}(k_{0}r)} - \frac{n}{k_{0}r} \right]$$
 (4.69)

where  $\eta_0 = \sqrt{\frac{\mu_0}{\epsilon_0}} = 377 \ \Omega$  is the intrinsic impedance of the free space.

Again we have introduced five unknown coefficients  $A_n$ ,  $B_n$ ,  $C_n$ ,  $D_n$  and  $E_n$ . However, now they will be eliminated by using transmission line definitions.

First, we note that since the Associated Legendre functions form a complete set, we can expand the tangential electric field on the surface of the metallic sphere in terms of these functions as

$$E_{\theta 1}(a,\theta) = \sum_{n=1}^{\infty} P_n^1(\cos \theta) F_n$$
 (4.70)

where  $F_n$  is an unknown expansion coefficient. To evaluate  $F_n$ , we use the boundary conditions of Equation (4.25) and the orthogonality of the functions  $P_n^1(\cos \theta)$  as shown in Equation (4.28). One gets

$$F_{n} = \frac{V}{a} P_{n}^{1}(0) \cdot \frac{(2n+1)}{2n(n+1)}$$
 (4.71)

where, again, n denotes odd integers only. Also, from Equation (4.60) we have another expression for  $E_{\theta\,l}\,(a,\theta)\,, \ \text{equating these two expressions we have}$ 

$$F_n = Z_{1n}^+(a)H_{\varphi 1n}^+(a) - Z_{1n}^-(a)H_{\varphi 1n}^-(a)$$
 (4.72)

where  $\mathbf{F}_{\mathbf{n}}$  is given in Equation (4.71). We will use Equation (4.72) later on. The boundary conditions on the tangential field components are used to get the following equations:

$$E_{\theta 1} = E_{\theta 2} \quad \text{at} \quad r = b;$$

$$z_{1n}^{+}(b)H_{\phi 1n}^{+}(b) - z_{1n}^{-}(b)H_{\phi 1n}^{-}(b)$$

$$= z_{2n}^{+}(b)H_{\phi 2n}^{+}(b) - z_{2n}^{-}(b)H_{\phi 2n}^{-}(b) \qquad (4.73)$$

$$H_{\varphi 1} = H_{\varphi 2}$$
 at  $r = b$ ;

$$H_{\varphi}^{+}\ln(b) + H_{\varphi}^{-}\ln(b) = H_{\varphi}^{+}\ln(b) + H_{\varphi}^{-}\ln(b)$$
 (4.74)

$$E_{\theta 2} = E_{\theta 3}$$
 at  $r = c$ ;

$$z_{2n}^{+}(c)H_{02n}^{+}(c) - z_{2n}^{-}(c)H_{02n}^{-}(c) = z_{3n}^{+}(c)H_{03n}^{+}(c)$$
 (4.75)

$$H_{02} = H_{03}$$
 at  $r = c$ ;

$$H_{\varphi}^{+}(c) + H_{\varphi}^{-}(c) = H_{\varphi}^{+}(c).$$
 (4.76)

To solve Equations (4.73) to (4.75), we introduce new unknowns as follows:

At r = b, the reflection and transmission coefficients are defined respectively as

$$R_{ln}(b) \equiv \frac{\prod_{\phi ln}^{-}(b)}{\prod_{\phi ln}^{+}(b)}, T_{ln}(b) \equiv \frac{\prod_{\phi ln}^{+}(b)}{\prod_{\phi ln}^{+}(b)}$$
 (4.77)

similarly at r = c;

$$R_{2n}(c) \equiv \frac{H_{\varphi 2n}(c)}{H_{z 2n}(c)}, T_{2n}(c) \equiv \frac{H_{\varphi 3n}(c)}{H_{z 2n}(c)}$$
 (4.78)

Note that these are the current coefficients in analogy with the transmission line theory. For example,  $R_{1n}(b)$  is the ratio of the reflected wave  $H_{\phi 1n}^{-}(b)$  to the incident wave  $H_{\phi 1n}^{+}(b)$  at r=b boundary. We also define a reflection coefficient looking from region 2 to region 1 of Figure 4.1 at r=b as

$$R_{2n}(b) \equiv \frac{H_{\varphi}^{+}(b)}{H_{\varphi}^{-}(b)}$$
 (4.79)

Finally, a reflection coefficient at r = a is defined as

$$R_{ln}(a) = \frac{H_{\varphi ln}^{+}(a)}{H_{\varphi ln}^{-}(a)}$$
 (4.80)

Of course, these coefficients are unknown since the amplitude coefficients  $A_n$ ,  $B_n$ ,  $C_n$ ,  $D_n$  and  $E_n$  are hidden in spherical waves  $H_{\phi}^+$  (b), etc. But the advantage is that the products of reflection coefficients are known. From (4.80) and (4.77) we have

$$R_{1n}(a) \cdot R_{1n}(b) = \frac{H_{n+1/2}^{(2)}(k_i a) H_{n+1/2}^{(1)}(k_i b)}{H_{n+1/2}^{(1)}(k_i a) H_{n+1/2}^{(2)}(k_i b)} = \frac{1}{K_{1n}(a,b)}$$
(4.81)

Similarly we can write

$$R_{2n}(b) \cdot R_{2n}(c) = \frac{H_{n+1/2}^{(2)}(kb)H_{n+1/2}^{(1)}(kc)}{H_{n+1/2}^{(1)}(kb)H_{n+1,2}^{(2)}(kc)} = \frac{1}{K_{2n}(b,c)}$$
(4.82)

If we use Equation (4.78) in Equations (4.75) and (4.76), we can then write

$$\begin{cases} z_{3n}^{+}(c) \cdot r_{2n}(c) = z_{2n}^{+}(c) - z_{2n}^{-}(c) R_{2n}(c) \\ r_{2n}(c) = 1 + R_{2n}(c) \end{cases}$$
(4.83)

From which we solve for  $R_{2n}(c)$ :

$$R_{2n}(c) = \frac{z_{2n}^{+}(c) - z_{3n}^{+}(c)}{z_{2n}^{-}(c) + z_{3n}^{+}(c)}$$
(4.84)

Equations (4.73) and (4.74) can also be written as

$$\begin{cases} z_{1n}^{+}(b) \cdot \frac{1}{T_{1n}(b)} - z_{1n}^{-}(b) \frac{R_{1n}(b)}{T_{1n}(b)} \\ = z_{2n}^{+}(b) - z_{2n}^{-}(b) \cdot \frac{1}{R_{2n}(b)} \\ 1 + R_{1n}(b) = T_{1n}(b) + \frac{T_{1n}(b)}{R_{2n}(b)} \end{cases}$$

$$(4.85)$$

From which one solves for the key quantity  $R_{ln}(b)$ :

$$R_{1n}(b) = \frac{z_{1n}^{+}(b) - z_{2n}^{+}(b) \cdot Q}{z_{1n}^{-}(b) + z_{2n}^{+}(b) \cdot Q}$$
(4.86)

with

$$Q = \frac{1 - K_{2n}(b,c)R_{2n}(c)Z_{2n}(b)/Z_{2n}^{+}(b)}{1 + K_{2n}(b,c)R_{2n}(c)}$$
(4.87)

Note that Q is now a known complex quantity.

To find an expression for the magnetic field on the surface of the spherical antenna, we start from Equation (4.72) to write

$$H_{\varphi}^{+}$$
ln(a) =  $\frac{F_{n}}{z_{ln}^{+}(a) - z_{ln}^{-}(a) \cdot \frac{1}{R_{ln}(a)}}$  (4.88)

or, since  $F_n$  is already known

$$H_{\varphi \ln}^{+}(a) = \frac{V/a \ P_{n}^{1}(0) \cdot \frac{2n+1}{2n(n+1)}}{z_{\ln}^{+}(a) - K_{\ln}(a,b) z_{\ln}^{-}(a) R_{\ln}(b)}$$

$$(n = 1, 3, 5, ...)$$
(4.89)

The total input current is given in Equation (4.49). The magnetic field is found from Equation (4.58) to be

$$H_{\varphi 1}(a, \theta = \pi/2 - \theta_0) = \sum_{n=1}^{\infty} H_{\varphi 1n}^{+}(a)[1 + R_{1n}(a)]P_{n}^{1}(\sin \theta_0)$$
(4.90)

With  $H_{\phi ln}^{+}(a)$  from Equation (4.89), we write the total input current, I, as

I = 2πa Cos 
$$\theta_0 \sum_{n=1}^{\infty} \frac{V}{a} P_n^1 (\sin \theta_0) P_n^1 (0) \cdot \frac{2n+1}{2n(n+1)}$$
 • (odd)

$$\cdot \frac{\frac{1 + K_{1n}(a,b) R_{1n}(b)}{z_{1n}^{+}(a) - K_{1n}(a,b) R_{1n}(b) z_{1n}^{-}(a)}}{(4.91)}$$

From which one finds the input admittance as

$$Y_{IN} = \frac{I}{V} = \cos \theta_0 \sum_{n=1}^{\infty} \frac{\pi (2n+1)}{n (n+1)} P_n^1 (\sin \theta_0) P_n^1 (0) \cdot \frac{1 + K_{1n}(a,b) R_{1n}(b)}{Z_{1n}^+(a) - K_{1n}(a,b) R_{1n}(b) Z_{1n}^-(a)}$$
(4.92)

The input impedance is the inverse of  $Y_{IN}$ .  $R_{ln}$  (b) is given in Equation (4.86) and is the most important

quantity to be computed. Note that expression (4.92) is physically more meaningful. For example, if we want to consider the case of a spherical antenna in a free space (a special case of the problem shown in Figure 4.1), we argue that  $R_{1n}$  (b) is zero and from (4.92) we get

$$Y_{IN} = \cos \theta_0 \sum_{n=1}^{\infty} \frac{\pi (2n+1)}{n (n+1)} P_n^1 (\sin \theta_0) P_n^1 (0) \frac{1}{Z_{1n}^+(a)}$$
 (4.93)

where, from Equation (4.61) we have

$$z_{1n}^{+}(a) = j \sqrt{\frac{\mu_0}{\epsilon_0}} \left[ \frac{H_{n-1/2}^{(2)}(k_0 a)}{H_{n+1/2}^{(2)}(k_0 a)} - \frac{n}{k_0 a} \right]$$
 (4.94)

with  $k_0^2 = \omega^2 \mu_0 \epsilon_0$ . For an infinitesimal gap,  $\theta_0 = 0^\circ$ , Equation (4.93) is exactly the same as that found in the literature [6].

The expression for the input admittance (or input impedance) is derived on the assumption of a finite gap as shown in Figure 4.2. However the expressions derived are also valid as  $\theta_0 \to 0^\circ$  or for a zero gap. The question of the convergence of the series expression for the admittance will be addressed in the Appendix A. But at this point it is necessary to mention that for a zero gap assumption the series will diverge [9] and in the computation of the admittance keeping a large number of terms will lead to an inaccurate result.

Based on the expression of Equation (4.92), another computer program was written. Although the same
Hankel function appeared in this expression, we did not
meet the computational difficulty we encountered in the
matrix inversion method discussed in the last section.

This was primarily due to the fact that we now mostly used
Hankel function in ratios and the effect of normalization
took place. Theoretical results of the input impedance
presented in the next section are based on the expression
derived in this section for the input admittance. To check
the validity of the theoretical results a comparison is
made for a special case with a classical theory. Also in
the next chapter we will show experimental evidence which
will verify the accuracy of the results for the input
impedance formulated in this section.

4.6. Some Theoretical Results of the Input Impedance
Computations

In this section, we discuss some numerical results calculated from the Equation (4.92) in the last section.

Basically, we are interested in electrically small spherical antennas and it is desirable to see how the input impedance of an insulated antenna of Figure 4.1 varies as a function of the parameters involved.

To begin with, the accuracy of our computations was checked in a special case of a spherical antenna in

free space. In Figure 4.3, we show the numerical results of the input conductance of an isolated, perfectly conducting sphere in free space calculated based on Equation (4.92). This case has been discussed by Stratton and Chu [10] and the results of Figure 4.3 agrees very well with their computations. A very small value of  $\theta_0$  was used corresponding to their assumption of zero (or infinitesimal) gap.

In order to see the effect of the dimension of the conducting body (or biological body) on the input impedance of the insulated spherical antenna depicted in Figure 4.1, we computed the input impedance as a function of c or the radius of the conducting body. For example, in Figure 4.4, we show the input reactance of a small insulated spherical antenna of radius a = 1 cm as a function of c in centimeters. The frequency of the antenna is 600 MHz and the relative dielectric constant of the insulating coating is  $\varepsilon_{ir} = 2.1$  (e.g. Teflon). The biological body is assumed to be of low loss with  $\sigma = 0.1$  mho/m , its dielectric constant is assumed to be  $\varepsilon_r = 70$ . Note that in general

$$Z_{TN} = R_{TN} + j X_{TN} \quad \text{ohms}$$
 (4.95)

is the input impedance to our spherical antenna. (The antenna is mainly capacitive and, therefore, its reactance is always negative.) However, for the construction of

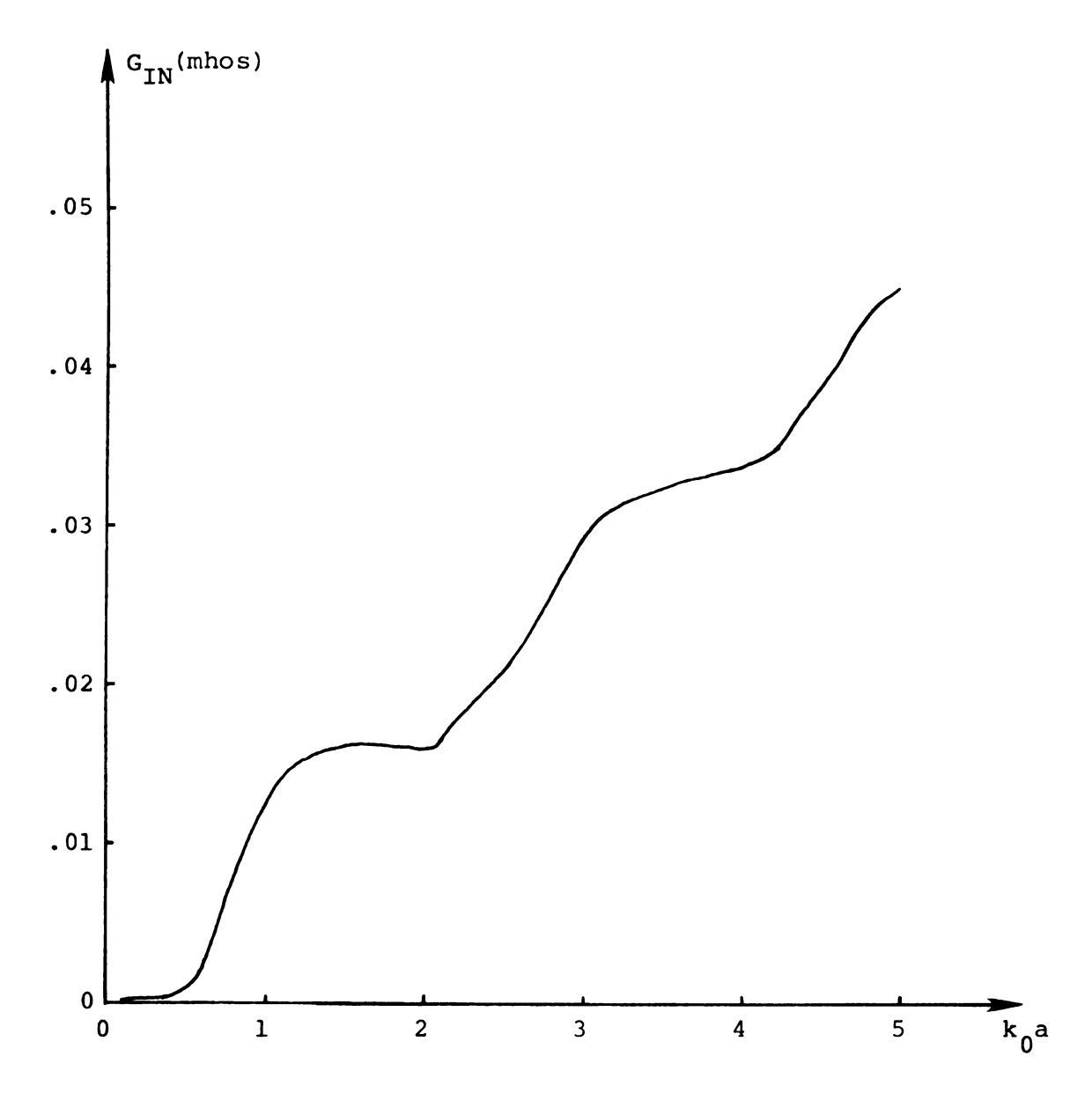


Figure 4.3. Input Conductance (or Radiation Conductance) of a Spherical Antenna in Free Space as a Function of  $k_0 a$ , where a is the Radius of Sphere and  $k_0 = \omega \sqrt{\mu_0 \epsilon_0}$  is the Free Space Wavenumber.

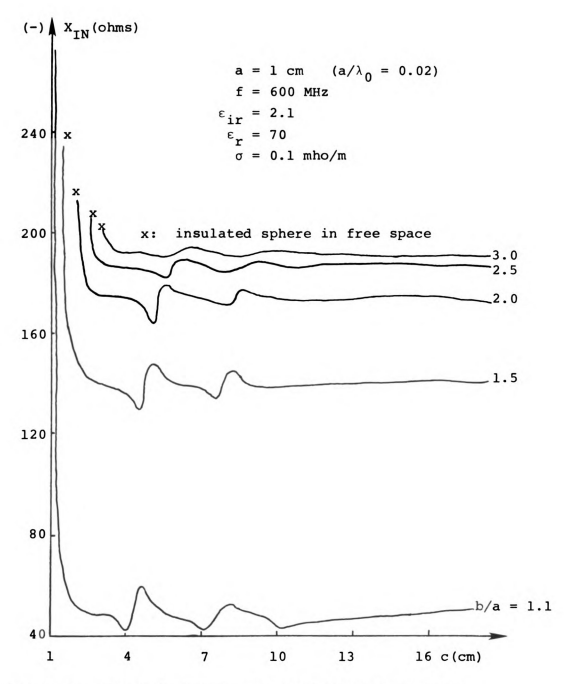


Figure 4.4. Input Reactance of a Small Spherical Probe as a Function of the Radius of the Conducting Sphere.

small probes we are only interested in electrically small antennas, thus, the input resistance  $\ensuremath{\,\text{R}_{\text{TN}}}$  is always small as compared with its reactance  $X_{IN}$ . Therefore, in most cases we only discuss the variation of the input reactance as a function of various parameters. Referring to Figure 4.4, we plot  $X_{TN}$  in ohms for various values of the dielectric coating thickness or the ratio b/a, as a function of c. It can be seen from this figure that for thin coating or for b/a close to unity, there is a considerable variation of the input impedance as the dimension of the conducting body changes. However, as the thickness of the coating or as b/a is increased,  $X_{TN}$ becomes less sensitive to the variation of c. When b/a = 3.0, there is practically no variation in the input impedance as the dimension of the conducting body is changed. This phenomena is desirable, since we want the probe to be insensitive to the relative probe location in the biological body; changing of c corresponds to the changing of the probe location in a conducting body of fixed dimensions.

Another interesting point which can be seen from Figure 4.4 is that for a thin coating (or b/a close to 1), and for small values of c, the input reactance (and hence the input impedance) changes very rapidly and becomes very large as c approaches b. (The limiting

cases of zero coating or c = b are shown by X's in Figure 4.4.) This suggests that if we use a very thin coating, then the field measured by the thinly coated probe at the edge of the biological body may be in error since the input impedance of the probe experiences a rapid change at this region and, thus, the output of the probe may be effected significantly as indicated by Equations (2.8) and (3.25) of the previous chapters. On the other hand, for a thick coating this problem disappears and the input impedance becomes nearly independent of c. This phenomenon has been observed experimentally in the literature [11], and will be explained in Figures 4.5 and 4.6.

Figure 4.5 is the measurement of the electric field induced in a finite conducting body (a box of saline solution of 0.5N) with dimensions of 16 cm × 16 cm × 1 cm. The incident plane wave is incident normally upon the body and is polarized in the x direction. In Figure 4.5, dots are theoretical values and the continuous line is the experimental results. In this experiment, a small dipole probe with a very thin coating was used. As indicated in this figure, the measured values are significantly lower than the theoretical values near the edge of the body. This can be explained as follows. The input impedance of the probe at the body edge becomes very large so that the output voltage of the probe becomes small consequently (see Equations (2.8) and (3.25)). Figure 4.6 shows similar

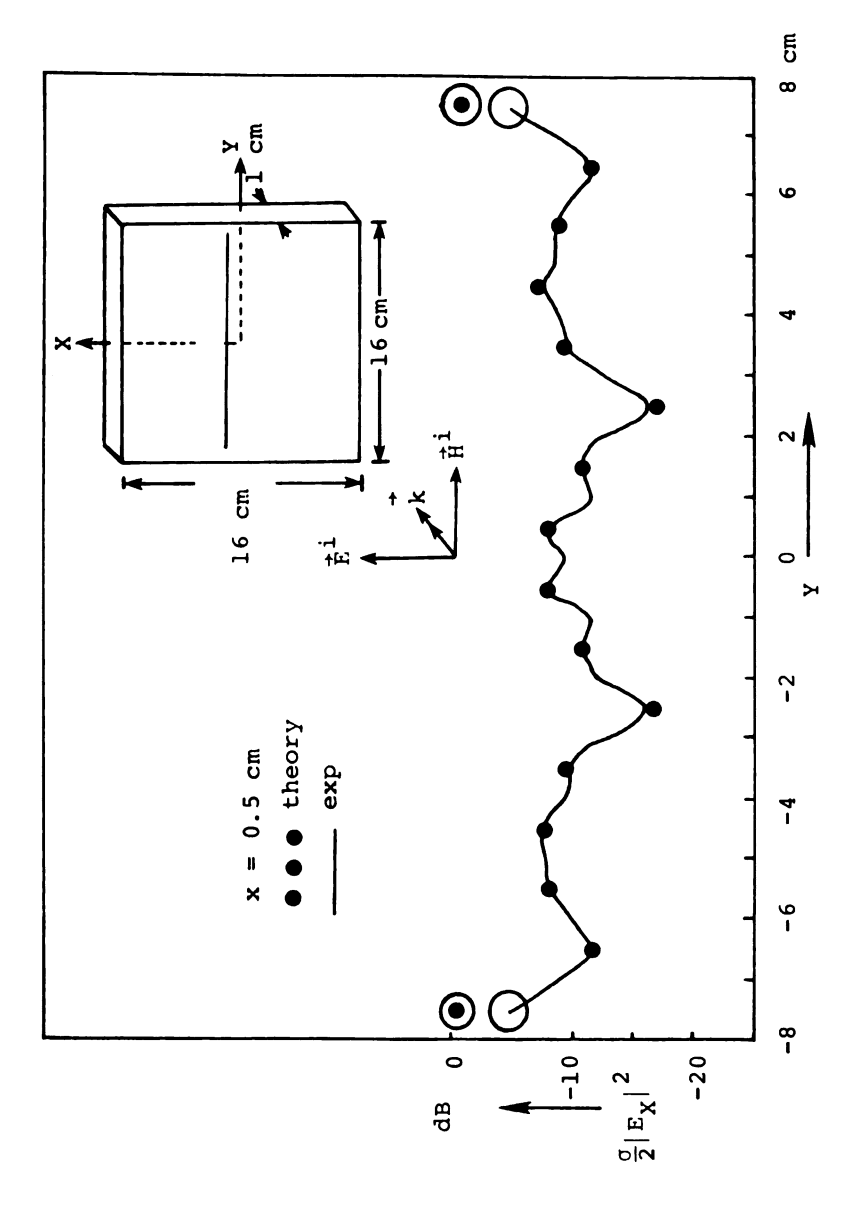


Figure 4.5. Theoretical and Experimental Values of the Dissipated Power Due ', as a Function of Y along x = 0.5 cm. Freq. 2.45 GHz,  $\sigma$  = 5.934 v/m,  $\varepsilon$  = 68.487  $\varepsilon_0$ . Salt Concentration = 0.5 normal.

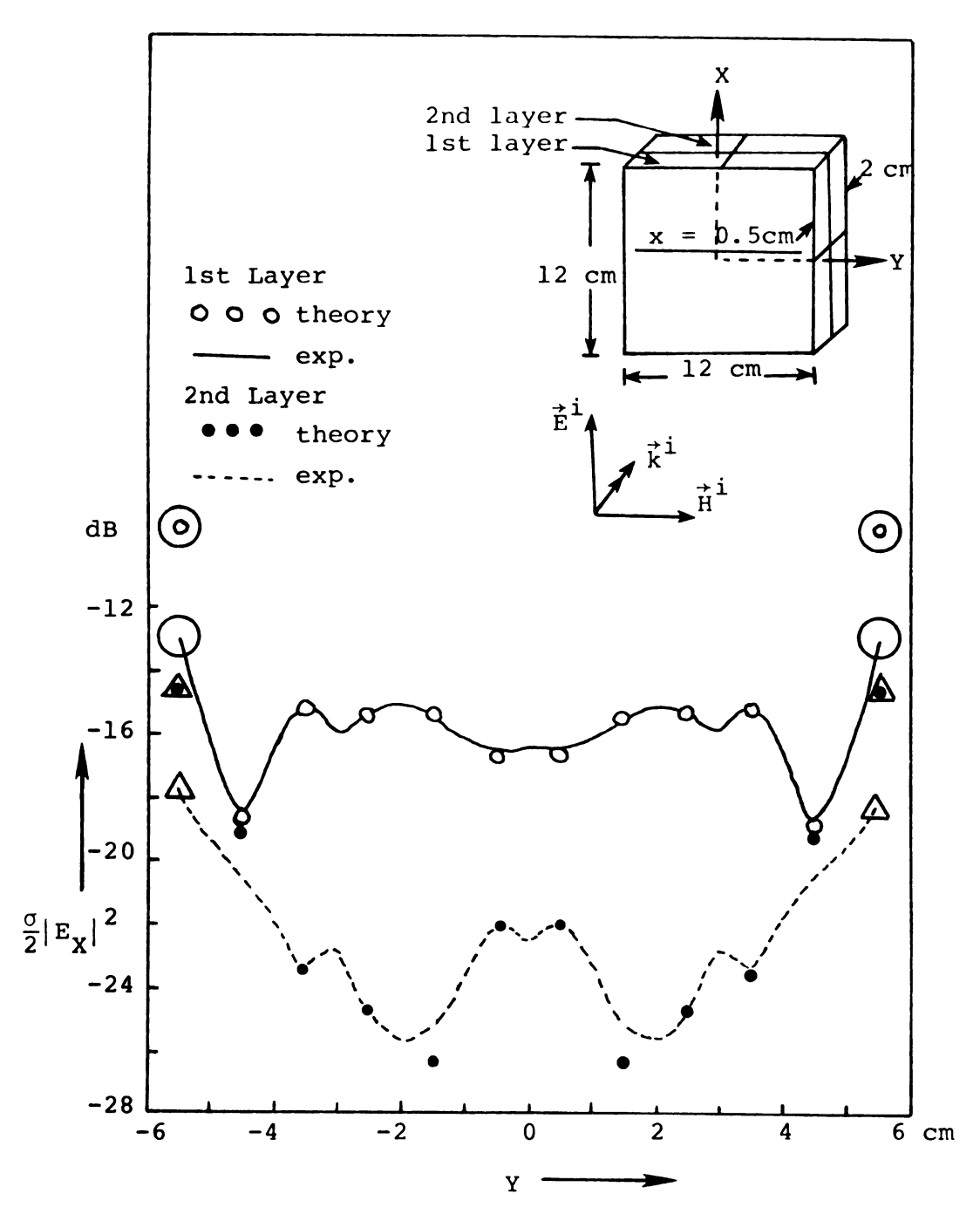


Figure 4.6. Theoretical and Experimental Values of the Dissipated Power Due to  $E_X$ ,  $\frac{\sigma}{2} \left| E_X \right|^2$ , as a Function of Y along X = 0.5 cm. Freq. = 2.45 GHz,  $\sigma$  = 5.934 U/m,  $\epsilon$  = 68.487  $\epsilon_0$ . Salt concentration = 0.5 normal.

measurements in a conducting body with dimensions of 12 cm × 12 cm × 2 cm. The field is measured over two layers as shown. Again, near the body edges, the experiment disagrees with the theory for the same reason mentioned above. (The values near the body edges are shown by circles and triangles.)

To see the effect of the parameters of the conducting body on the input impedance, we evaluated the input reactance as a function of the relative dielectric constant of the medium. For example, in Figure 4.7a, we show the family of curves for the input reactance of a spherical probe. The radius of the sphere is a = 1 cm while the conducting body is of radius c = 10 cm and the frequency of operation is f = 600 MHz (corresponding to the free space wavelength of  $\lambda_0 = 50$  cm). The dielectric coating is assumed to have relative dielectric constant of  $\epsilon_{ir}$  = 2.1 (Teflon) and the conductivity of the body is  $\sigma = 0.01 \text{ mmho/m}$  (very low loss body). The curves are plotted for different thicknesses of the dielectric coating or b/a ranging from 1.0 (bare antenna in the conducting body) to 3.0 (relatively thick coating). The independent variable is  $\epsilon_r$  or the relative dielectric of the conducting body.

As can be seen from Figure 4.7a, for thin coatings, there is a considerable amount of variation of the input ractance as  $\varepsilon_r$  varies while, for thicker coatings, the

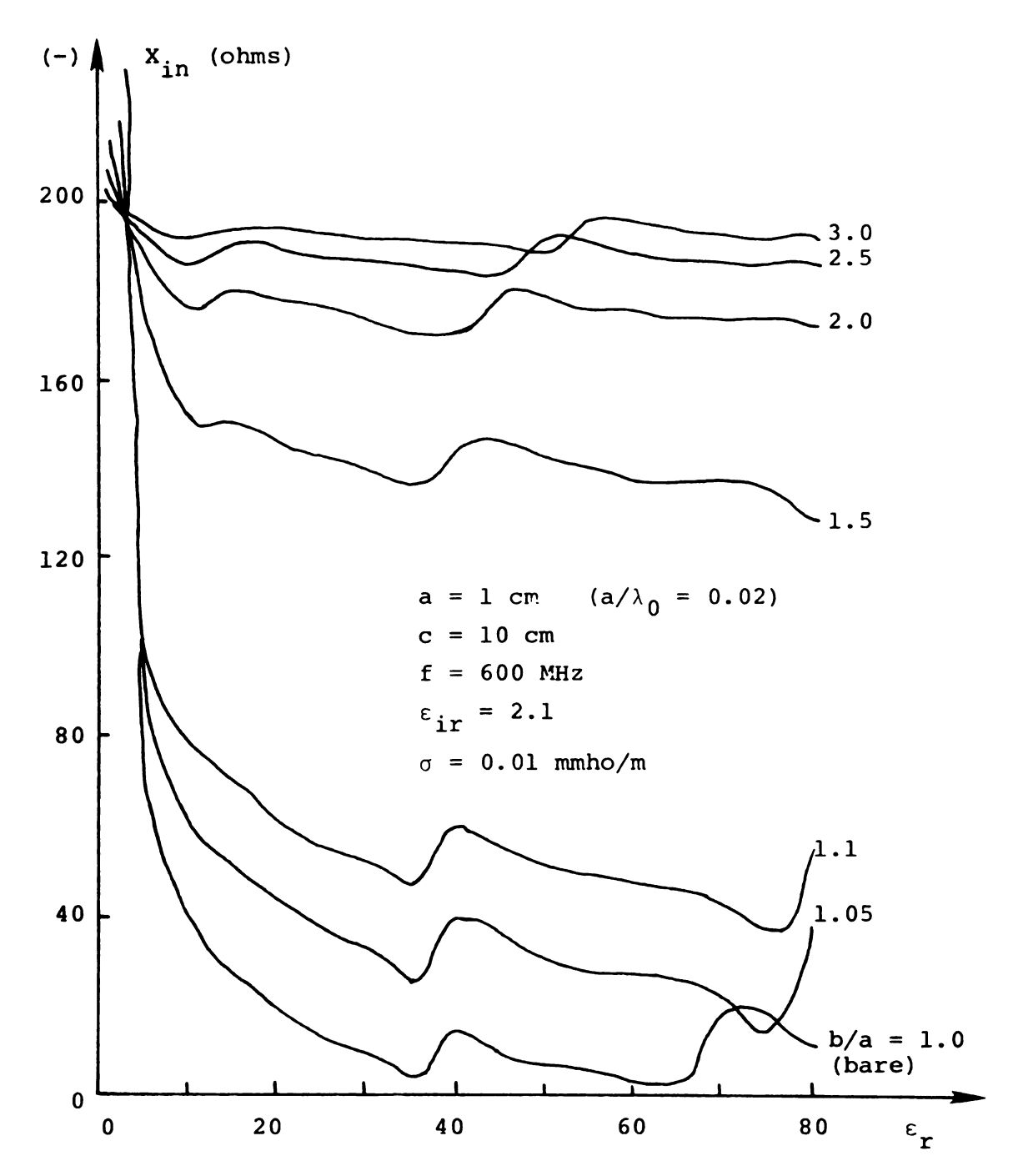


Figure 4.7. a. Input Reactance of a Small Spherical Probe as a Function of the Permittivity of the Conducting Sphere.

input impedance seems to be almost independent of this parameter. As mentioned previously, only the input reactance is shown because the input resistance is usually very small compared to  $X_{IN}$ . For example for the case of b/a = 1.0,  $R_{IN}$  is only 0.32  $\Omega$  at  $\varepsilon_r$  = 1.0 compared to -234  $\Omega$  for  $X_{IN}$  and 1.1  $\Omega$  at  $\varepsilon_r$  = 70.0 compared to -136  $\Omega$  for the input reactance. Figure 4.7b shows the case of the same probe but in a conducting body with c = 5 cm and  $\sigma = 1.0$  V/m.

Up to this point, we have seen that to construct a probe whose input impedance is rather independent of the radius of the conducting body and its relative dielectric constant, one may use a thick dielectric coating on the probe.

We have also investigated the dependence of the input impedance of the probe on the conductivity of the conducting body. In Figure 4.8, we observe the variation of the input impedance (both  $R_{IN}$  and  $X_{IN}$ ) as a function of the conductivity  $\sigma$  (mho/m) of the conducting body. Three curves are plotted for each part (i.e. real and imaginary parts of  $Z_{IN}$ ), for the cases of b/a = 1.1, 1.5 and 2.0. The sphere has a radius of a = 1 cm and the radius of the conducting body is c = 5 cm. The frequency is f = 600 MHz (i.e.  $a/\lambda_0 = 0.02$ ) and the relative dielectric constant of the coating is again  $\varepsilon_{ir} = 2.1$ . The body is assumed to have a relative dielectric constant

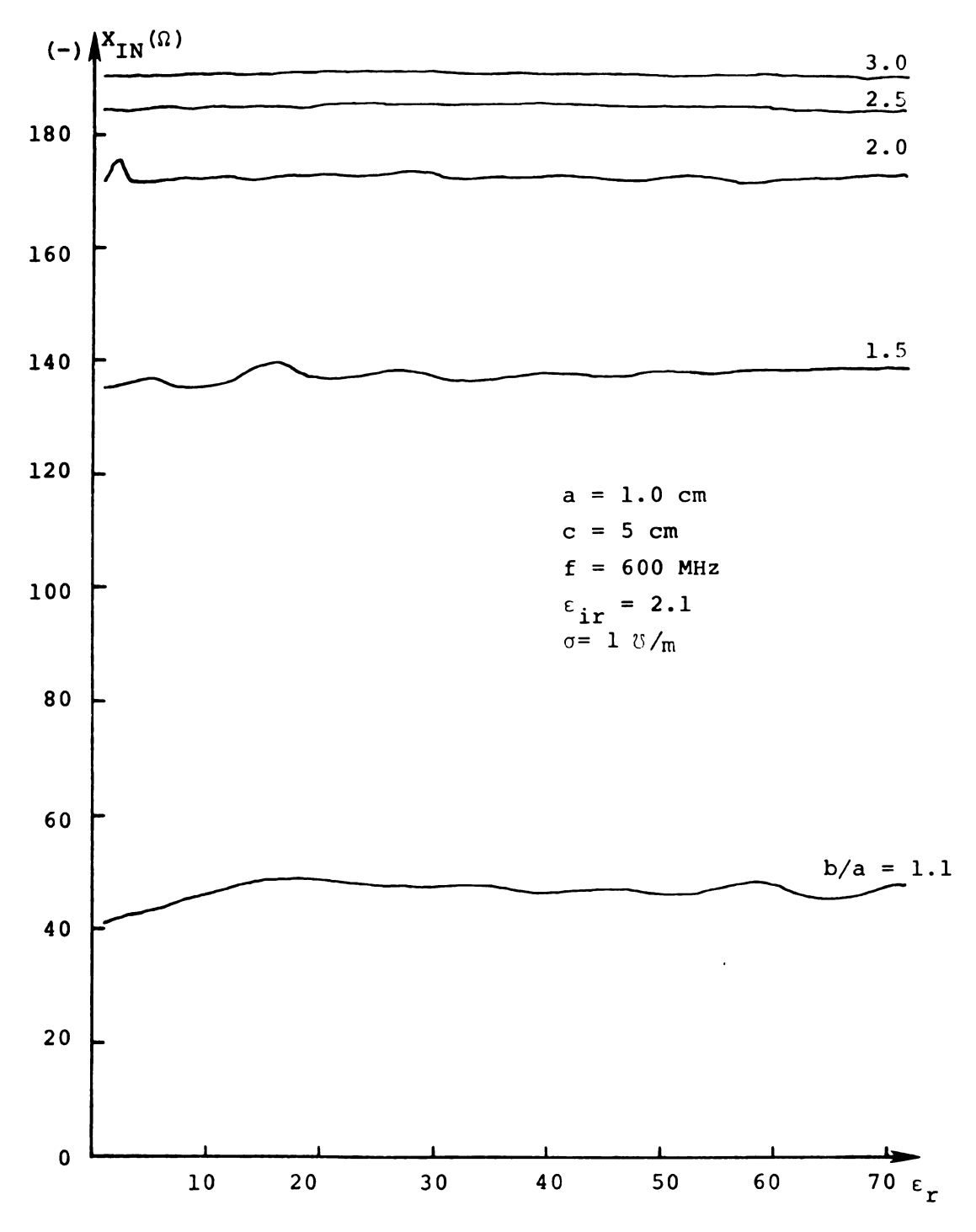


Figure 4.7. b. Input Reactance of a Small Spherical Probe as a Function of the Permittivity of the Conducting Body; b/a = 1.1, ..., 3.0.

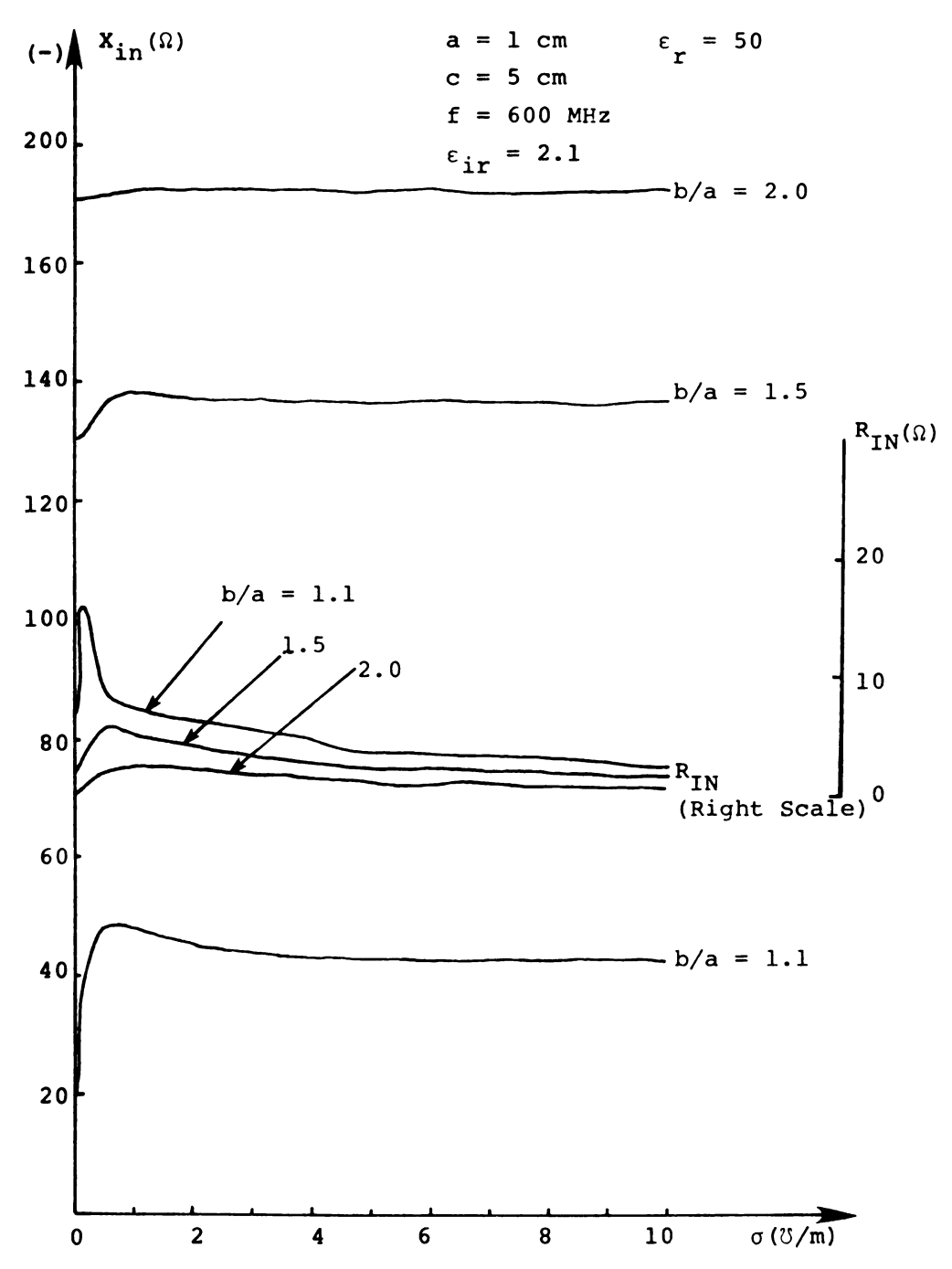


Figure 4.8. Input Impedance of a Dielectrically Coated Spherical Antenna as a Function of the Conductivity of the Conducting Body.

of  $\varepsilon_{\mathbf{r}}=50$ . Figure 4.8 shows clearly that for thick coating (i.e. b/a=2.0) the input impedance of the insulated spherical antenna is almost insensitive to the variation of the conductivity of the conducting body. For the case of thin coating (i.e. b/a=1.1), we see that the input impedance (both input resistance and input reactance) depends more significantly on the conductivity of the body.

To fabricate a probe to be used in finite biological bodies, it is desirable to make it as small as possible to have a good resolution of the field and minimize the perturbation caused by the introduction of the probe.

Therefore, it is not desirable to increase the thickness of the dielectric coating a great deal.

Another parameter of interest seems to be the relative dielectric constant of the insulating materials. In Figure 4.9a, we show the dependence of the input reactance of a spherical antenna of radius a=1.0 cm when coated by a dielectric spherical shell of outer radius b=1.1 cm. (i.e. b/a=1.1) on the dielectric constant of the coating. The radius of the conducting body is c=10.0 cm and the frequency is f=600 MHz. The body is assumed to have the conductivity of  $\sigma=1.0$  mmho/m. Five curves are plotted as a function of the relative dielectric constant of the conducting body,  $\epsilon_r$ , for five different relative dielectric constant of the coating;  $\epsilon_{ir}$  varies from 1.0 to 10. As

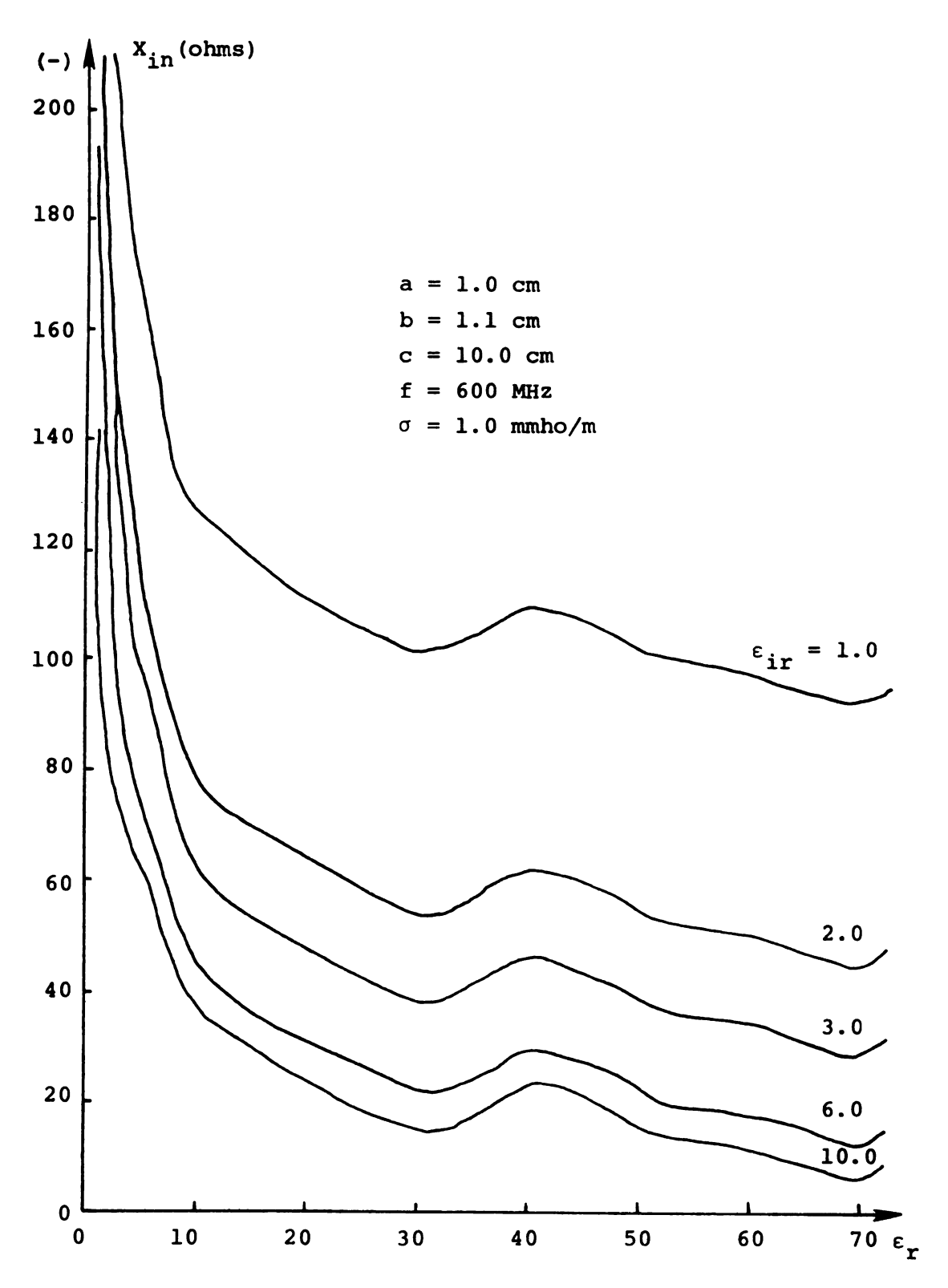


Figure 4.9. a. Input Reactance of a Small Spherical Probe as a Function of the Relative Dielectric Constant of the Conducting Body.

observed in Figure 4.9a, for small values of  $\epsilon_{ir}/\epsilon_r$ , the input reactance has less variation (in percentage) than the case of larger values of  $\epsilon_{ir}/\epsilon_r$  as the relative dielectric constant of the conducting body is changed. For most biological bodies  $\epsilon_r > 10$ , therefore to fabricate a probe which is insensitive to the dielectric constant of the body, the insulating material should have a low value of dielectric constants  $\epsilon_{ir}$ . Figure 4.9b shows the problem for  $\sigma = 1$  mho/m. It can be seen that for higher values of  $\sigma$ ,  $X_{IN}$  is not strongly affected by the values of  $\epsilon_r$ .

From the discussion of the last few figures, it is concluded that to construct a spherical probe whose input impedance is nearly independent of the electrical parameters and the configuration of the biological (or conducting) body, it is desirable to choose the dielectric coating as thick as possible within the allowable limit, and at the same time, to keep the ratio  $\varepsilon_{\rm ir}/\varepsilon_{\rm r}$  as small as possible. The receiving characteristics of the spherical probe was considered in the last chapter and a similar conclusion was reached.

Before going to the experimental verification of the theory presented in this chapter, the difference between theoretical and experimental input impedances should be studied. Theoretically the input impedance of the spherical antenna was calculated at the "edge" expressed by r = a and  $\theta = \pi/2 - \theta_0$ . However, in the experiment,

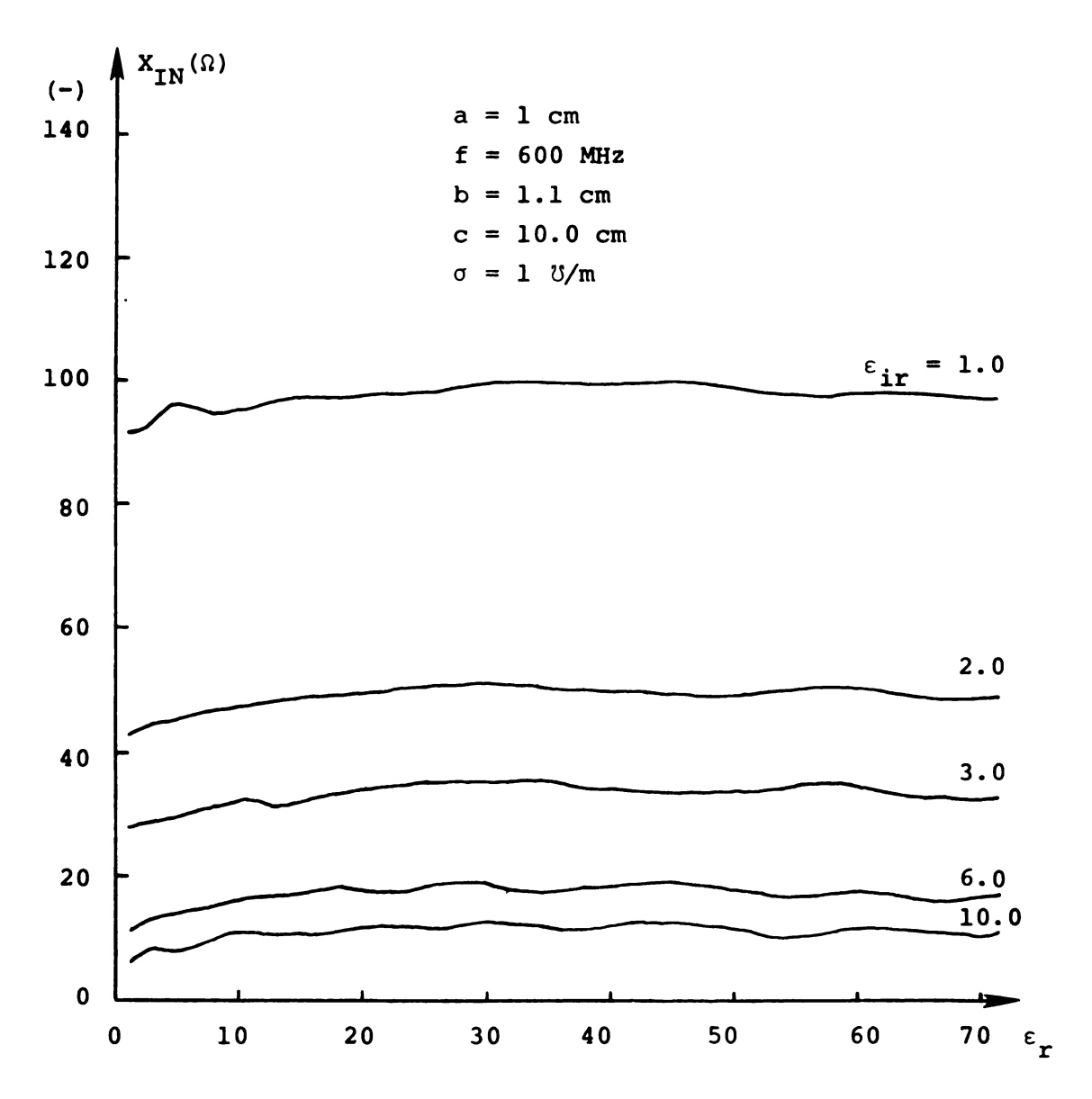


Figure 4.9. b. Input Reactance of a Small Spherical Probe as a Function of the Relative Dielectric Constant of the Conducting Body. The Parameters are Relative Dielectric Constants of the Insulating Dielectric Shell.

the antenna was driven at a point r = 0 by a small coaxial line. Therefore, it is necessary to transform the
"edge" impedance computed in this chapter to the center
of the antenna, before it can be compared with the measured
results. Such an impedance transformation is discussed
in the next section.

## 4.7. Radial Transmission Lines

The gap region of the spherical antenna discussed in the last sections is shown in Figure 4.2. This gap region can be treated as the medium between two conducting circular plates and, thus, the problem of the transformation of the input impedance from the edge  $(r=a,\theta=\pi/2-\theta_0)$  to the central feeding point  $(r=r_i,\theta)$  where  $r_i$  is the small radius of the coaxial line used to excite the antenna) becomes the impedance transformation in a radial transmission line [12]. The geometry of the problem to be studied here is shown in Figure 4.10.

There are two identical conducting plates of radius  $r = r_L$  separated by a dielectric medium (gap region). The upper plate is connected to the center conductor of a coaxial line and the lower plate to the outer conductor of the coaxial line. Thus, a potential difference (voltage) is maintained across the plates. The problem is to find an expression relating the impedance seen at  $r = r_L$  to that at  $r = r_L$  as shown in Figure

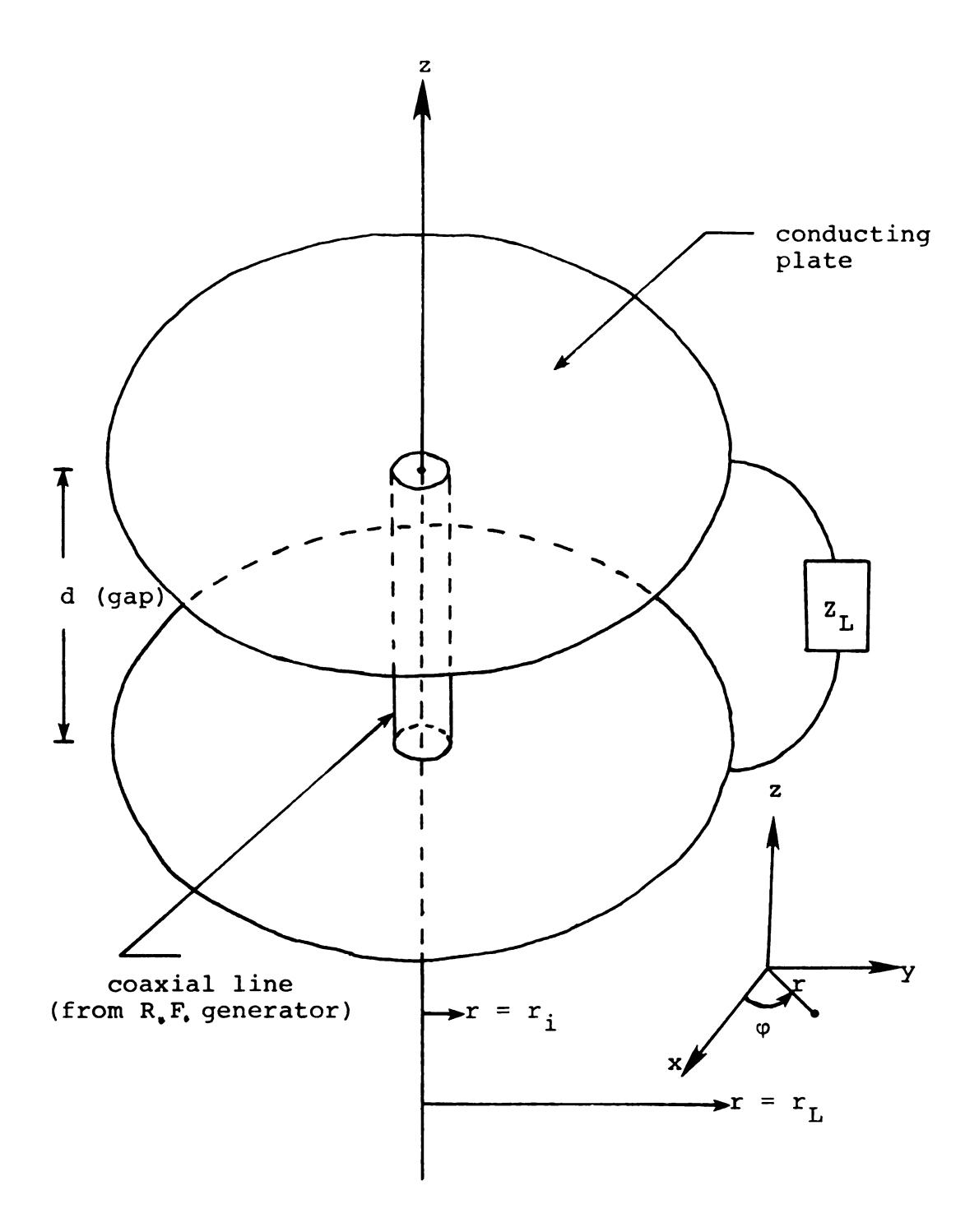


Figure 4.10. The Geometry of Radial Transmission Line.  $\mathbf{Z}_{L} \quad \text{is the "edge" Impedance of the Spherical} \\ \text{Antenna.} \quad \text{The Gap Corresponds to the Medium} \\ \text{Between the Conducting Plates.}$ 

4.10. The separation of the plates is "d" and the load impedance at  $r = r_L$  is  $Z_L$ . (Note that this  $Z_L$  represents the input impedance of the spherical antenna as discussed in this chapter).

The solution to the problem can be constructed using the cylindrical coordinates r,  $\varphi$  and z as shown in Figure 4.10. The simplest EM wave that can be guided in this system is a TEM mode with field components  $E_z$  and  $H_{\varphi}$ . Also field components are functions of r only. We will analyze other fields starting with Helmholtz Equation for  $E_z$ ,

$$\frac{\partial^2}{\partial r^2} E_z(r) + \frac{1}{r} \frac{\partial E_z(r)}{\partial r} + \omega^2 \mu_0 \varepsilon_g E_z(r) = 0 \qquad (4.96)$$

where  $\varepsilon_g = \varepsilon_{gr} \varepsilon_0$  is the dielectric permittivity of the gap region and  $r_i \le r \le r_L$  (see Figure 4.10). With  $k_g^2 = \omega^2 \mu_0 \varepsilon_g$ , Equation (4.96) is a Bessel Equation of zeroth order. Noting that we are in a bounded region, the solution to Equation (4.96) can be expressed as

$$E_z(r) = AH_0^{(1)}(k_g r) + BH_0^{(2)}(k_g r)$$
 (4.97)

where  $H_0^{(1)}$  and  $H_0^{(2)}$  are the first and second Hankel functions of order zero, respectively.  $\vec{H}$  has only the  $\phi$ -component and can be found from Equation (4.2) and Equation (4.97) to be

$$H_{\varphi}(r) = \frac{1}{j\omega\mu_0} \frac{\partial E_{z}(r)}{\partial r}$$
 (4.98)

or

$$H_{\varphi}(r) = \frac{1}{j\omega\mu_0} [A \frac{\partial}{\partial r} H_0^{(1)}(k_g r) + B \frac{\partial}{\partial r} H_0^{(2)}(k_g r)]$$
 (4.99)

The following relations of Hankel functions are used:

$$\begin{cases} \frac{\partial}{\partial r} H_0^{(1)}(k_g r) = -k_g H_1^{(1)}(k_g r) \\ \frac{\partial}{\partial r} H_0^{(2)}(k_g r) = -k_g H_1^{(2)}(k_g r) \end{cases}$$
(4.100)

Equation (4.99) then becomes

$$H_{\varphi}(r) = \frac{jk_g}{\omega\mu_0} \left[AH_1^{(1)}(k_gr) + BH_1^{(2)}(k_gr)\right]$$
 (4.101)

Note that the dielectric region between the plates is assumed to be lossless, i.e.  $k_g$  is a real quantity. Since Hankel functions are complex quantities, they can be expressed as

$$H_0^{(1)}(x) \equiv h_0(x) e^{j\theta(x)}, H_0^{(2)}(x) \equiv h_0(x) e^{-j\theta(x)}$$
 (4.102)

$$jH_1^{(1)}(x) = h_1(x)e^{j\psi(x)}, jH_1^{(2)}(x) = -h_1(x)e^{-j\psi(x)}$$
 (4.103)

where h, h<sub>1</sub>,  $\theta$  and  $\psi$  are the amplitudes and phase functions. With these definitions, expressions for the impedance transformation can be simplified.

Using Equations (4.102) and (4.103), Equations (4.97) and (4.101) are written as

$$E_z(r) = h_0(k_q r)[Ae^{-j\theta(k_q r)} + Be^{-j\theta(k_q r)}]$$
 (4.104)

and

$$H_{\varphi}(r) = \frac{h_1(k_g r)}{n_g} [Ae^{j\psi(k_g r)} - Be^{-j\psi(k_g r)}]$$
 (4.105)

where  $\eta_g = \sqrt{\frac{\mu_0}{\epsilon_g}}$ . Equation (4.105) may be put in a different form by defining a wave impedance as

$$Z_0(k_g r) \equiv \eta_g \frac{h_0(k_g r)}{h_1(k_g r)}$$
 (4.106)

such that Equation (4.105) becomes

$$H_{\varphi}(r) = \frac{h_0(k_g r)}{Z_0(k_g r)} [Ae^{j\psi(k_g r)} - Be^{-j\psi(k_g r)}]. \qquad (4.107)$$

Note that the unknown amplitude coefficients A and B have the dimensions of electric field (volts/meter).

To evaluate the constants A and B, we specify the fields at  $r=r_i$  (input terminals) and at  $r=r_L$  (load). We can write,

$$\begin{cases} E_{zi} = h_0(k_g r_i) & [Ae^{j\theta_i} + Be^{-j\theta_i}] \\ H_{\phi i} = \frac{h_0(k_g r_i)}{Z_0(k_g r_i)} & [Ae^{j\psi_i} - Be^{-j\psi_i}] \end{cases}$$
(4.108)

where  $\theta_{i} \equiv \theta (k_{q}r_{i})$  and  $\psi_{i} \equiv \psi(k_{q}r_{i})$ .

$$\begin{cases} E_{zL} = h_0(k_g r_L) & [Ae^{j\theta}L + Be^{-j\theta}L] \\ H_{\varphi L} = \frac{h_0(k_g r_L)}{Z_0(k_q r_L)} & [Ae^{j\psi}L - Be^{-j\psi}L] \end{cases}$$
(4.109)

where  $\theta_L \equiv \theta$  ( $k_g r_L$ ) and  $\psi_L \equiv \psi(k_g r_L)$ .  $\theta$  and  $\psi$  functions are as defined by Equations (4.102) and (4.103).

From Equations (4.108) and (4.109) one obtains

$$\frac{E_{zi}}{H_{\phi i}} = Z_0(k_g r_i) \frac{Ae^{j\theta_i} - j\theta_i}{Ae^{j\psi_i} - Be^{-j\psi_i}}$$
(4.110)

and

$$\frac{\mathbf{E}_{\mathbf{zL}}}{\mathbf{H}_{\mathbf{\varphi}\mathbf{L}}} = \mathbf{Z}_{0} (\mathbf{k}_{\mathbf{g}} \mathbf{r}_{\mathbf{L}}) \frac{\mathbf{A} \mathbf{e}^{\mathbf{j}\theta} \mathbf{L} - \mathbf{B} \mathbf{e}^{-\mathbf{j}\theta} \mathbf{L}}{\mathbf{j}\psi_{\mathbf{L}} - \mathbf{B} \mathbf{e}^{-\mathbf{j}\psi_{\mathbf{L}}}}$$
(4.111)

Next, the voltage and current at any radius r are defined as follows:

$$\begin{cases}
V = -E_{Z}(r) d \\
I = 2\pi r H_{\varphi}(r)
\end{cases}$$
(4.112)

With Equation (4.112) the "total" impedance becomes

$$z_{\text{total}} = \frac{V}{I} = -\frac{d}{2\pi r} \left[ \frac{E_z(r)}{H_{\varphi}(r)} \right]$$
 (4.113)

Now, Equations (4.110) and (4.111) can be written in terms of the total impedances as

$$-\frac{2\pi r_{i}}{d} z_{in} = z_{0}(k_{g}r_{i}) \frac{Ae^{j\theta_{i}} Be^{-j\theta_{i}}}{Ae^{j\psi_{i}} - Be}$$
(4.114)

and

$$-\frac{2\pi r_{L}}{d} z_{L} = z_{0}(k_{g}r_{L}) \frac{Ae^{j\theta_{L}} + Be^{-j\theta_{L}}}{Ae^{j\psi_{L}} - B}$$
(4.115)

We solve Equation (4.115) for B as

$$B = \begin{pmatrix} e^{j\theta} L_{Z_{0L}} + \frac{2\pi r_{L}}{d} e^{j\psi} L_{Z_{L}} \\ \frac{2\pi r_{L}}{d} e^{-j\psi} L_{Z_{L}} - e^{-j\theta} L_{Z_{0L}} \end{pmatrix} A$$
 (4.116)

where  $Z_{0L} = Z_0(kr_L) = \eta_g \frac{h_0(k_g r_L)}{h_1(k_g r_L)}$ . Substituting (4.116) in (4.114), one gets (after some algebra)

$$z_{in} = \frac{1}{\alpha_{i}} z_{0i} \left[ \frac{\alpha_{L} z_{L} \cos(\theta_{i} - \psi_{L}) - j z_{0L} \sin(\theta_{i} - \theta_{L})}{z_{0L} \cos(\psi_{i} - \theta_{L}) - j \alpha_{L} z_{L} \sin(\psi_{i} - \psi_{L})} \right]$$
(4.117)

where

$$\alpha_{i} \equiv \frac{2\pi r_{i}}{d}, \alpha_{L} \equiv \frac{2\pi r_{L}}{d}$$
 (4.118)

and  $Z_{0i} = Z_{0}(k_{g}r_{i})$ . Note that in deriving Equation (4.117), Euler's identity,  $e^{j\theta} = \cos \theta + j \sin \theta$  was used

Equation (4.117) is the desired impedance transformation formula of the radial transmission line of Figure 4.10.  $\mathbf{Z_L}$  is to be interpreted as  $\mathbf{Z_{IN}}$  of our spherical antenna as shown in Figure 4.1 and  $\mathbf{Z_{in}}$  is the input impedance measured experimentally (Chapter 5).

Before closing this chapter, we consider a simpler method of correcting the end effect or transforming the impedances as discussed above. Some numerical examples are also given.

## 4.8. Apparent Antenna Impedance and Capacitive End Correction

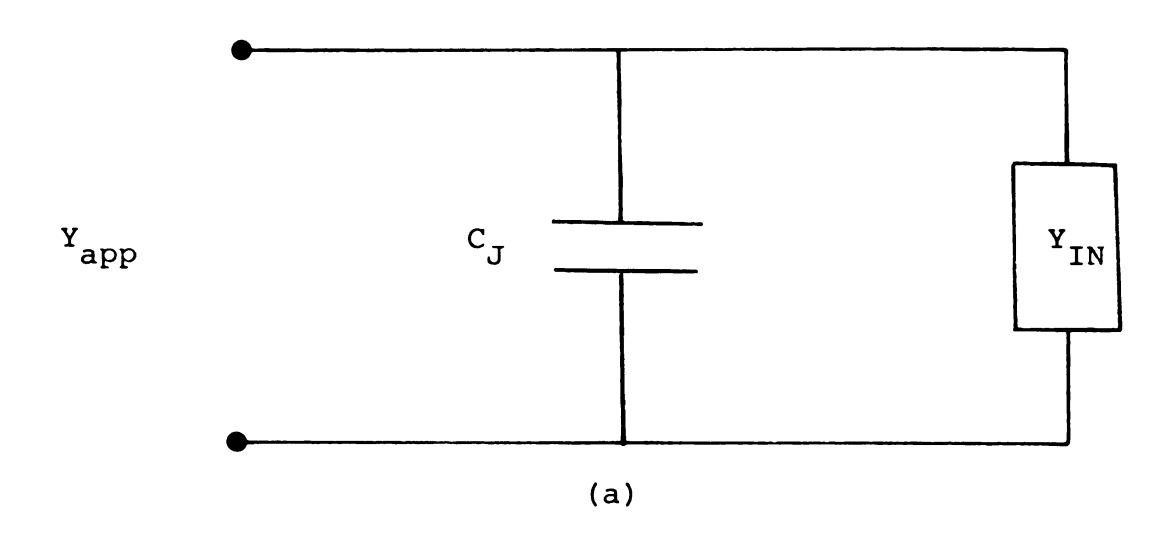
Although the expression of Equation (4.117) in the last section rigorously transforms the edge impedance to the center of the spherical antenna of Figure 4.2, there is a simpler method of treating this problem if the radius of the sphere (or the radius of the plates shown in Figure 4.10) is electrically small and the electric field in the gap region is uniform.

King [5] used the terminology of "apparent" antenna impedance as the impedance measured at the input or feeding terminals as compared to that of the theoretical antenna terminals. In our case, the important factor is the "junction" capacitance and the terminal zone equivalent circuit can be visualized as shown in Figure 4.11.

In electrostatic, it is known that when the electric field between two parallel plates is uniform, the capacitance is simply given by

$$C_{J} = \varepsilon_{g} \frac{A}{d}$$
 (4.119)

where  $\varepsilon_g = \varepsilon_{gr} \varepsilon_0$  is the permittivity of the dielectric



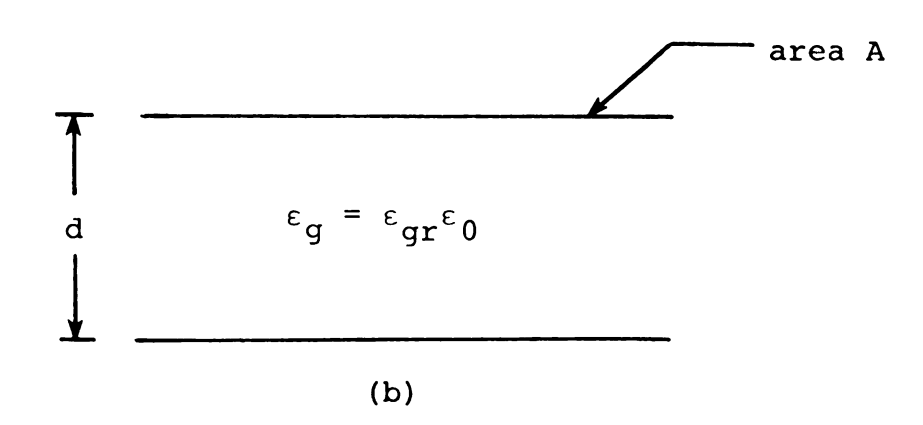


Figure 4.11. (a) is the Junction Equivalent Circuit of the Spherical Antenna with an Edge Input Admittance of  $Y_{\overline{1N}}$ . (b) is the Configuration of the Circular Parallel Plates of Area A which Approximates the Gap of the Antenna.

region between the two plates. A is the area of the plates and d is the separation between the plates as shown in Figure 4.11.

The measured input impedance is given by

$$z_{in}(exp.) = \frac{1}{Y_{app}} = \frac{1}{C_J + Y_{IN}}$$
 (4.120)

where  $Y_{IN}$  is the input admittance of the insulated spherical antenna in the conducting body as given by Equation (4.92). As will be seen from the following numerical examples, the junction capacitance has a significant effect on the measured value of the input impedance. Also, in the following examples, we show a close agreement between the results calculated from the simple method just discussed and that from the more rigorous radial transmission line theory.

Numerical Example #1. Let us now consider some cases where we transform the input impedance from the edge of the spherical antenna to its center. First we have  $\mathbf{Z}_{\mathrm{IN}} = \mathbf{Z}_{\mathrm{L}} \doteq -\mathrm{j}235~\Omega \quad \text{as the edge input impedance for a dielectrically coated spherical antenna in the free space (a = 1.0 cm, b = 1.5 cm, <math>\epsilon_{\mathrm{gr}} = 2.1$  and f = 600 MHz). This is computed from the expression in Equation (4.92). The angular width of the gap is assumed to be  $2\theta_0 = 10^\circ$ . Also the following data are used:  $\mathbf{a} = \mathbf{r}_{\mathrm{L}} = 1$  cm.  $\mathbf{r}_{\mathrm{i}} = 0.025~\mathrm{cm}, \ \mathbf{d} \doteq 0.2~\mathrm{cm}.$  With these data, we use the

radial transmission line expression of Equation (4.117) to find the input impedance at the feeding point as follows:

$$\begin{cases} k_g r_i = \frac{\sqrt{2.1} \times 2\pi \times 0.025}{50} = 0.0045 \\ k_g r_L = \frac{\sqrt{2.1} \times 2\pi \times 1}{50} = 0.182 \end{cases}$$

$$\begin{cases} h_0 (k_g r_i) \doteq \frac{2}{\pi} \rho_m (\frac{1.781 \times 0.0045}{2}) = 3.514 \\ h_1 (k_g r_i) \doteq \frac{2}{\pi \times 0.0045} = 141.47 \end{cases}$$

$$h_0(k_g r_L) \doteq 1.158$$
 ,  $h_1(kr_L) \doteq 3.498$ 

$$\begin{cases} \theta_{i}(k_{g}r_{i}) = \theta_{i} = \tan^{-1}\left[\frac{2}{\pi} \varrho_{n}(\frac{1.781 \times 0.0045}{2})\right] = -1.295 \text{ rad.} \\ \theta_{L}(k_{g}r_{L}) = \theta_{L} = \tan^{-1}\left[\frac{2}{\pi} \varrho_{n}(\frac{1.781 \times 0.182}{2})\right] = -0.858 \text{ rad.} \end{cases}$$

(for small argument approximations of the Hankel functions involved, see Appendix B).

$$\begin{cases} \psi_{i}(k_{g}r_{i}) = \tan^{-1}\left[\frac{\pi \times (0.0045)^{2}}{4}\right] = 0.000016 \text{ rad.} \\ \psi_{L}(k_{g}r_{L}) = \tan^{-1}\left[\frac{\pi \times (0.182)^{2}}{4}\right] = 0.026 \text{ rad.} \end{cases}$$

$$\begin{cases} z_{0i} = 260.15 \times \frac{3.514}{141.47} = 6.462 \Omega \\ z_{0L} = 260.15 \times \frac{1.158}{3.498} = 86.12 \Omega \end{cases}$$

$$Cos(\theta_{i} - \psi_{L}) = 0.247, Cos(\psi_{i} - \theta_{L}) = 0.654 \end{cases}$$

$$\cos(\theta_i - \psi_L) = 0.247, \cos(\psi_i - \theta_L) = 0.654$$
  
 $\sin(\theta_i - \theta_L) = -0.423, \sin(\psi_i - \psi_L) = -0.026$ 

$$\alpha_{i} = \frac{2\pi \times 0.025}{0.2} = 0.785$$
,  $\alpha_{L} = \frac{2\pi \times 1}{0.2} = 31.416$ 

All these are computed according to the definitions given in the last section. Finally, putting all these values in Equation (4.117), we have

$$Z_{in}(center) = -j61.3845 \Omega$$
 (4.121)

that is the edge input impedance of  $-j235~\Omega$  (with a very small resistive part), reduces to that given above after going through the transformation of Equation (4.117). As is seen from the above computation, the procedure is rather involved. Since  $a/\lambda_0$  is 0.02 in this case, the capacitive approximation may be used as follows:

$$C_J = \epsilon_{gr} \epsilon_0 \frac{A}{d} = 2.1 \times 8.854 \times 10^{-12} \times \frac{\pi \times 10^{-4}}{2 \times 10^{-3}}$$

or

$$C_{J} = 2.92 \mu \mu F$$

and

$$j\omega c_J = j1.1 \times 10^{-12}$$
 mho

According to the theory;  $Y_{IN} = j0.42 \times 10^{-2}$  mho. Therefore  $Y_{IN} + j\omega c_J = Y_{app} = j1.52 \times 10^{-2}$  mho and

$$z_{in} = \frac{1}{Y_{IN} + j\omega c_{J}} = -j65.78 \Omega$$
 (4.122)

Comparing Equations (4.121) and (4.122), it is evident that a simple junction capacitance correction can transform the edge impedance to the input impedance.

Numerical Example #2. In this example, we use some data from the case of a dielectrically coated spherical antenna in a finite low-conducting body. The values used are:

a = 1.0 cm, b = 2.0 cm, c = 10 cm, 
$$\epsilon_{ir}$$
 = 2.1  $\epsilon_{r}$  = 28,  $\sigma$  = 0.01 mmho/m  $z_{IN}$  = -j174  $\Omega$ ,  $\epsilon_{gr}$  = 1.0 (air gap) f = 600 MHz, a =  $r_{L}$  = 1.0 cm,  $r_{i}$  = 0.01 cm d = 4.0 mm.

The impedance calculated from Equation (4.117) is

$$z_{in} = -j116.54 \Omega$$

and that from the capacitive correction is found to be

$$z_{in} = -j119.59 \Omega$$

Again a good agreement between these two methods is obtained.

No theory is complete without experimental verification. In order to check the numerical accuracy of the theoretical values of the input impedance calculated from Equation (4.92) of this chapter, we have performed some experiments. Details are presented in the next chapter.

## CHAPTER V

## SOME EXPERIMENTAL RESULTS

In order to verify the theory presented in the preceding chapter, some experiments were performed in which the input impedances of some cases discussed previously were measured and compared with the theory. A good agreement between theory and experiment was obtained.

Two methods for measuring the input impedance of the antenna were used in the present study. The first is the conventional minimum shift method in which a slotted line is used together with an impedance chart (Smith chart). The second method employs E-H probes and a vector voltmeter. This method has been reported by Scott [13], [14]. We will first discuss the second method and then present some experimental measurements of the input impedance.

Finally, since the probe is to be used to measure the intensity of EM fields induced in finite conducting bodies, we will present some experimental results on the spherical probe when it is used to measure the induced electric field in finite experimental models containing saline solution.

5.1. V-I (or E-H) Probe Impedance Measuring Techniques

The method to be described here is based on the very definition of the impedance on the transmission line which states: The impedance at any point on a transmission line is the ratio of the voltage to the current at that point. Since coaxial transmission lines are most commonly used in experiments and practice, we will first study the nature of voltage and current waves on a coaxial transmission line (or cable).

Figure 5.1 shows the cross sectional and longitudinal views of the coaxial transmission line used to construct the E-H probe device. The inner conductor, assumed to be perfectly conducting, is of radius a and is maintained (by a generator) at the potential +V. The outer conductor which has an internal radius of b is kept at the zero potential. The dielectric between the conductors (a  $\leq$  r  $\leq$  b) is assumed to be air.

The electric field in the air region between the conductors, can be determined from the Gauss' Law. Assuming that the charge density (charge per unit length) on the center conductor is  $\rho_{\ell}$  (coul./m), we can write this law as

$$\oint_{S} \vec{E} \cdot d\vec{s} = \frac{Q}{\epsilon_0}$$
 (5.1)

where Q is the total charge enclosed by the closed surface S. Choosing a cylindrical surface as shown by

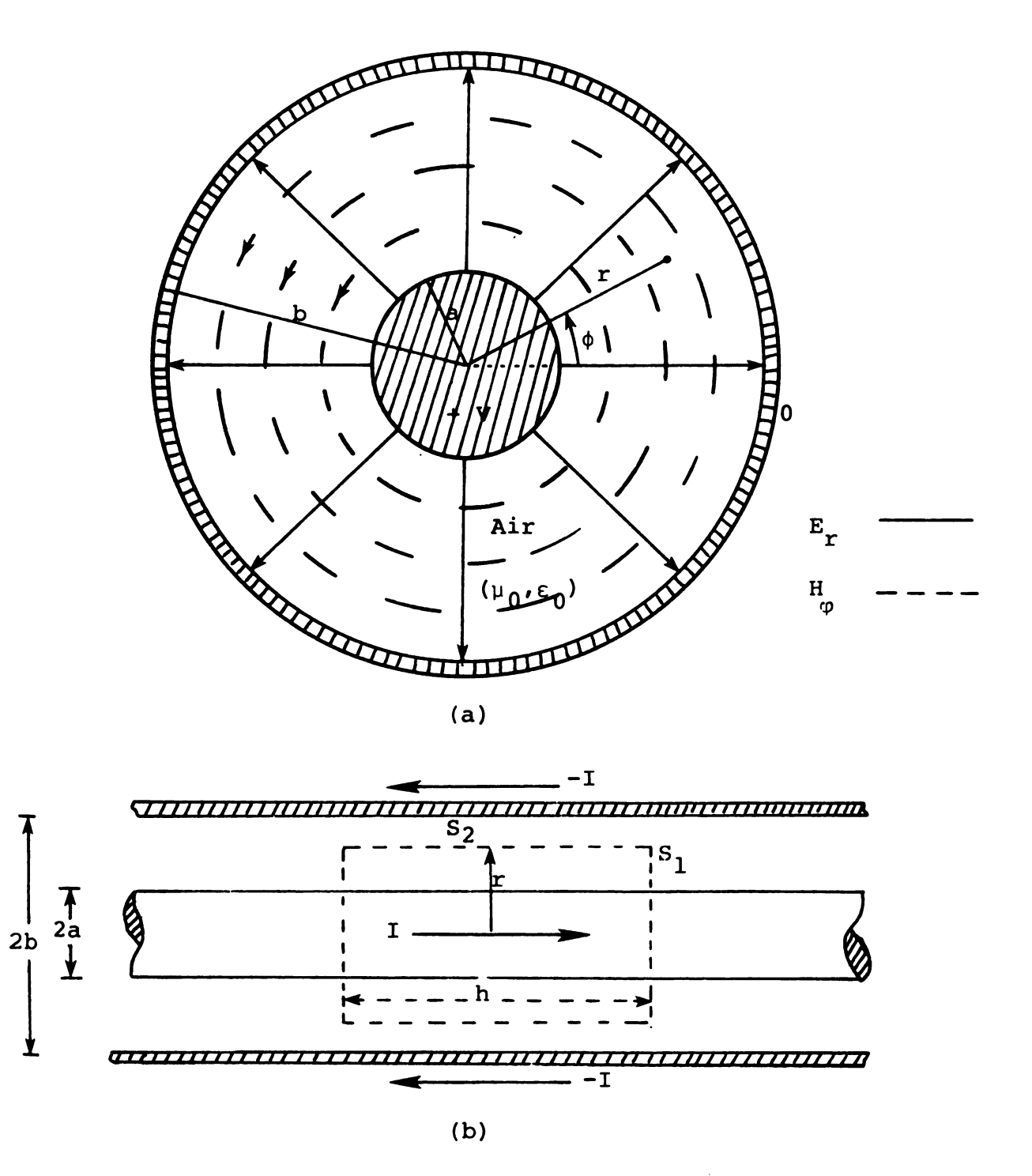


Figure 5.1. Cross-sectional (a) and Longitudinal (b)
Views of the Cylindrical Coaxial Transmission Line. A Generator Maintains a
Voltage (or Potential Difference) V
Between the Inner and Outer Conductors.

the dotted lines of Figure 5.1 (b), Equation (5.1) can be written as

$$\int_{S_1} \vec{E} \cdot d\vec{s} + \int_{S_2} \vec{E} \cdot d\vec{s} = \frac{Q}{\epsilon_0}$$
 (5.2)

Now, from the symmetry consideration, it is evident that there is only a radial component of  $\vec{E}$  field,  $E_r$ , which is a function of r only. Therefore, there is no contribution from  $S_1$  integral, and Equation (5.2) becomes

$$\int_{S_2} \vec{E} \cdot d\vec{s} = E_r(r) \int_{S_2} ds = E_r(r) (2\pi r \cdot h) = \frac{Q}{\epsilon_0}$$
 (5.3)

Since  $Q = h\rho_{\varrho}$ , Equation (5.3) yields

$$E_{\mathbf{r}}(\mathbf{r}) = \frac{\rho_{\ell}}{2\pi\epsilon_{0}\mathbf{r}}$$
 (5.4)

where a  $\leq$  r  $\leq$  b. The potential difference between the center conductor and outer conductor, V, can be expressed in terms of the charge density,  $\rho_{\ell}$ , as follows:

By the definition of the potential difference (voltage);

$$\Phi(a) - \Phi(b) = V = \int_{a}^{b} E_{r}(r) dr$$
 (5.5)

Substituting Equation (5.4) in Equation (5.5), we have

$$V = \frac{\rho_{\ell}}{2\pi\epsilon_0} \ell_n \, b/a \tag{5.6}$$

Combining Equation (5.6) and Equation (5.4), the r component of the  $\vec{E}$  field can be found as

$$E_{r}(r) = \frac{V}{r _{m}(b/a)}, a \leq r \leq b$$
 (5.7)

Equation (5.7) can also be found based on the Laplace Equation:

$$\nabla^2 \Phi(\mathbf{r}) = 0 \tag{5.8}$$

subject to the boundary conditions of  $\phi(a) = V$  and  $\Phi(b) = 0$ . Writing out Equation (5.8) in the cylindrical coordinates, one gets

$$\frac{1}{r} \frac{\partial}{\partial r} \left[ r \frac{\partial \Phi(r)}{\partial r} \right] = 0$$
 (5.9)

Equation (5.9) is easily solved to give

$$\frac{\partial \Phi(\mathbf{r})}{\partial \mathbf{r}} = \frac{\mathbf{c}_1}{\mathbf{r}} \tag{5.10}$$

where  $c_1$  is a constant to be determined by the boundary conditions. Integrating (5.10) one more time, we have

$$\Phi(r) = c_1 2n r + c_2$$
 (5.11)

c<sub>2</sub> being another unknown constant. Using  $\Phi(a) = V$  and  $\Phi(b) = 0$ , one gets

$$c_1 = -\frac{V}{\gamma_m b/a}, c_2 = \frac{V}{\gamma_m b/a} \cdot \gamma_m b$$
 (5.12)

Now, 
$$\vec{E} = -\nabla \Phi(\mathbf{r}) = -\frac{\partial \Phi(\mathbf{r})}{\partial \mathbf{r}} \hat{\mathbf{r}} = -\frac{\mathbf{c}_1}{\mathbf{r}} \hat{\mathbf{r}}$$
 (5.13)

and with the value of  $c_1$  as given in Equation (5.12), one gets Equation (5.7) for  $E_r$ .

Equation (5.7) shows that electric field in the region between the two conductors of the coaxial line is proportional to the voltage on the line.

The magnetic field  $\overrightarrow{H}$  is found by the application of Ampere's circuital law:

$$\oint_{\mathbf{C}} \vec{H} \cdot d\vec{k} = \mathbf{I}$$
(5.14)

where I is the total current enclosed by the contour c. From Maxwell's Equation (4.1), it follows that with  $\vec{E} = E_r(r)\hat{r}$ , there is only the  $\phi$ -component of  $\vec{H}$  field which is a function of r only. Thus, Equation (5.14) can be written as

$$\int_{0}^{2\pi} H(r) r d\phi = I$$
 (5.15)

Equation (5.15) gives rise to

$$H_{o}(r) = \frac{I}{2\pi r}$$
 (5.16)

where  $a \le r \le b$ .

Equation (5.16) shows that the magnetic field in the region between the conductors is proportional to the current I on the line. The sketches of the  $\vec{E}$  and  $\vec{H}$  field lines, are shown in Figure 5.1.

It is well known that a small dipole (or monopole) can be used to measure, or to sample, the electric field in a medium. The electrical length of the dipole should be kept to a minimum in order not to disturb the

field distribution. On the other hand, an electrically small, shielded loop can be used to measure the intensity of the magnetic field in a given medium. The theory for these probes can be found in the literature [15] and is not repeated here.

At this point, it is clear that for measuring the impedance  $Z = \frac{V}{T}$  at any point on a transmission line, the  $\vec{E}$  and  $\vec{H}$  fields (both magnitudes and phases) at that point need to be measured. Therefore, electric and magnetic field probes should be introduced from the outer conductor into the medium between the inner and outer conductors (which is usually air). Two points chosen for entrance should be on diametrically opposite sides to ensure that voltage and current (or the electric and magnetic fields) are being measured at the same location on the line. In order that the presence of these probes doesn't cause any significant change in SWR (Standing Wave Ratio) on the line, the sizes of the probes should be kept electrically small. In the case of our device, we are interested in the frequency range of 1 to 1000 MHz. The dimensions of the probes constructed are in the order of 2 mm. For one device, when the test line was attached to one end of the Slotted Line and a 50  $\Omega$  matched termination was placed at the other end of one test line, it was found that SWR did not change (i.e. SWR  $\doteq$  1.0). This means that the probes were not loading the line.

The over-all block diagram of the E-H probe constructed for the experiments is shown in Figure 5.2.

The main equipment used is the HP Model 8405A Vector

Voltmeter which is capable of measuring both the magnitude and the phase of a signal. It has two channels, "A" and "B". In our set up, the channel A is always connected to the outlet of the current probe. The B channel is connected to the voltage (or electric field) probe.

Therefore, the phase reading is the angle, in degrees, between the voltage and the current, with the current signal being the reference. The signal generator or oscillator is to be used without any modulation.

To mount the E and H probes, we need a section of a coaxial line. For this purpose, a section of the coaxial line was constructed and a "block" supporting the probes was attached to the coaxial line as shown in Figure 5.3. It is noted that since all the lines used are standard 50  $\Omega$  coaxial lines, the test line section should also have a 50  $\Omega$  characteristic impedance as computed from the following formula:

$$Z_{C} = \frac{\eta_{0}}{2\pi} \mathcal{D}_{n} \left(\frac{b}{a}\right) \tag{5.17}$$

where  $\eta_0 = \sqrt{\frac{\mu_0}{\epsilon_0}} = 120\pi \ \Omega$ , b and a are the dimensions as shown in Figure 5.1. In the construction of the test line we chose  $a = \frac{1}{8}$ " and  $b = \frac{9}{32}$ " such that  $Z_C$  was very close to 50  $\Omega$ . The total physical length of the

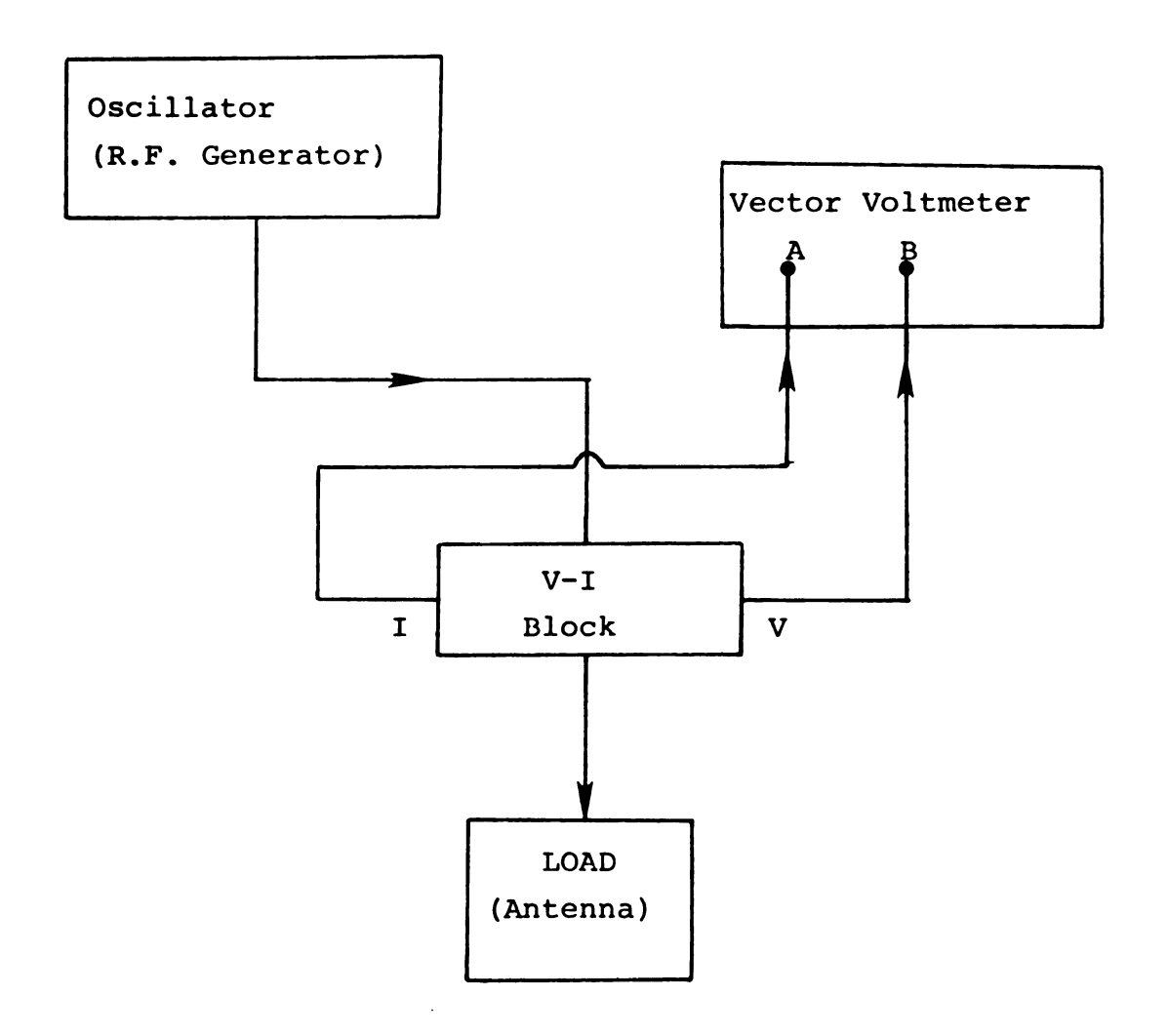


Figure 5.2. Block Diagram for E-H (or V-I) Probe Impedance Measuring Device. All the Lines Shown are Standard GR 50  $\Omega$  Coaxial Transmission Lines.

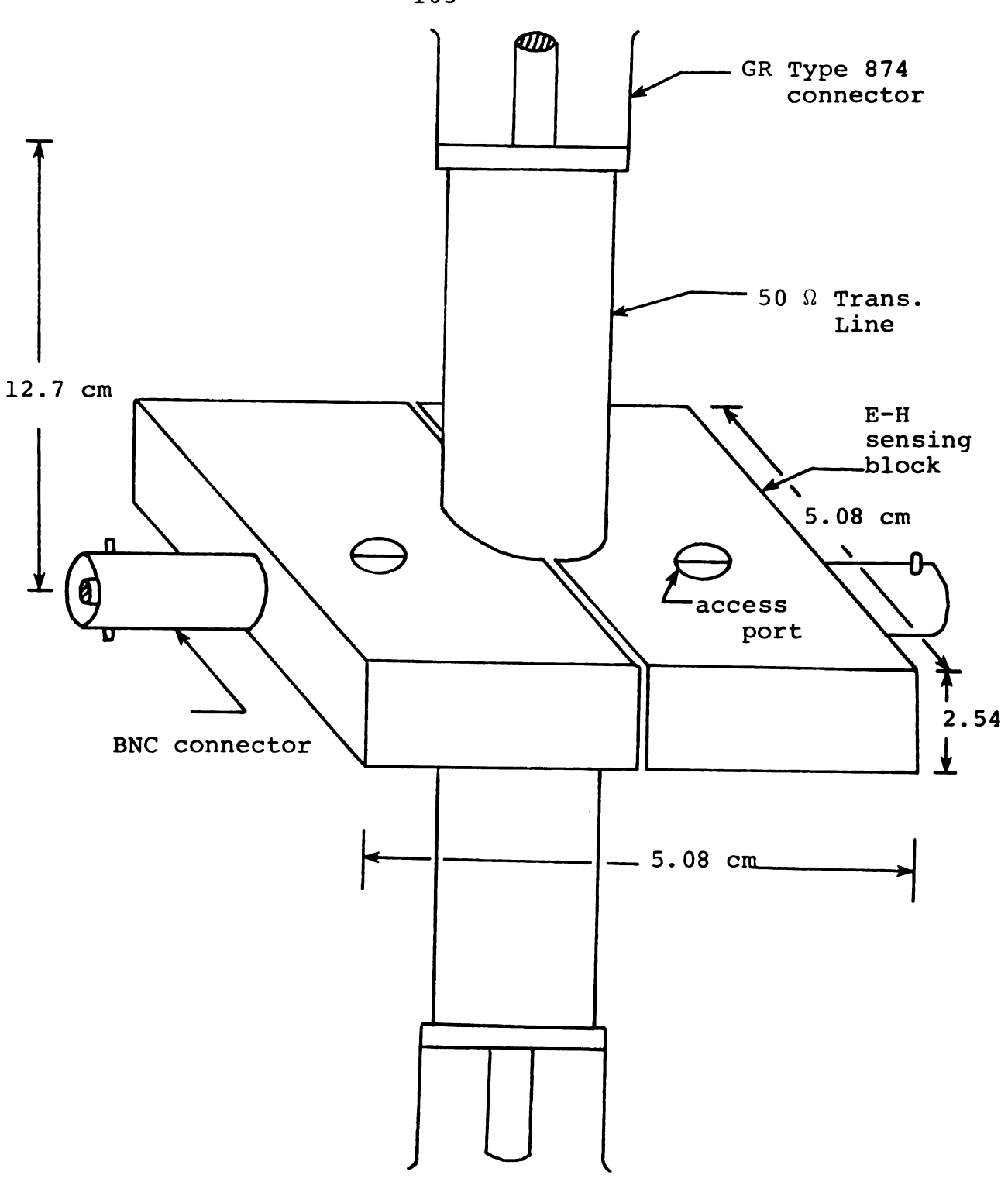


Figure 5.3. Test Line Together with E-H Block which Supports the Voltage and Current Probes

line was 25.4 cm. The V-I block was constructed from brass and had the dimensions 5.08 cm × 5.08 cm × 2.54 cm. To facilitate the connection to other parts of the experimental set-up, GR Type 874 standard connectors were used at both ends of the test line.

As mentioned previously, E and H probes are a small monopole and a small half shielded loop, respectively. The dimensions of these probes are shown in Figure 5.4. It is noted that the plane of the loop is parallel to the axis of the coaxial line.

After the test line and the V-I block were constructed, they were connected in the experimental setup shown schematically in Figure 5.2. Before actual measurements of the input impedance, we tried to measure some known impedances using this E-H probe device. It is worth mentioning that the calibration of the probes depends on the direction of the current flowing on the center conductor. Therefore, we should try to use one side of the test line always for the generator connection and the other side for the load connection. To avoid confusion, both ends of the test line were marked as "Gen." and "Load". In order to use the vector voltmeter for the measurements, the following steps should be taken:

1. The vector voltmeter has two main parts:
"Magnitude" and "Phase". Since the phase is relative

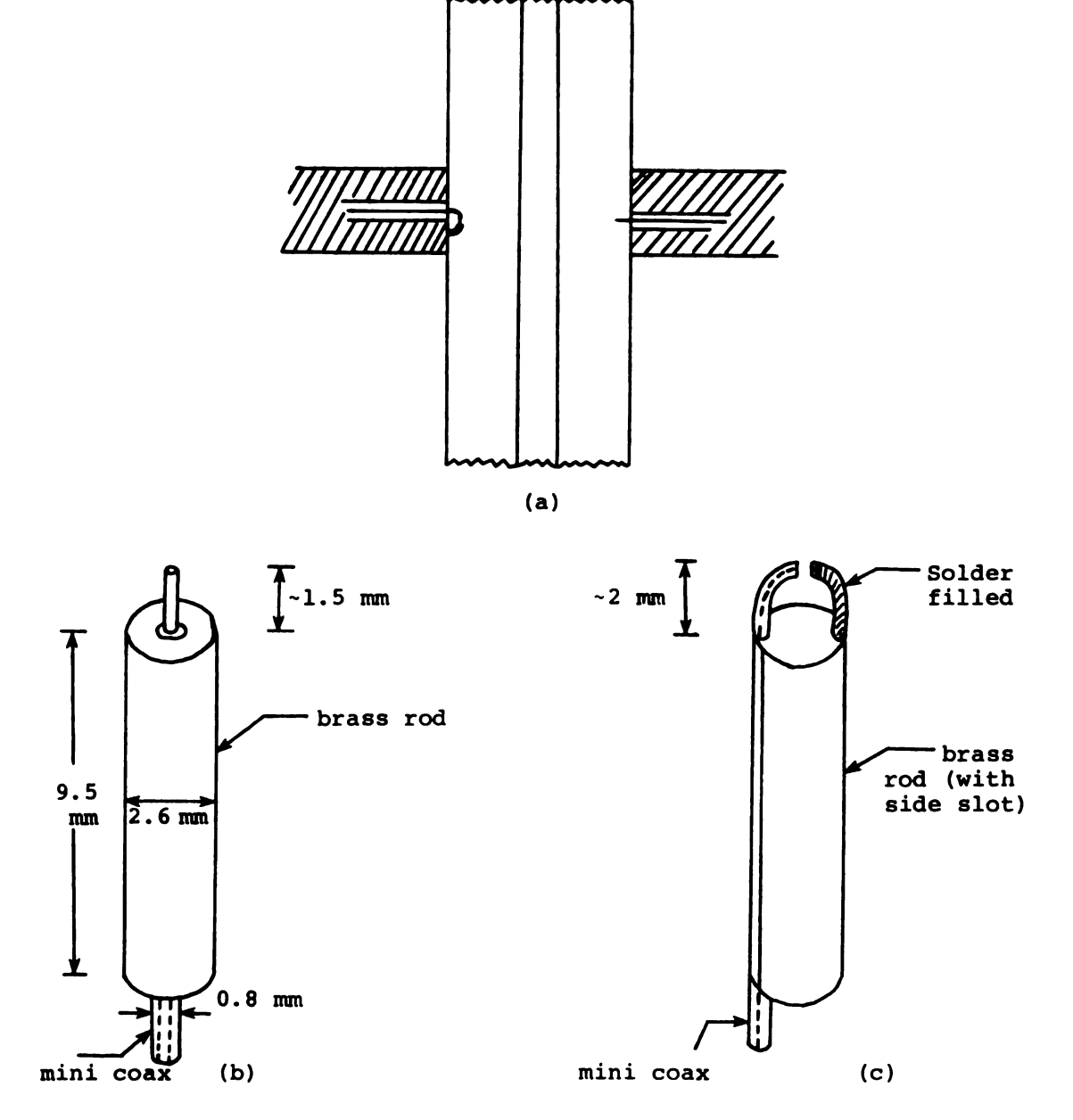


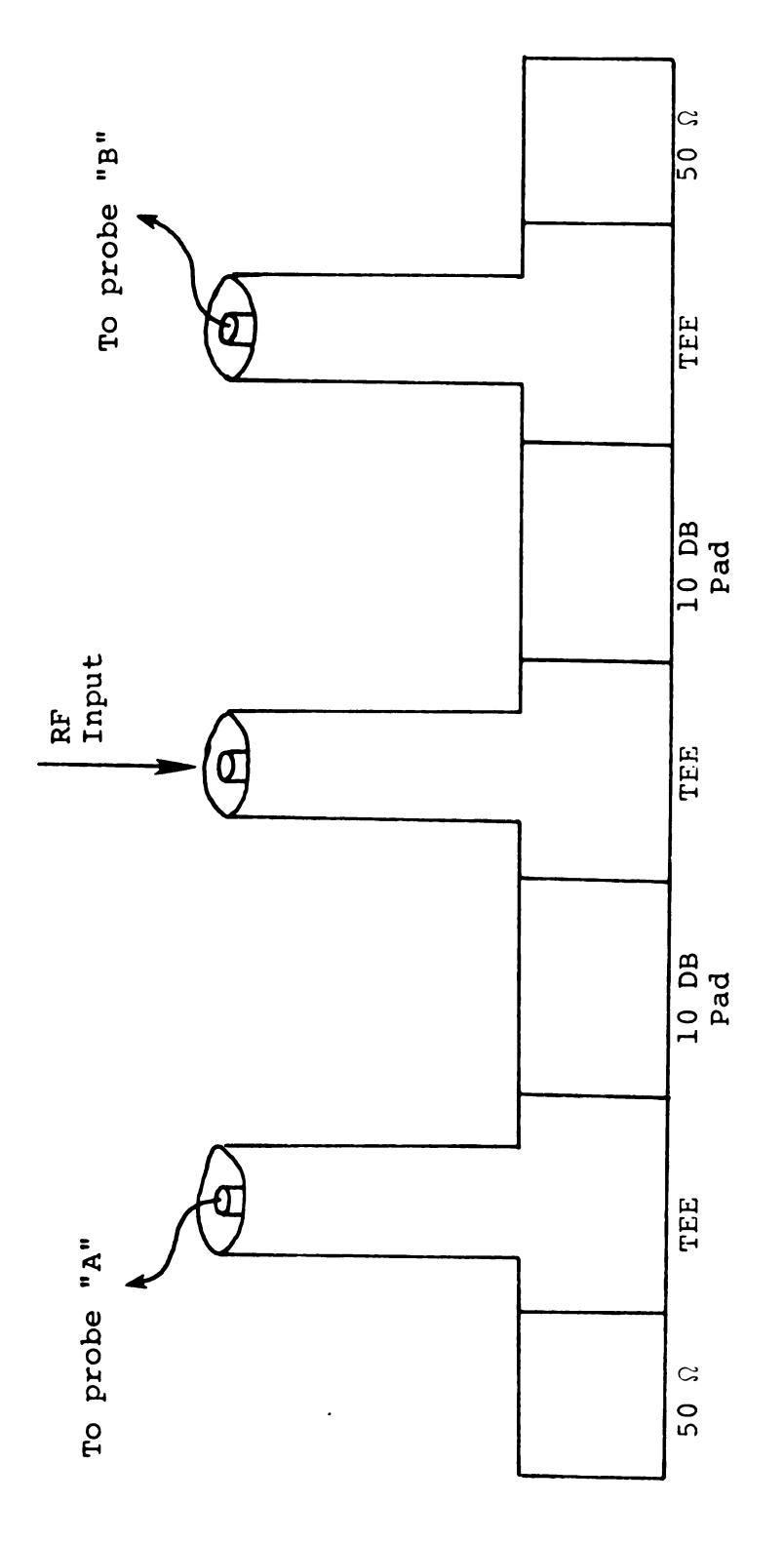
Figure 5.4. Cross-sectional View of the V-I Probe Assembly, Electric Probe (b), and Magnetic Probe (c).

meter before attempting to take any reading. To do this, a simple arrangement as shown in Figure 5.5 is used.

When the A and B probes are connected as shown, the two signals are in phase, thus, the phase meter should be adjusted to read zero degree. When using the R.F. generator, the FREQ. RANGE (in MHz) dial of the vector voltmeter should be adjusted to include the operating frequency. The APC UNLOCKED light should go out indicating that the meter is tuned to the generator's frequency.

Note that vector voltmeter can operate in the frequency range of 1 to 1000 MHz. The phase is now calibrated and the phase meter should not be touched during the experiment.

2. After calibrating the phase of the vector voltmeter as in step 1, we should calibrate the E-H probe, or the impedance sensing block, experimentally. As mentioned earlier, the voltage signal  $V_A$  (or the signal from the current, I, probe) is proportional to the total current on the line, while the voltage signal  $V_B$  (the signal from the voltage, V, probe) is proportional to the total voltage on the transmission line. Since the voltage and current on a line, in general, are out of phase relative to each other, the ratio of the two signals measured (i.e.  $V_A$  and  $V_B$ ) is generally a complex quantity which is proportional to the impedance measured at the location of the probes, i.e.,



The Calibration of the Phase Meter Used in the Vector Voltmeter Measurements. For the Configuration Shown the Phase Meter Should Measurements. Read "Zero". Figure 5.5.

$$\overline{K} \cdot \frac{\overline{V}_B}{\overline{V}_A} = Z_p$$
 (5.18)

where  $\overline{K}$ , the complex calibration constant, is, in general, a complex quantity and  $Z_p$  denotes the impedance measured at the E-H probe location. Bars on the signals  $V_A$  and  $V_B$  emphasize that these, in general, are complex voltages having both magnitudes (usually in mV) and phase angles in degrees. Before comparing  $Z_p$  with the impedance at the end of the test line (which is attached to its "LOAD" end), one needs to transform this impedance via the length  $\ell$  (electrical length) to the load plane. Such a transformation is given by a well known formula from the transmission line theory:

$$z_{L} = \left[\frac{z_{p} - jz_{c} \tan \beta_{0} \ell}{z_{c} - jz_{p} \tan \beta_{0} \ell}\right] z_{c}$$
 (5.19)

where  $Z_C = 50~\Omega$  is the characteristic impedance of the line,  $\beta_0 = 2\pi/\lambda_0$  ( $\lambda_0$  is the free space wavelength).  $Z_D$  is the impedance measured at the location of V-I block and is computed from Equation (5.18).  $Z_L$  is then the value of unknown impedance attached to the load side of the test line (e.g.  $Z_{IN}$  for the spherical antenna of our problem).

The easiest way to find the calibration constant  $\overline{K}$  is to place a "matched termination" ( $Z_L = 50~\Omega$ ) at the load end of the test line. Then from Equations (5.18) and (5.19) one gets,

$$\overline{K} \cdot \frac{\overline{V}_{B1}}{\overline{V}_{A1}} = Z_p = 50 \Omega \qquad (5.20)$$

Since  $\overline{V}_{B1}$  and  $\overline{V}_{A1}$  can now be read directly from the vector voltmeter, Equation (5.20) gives us the value of  $\overline{K}$  for the frequency of operation. It should be noted that  $\overline{K}$  is a function of frequency and the device should be calibrated for each frequency. Also note that  $V_A$  is a reference signal and therefore,  $/V_A = 0^\circ$  and  $/V_B$  is the angle (in degrees) as read from the vector voltmeter.

3. As can be seen from Equation (5.19), we need to know the electrical length from the location of the E-H probe to the plane of the unknown load. The electrical length is different from the physical length (which is known) because of the dielectric supports used in the connectors. In general, the actual electrical length is longer than the physical length. The best way to measure this length is to place a short termination ( $\mathbf{Z}_{\mathbf{L}} = \mathbf{0}$ ) at the load part of the test line. This leads to

$$Z_p(short) = jZ_c tan \beta_0 \ell$$
 (5.21)

which is obtained from Equation (5.19) with  $Z_L = 0$ . Recording the measurement at the probe location,

$$z_{p}(short) = \overline{K} \cdot \frac{V_{B2} \frac{/V_{B2}}{V_{A2} \frac{/0}{0}}}{V_{A2} \frac{/0}{0}}$$
 (5.22)

where  $\overline{K}$  has been found in the previous step. By this method one can find the unknown electrical length. The value of the physical length should always be used to check the algebra involved. One has to be careful in computing the electrical length  $\ell$  because a small error in  $\ell$  can lead to a significant error in  $\overline{Z}_L$  due to rapid variation of  $\tan \beta_0 \ell$  in Equation (5.19). This is a drawback of this method.

The advantage of the E-H probing method is that it can be used for a wide range of the operating frequency (e.g. from 1 MHz to 1000 MHz). While for the conventional slotted line method we are restricted to a shorter range of frequency because at low frequency an excessively long slotted line is needed. Another point, which is important in the measurement of impedances for our problem, is that if the resistive part of the impedance is very small, it is very difficult to employ the slotted line technique. The reason is that a low resistance causes a high SWR on the transmission line and it cannot be measured accurately. On the other hand, with the E-H probe method, we can measure resistances as low as 0.5 ohm. For the case of small spherical antennas we encounter small values of  $R_{TN}$  (input resistance) and it was only possible to measure a small  $\,R_{_{T\,N}}^{}\,\,$  with

the E-H probe device. One source of errors in using the E-H probe device may be due to inaccuracy in phase readings and a possible error in measuring the electrical length & mentioned previously. To check the accuracy of the device and to clarify the steps needed for using the V-I impedance device, a numerical example is worked out here.

NUMERICAL EXAMPLE: To check the calibration of the E-H probe and its accuracy, we select a known  $100-\Omega$  GR termination as our "unknown" load. First we choose the frequency of operation as f = 600 MHz and the steps outlined above are taken with the following results:

- (a) Phase meter is calibrated according to Figure 5.5(i.e. "0" phase reading).
- (b) A matched load (50  $\Omega$ ) is placed at the "LOAD" side of the test line and the readings from the vector voltmeter are recorded as

$$V_B = 6.55 \text{ millivolts}, \ \underline{V}_B = +101^{\circ}$$
 $V_A = 69.9 \text{ mV}, \ \underline{V}_A = 0^{\circ}$ 

such that the calibration constant  $\overline{K}$  found from Equation (5.18) is

$$\overline{K} \frac{\overline{V}_B}{\overline{V}_A} = 50 \Omega; \overline{K} = 533.587 /-101^{\circ} \Omega$$

(c) With the load in place, the following readings are obtained:

$$V_B = 6.45 \text{ mV}, \ \underline{/V_B} = 138^{\circ}$$
  
 $V_A = 74 \text{ mV}, \ \underline{/V_A} = 0^{\circ}$ 

The impedance at the probe location can now be found from Equation (5.18) as

$$z_p = \overline{K} \frac{\overline{V}_B}{\overline{V}_A} = 46.5 /+37^\circ = 37.136 + j27.984 \Omega$$
 (5.23)

This impedance  $\mathbf{Z}_{\mathbf{p}}$  is the one measured at the probe location looking toward the load and should be transformed through the electrical length  $\ell$  to get the actual load impedance.

(d) The electrical length  $\ell$  is found by placing a GR-WN short termination at the "LOAD" side of the test line. The following readings are recorded:

$$V_B = 12.2 \text{ mV}, /V_B = +12^{\circ}$$
  
 $V_A = 43.7 \text{ mV}, /V_A = 0^{\circ}$ 

Using Equation (5.18) one gets

$$z_p$$
(short) = 533.587  $/-101^\circ$  ·  $\frac{12.2 /12^\circ}{43.7 /0^\circ}$ 

or 
$$Z_p(short) \doteq -j 148.965 \Omega$$

Equation (5.21) can now be used:

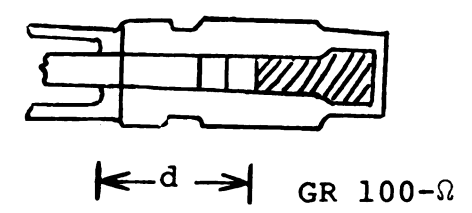
-j 148.965 = j 50 tan 
$$\beta_0 \ell$$

i.e. 
$$\tan \beta_0 \ell = -2.9793$$

For  $\lambda_0 = 50$  cm (f = 600 MHz) we get

$$\beta_0 l = 108.5543$$
° or  $l = 15.077$  cm.

It is noted that the physical length was roughly 14 cm. Before transforming  $Z_p$  of Equation (5.23) we note that the actual position of our unknown load is at  $\ell + d$  (see the illustration) from the probe location, where from the GR catalog,



$$d = 3.2 + 0.55 = 3.75$$
 cm

Thus,

$$\ell + d = 15.077 + 3.75 = 18.827 \text{ cm} = \ell'$$

(e) The last step is to transform the impedance  $\mathbf{Z}_{\mathbf{p}}$  through the length  $\ell$ '. This can be done by using Equation 5.19 (or by the use of the Smith chart) to find

$$Z_{L} = 99.2 + j10.5 \Omega$$
 (5.24)

as the unknown load impedance. Considering the fact that this is a 100  $\Omega$  termination and that there is always a reactive component of the impedance in the R.F. range, we see that the E-H probe system gives an accurate measurement of the impedance to be measured.

To see the effect of the frequency change, we repeated the above example at f = 250 MHz. Skipping the steps (a) to (e) we found the following values:

$$\overline{K} = 252.84 / +80^{\circ}$$

Comparing this to  $\overline{K} = 533.587 / -101^{\circ}$  for the case of f = 600, we see the frequency dependence of the calibration factor.

At 250 MHz, we have found

$$Z_{\tau} = 99.95 + j1.92 \Omega$$
 (5.25)

as the value of the load impedance (100  $\Omega$  termination). Again there is a good agreement between the measured value and the known value of the impedance.

5.2. Experimental Setup for the Measurement of the
Input Impedance of a Dielectrically Coated Spherical
Antenna in a Finite Conducting Body

In this section we discuss the experimental arrangements for measuring the input impedance which was theoretically discussed in Chapter 4. Although the far zone radiation characteristics of a coated spherical antenna were measured by other investigators [16] at microwave frequencies, to our best knowledge, the input impedance of a coated spherical antenna has not been measured before. A difficulty here was the construction

of the conducting body filled with Saline solution and the problem of water leaking which was solved by a proper sealing. If phantom materials which approximate actual biological tissues are used, the leaking problem can be eliminated.

Figure 5.6 shows the complete experimental setup used to measure the input impedances. An anechoic chamber (6' × 6' × 5') was covered at the top side with an aluminum ground plane. As the experimental results in the next section will show, this chamber lined with the microwave absorbers was sufficient to simulate the free space needed for the experimentation.

The cross sectional view of the metallic hemisphere together with the dielective coating and the conducting body is shown in Figure 5.6. The radius of the hemisphere (made from aluminum) was of the order of 1 cm and that of the conducting body was 5.5 cm. The dielectric coating shells were constructed of different outer radii and the actual datas are indicated in the next section. The metallic hemisphere was insulated from the ground plane with a narrow dielectric disk (Nylon or Teflon) of the thickness of about 1 mm. (This corresponds to  $\theta_0 = 5^{\circ}$  as the half angular width of the gap region discussed in Chapter 4). The insulating dielectric shell was supported by plastic screws from the ground plane. The saline solution was stored in a small tank and small

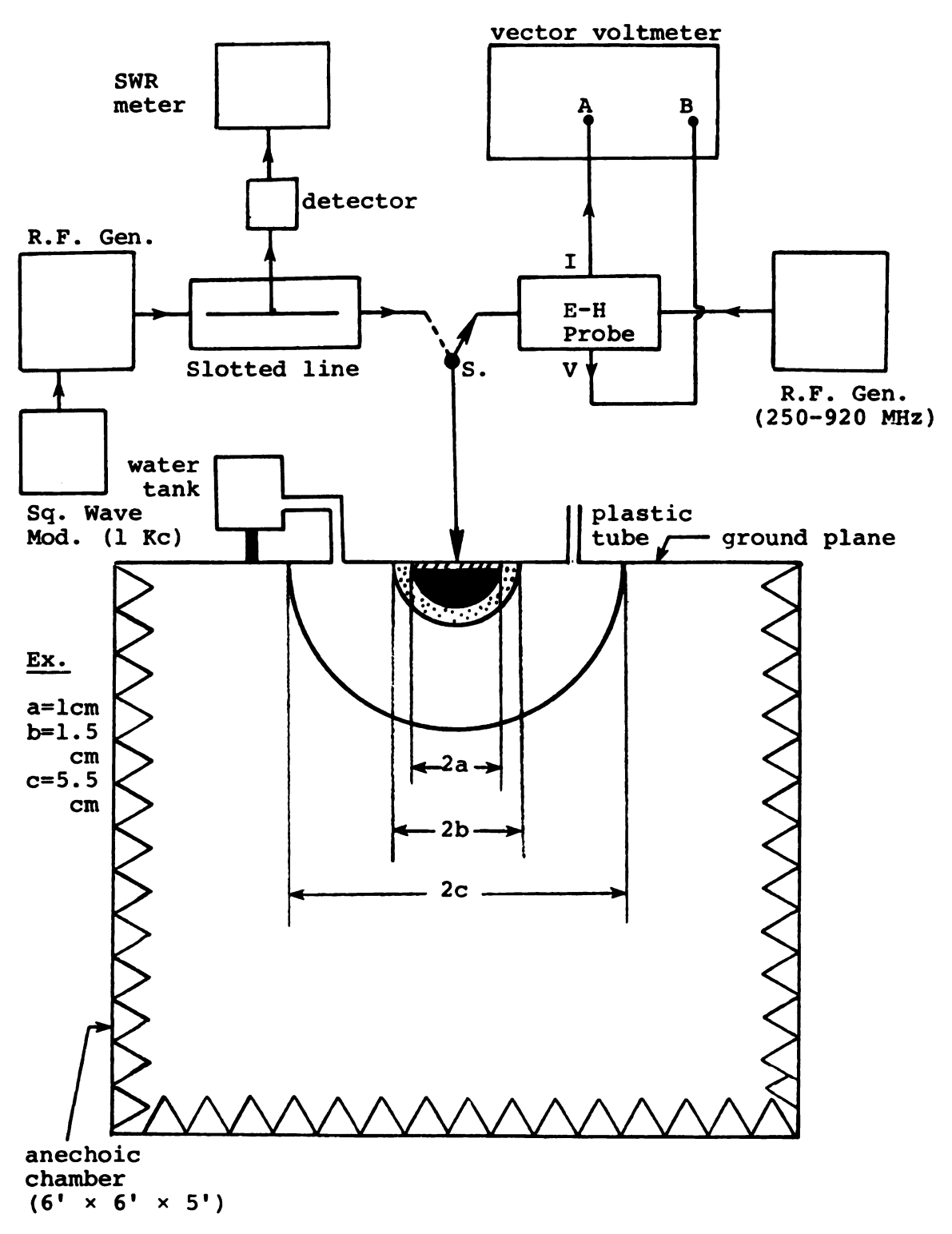


Figure 5.6. Experimental Setup for Measuring the Input Impedance of a Dielectrically Coated Hemisphere in a Finite Conducting Body.

plastic tubes were used to connect between the tank and the conducting body in such a way that the saline solution inside the conducting body was in close touch with the ground plane and air bubbles were thus avoided. The conducting body was constructed from a thin plastic material. To feed the antenna, we need a transition from a standard coaxial line (which has a center conductor with a diameter in order of 1 cm) to a smaller size connector in which it has a center conductor with a much smaller cross section compared with that of the hemisphere.

After constructing the chamber and the spherical antenna, the whole system was connected as shown in Figure 5.6 to measure the input impedance with the two methods mentioned previously. In the top left of Figure 5.6, we show the connection for the slotted line measurements. For this measurement, the minimum point is located in the slotted line with the antenna connected and then it is removed and replaced with a short circuit. The shift in the minimum points for the cases of the antenna and the short circuit is then used in the Smith chart calcula-The SWR was measured by a SWR meter. It is tion. mentioned that the reactance part of the impedance usually can be measured very accurately by this method. top right of Figure 5.6, we show the E-H probe connection discussed in the last section. Note that IKC modulation used in the slotted line measurement was not used in the E-H probe technique.

Using the experimental setup presented in this section, we were able to measure some input impedances of the insulated hemispheres imbedded in a conducting medium and in free-space. These experimental results are compared with theoretical results. Due to constructional difficulty and the time limitation, it was only possible to measure some typical cases in the experiment. However, a limited amount of experimental results was sufficient to verify the accuracy of the theoretical results presented in the preceding sections.

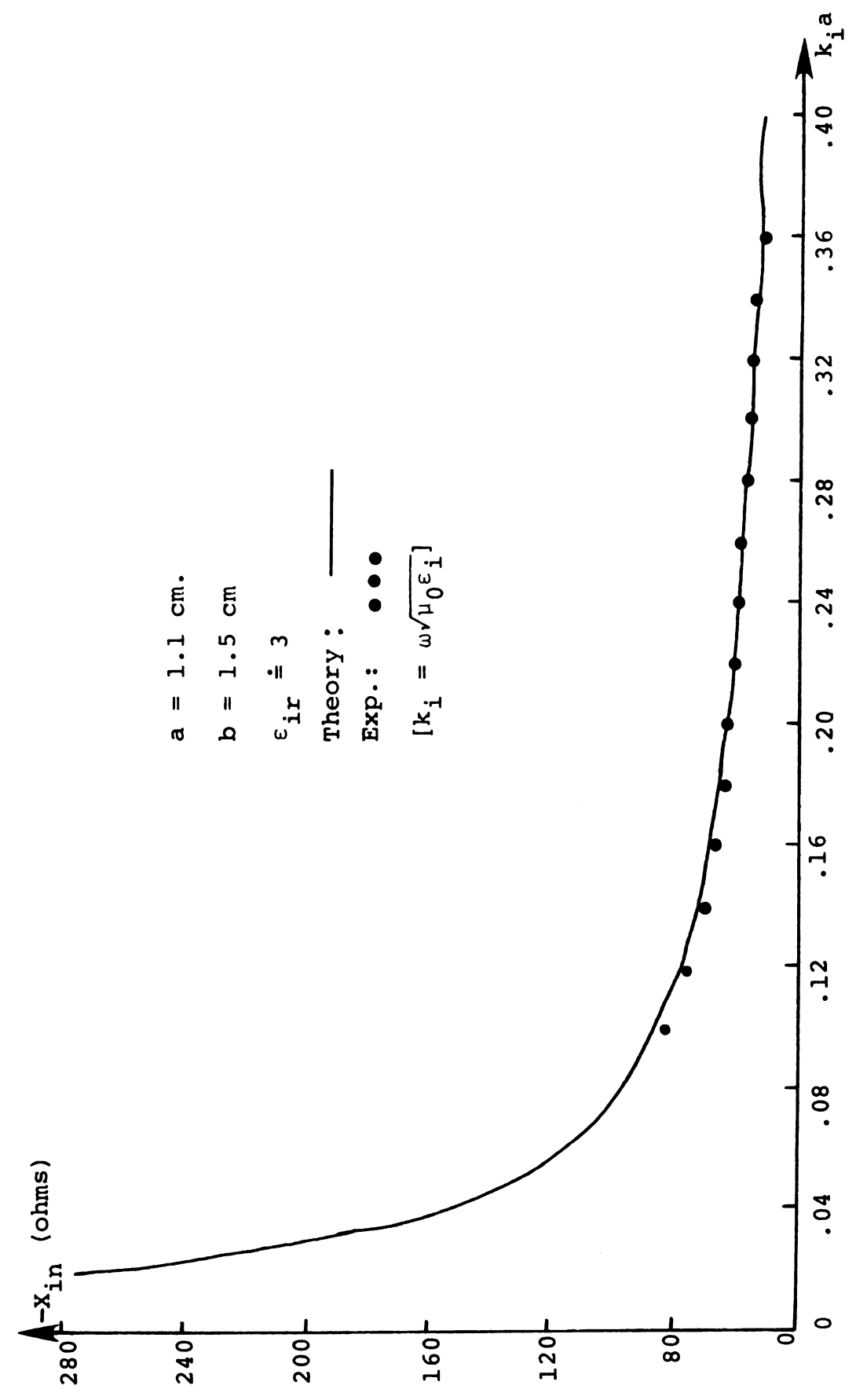
## 5.3. Comparison of Theory and Experiment

Before attempting to compare the values of input impedances based on the Equation (4.92) of the last chapter with experimental results, it is reminded that experimental results of the input impedance were measured at the center of the antenna, instead of the edge. Therefore, as discussed in the last section of Chapter 4, it is necessary to transform the "edge" impedance to the center of the sphere by using either the radial transmission line theory or the junction capacitance correction. Furthermore, since an image ground plane was used in the experiments, only 1/2 of the input impedance of the antenna was actually measured. In other words,

$$Z_{IN}$$
 (hemisphere) = 1/2  $Z_{in}$  (5.26)

where  $Z_{\text{in}}$  is the input impedance of the spherical antenna (sections 4.7 and 4.8) at the center and  $Z_{\text{IN}}$  (hemisphere) is the value measured experimentally. These facts have been taken into account in the comparison of theory and experiment.

Figure 5.7 shows the input reactance of a dielectrically coated hemisphere in free space. This can be regarded as a special case of our general problem. The curve is plotted against  $k_i$  a where  $k_i = \omega \sqrt{\mu_0 \epsilon_i}$ ,  $\varepsilon_i = \varepsilon_{ir} \varepsilon_0$  and  $\varepsilon_{ir}$  is the relative dielectric constant of the insulating material (Nylon) and is estimated to be  $\epsilon_{ir} \doteq$  3.0, a is the radius of the antenna. The dots are experimental results while the solid curve is the theoretical result based on the computation of Chapter 4 ( $\theta_0$  is about 5 degrees). Only the reactance is shown because the input resistance is negligible compared with  $\mathbf{X}_{\tau\mathbf{N}}$  for small  $\mathbf{k}_{\mathbf{i}}$ a. Naturally, the input resistance increases as the frequency is increased. Note that the plot can be considered to be as a function of frequency because in the actual experiment the radius a of the hemisphere was kept constant and the frequency was increased. It is noted that the input resistance was measured to be approximately one ohm. This value is about 0.5 ohm bigger than the theoretical value. This is due to the losses in the system and insulating materials. The diameter of the hemisphere shown in Figure 5.7 is



Theoretical and Experimental Input Reactance of a Dielectrically Coated Hemisphere in Free Space as a Function of Frequency. Figure 5.7.

2.2 cm and that of the insulating shell is 3.0 cm. It is observed in the figure that a good agreement between theory and experiment was obtained.

As mentioned previously, the experimentation for the general case of an insulated spherical antenna in a finite conducting body was difficult to perform, however, some good results were obtained. They are summarized in the next few tables. In Table 5.1, we show the values of the input reactance of a coated hemisphere with a = 1.1cm and b = 1.21 cm (b/a = 1.1) when imbedded in a finite conducting body of c = 5.5 cm. The frequency used was 600 MHz and the insulating material had  $\epsilon_{ir} = 3.0$ . medium in the conducting body was changed from air, distilled water, to saline solutions of various normality ranging from 0.5N to 2.0N. The electrical parameters of the solution were computed based on the available theory [17]. As shown in the last two columns of the table, there is a good agreement between theory and experiment. Also note that this is the case of relatively thin coating and there is a considerable variation in  $X_{TN}$  (and hence in  $\mathbf{Z}_{\mathsf{TN}}$ ) of the spherical antenna as the properties of the external medium are changed. The input resistance was small but it was increased as the normality of the solution was increased from 0 to 2.

Next, the thickness of the dielectric coating was increased. Table 5.2 shows similar results as that of

Table 5.1. Theoretical and Experimental Values of the Input Impedance of a Coated Hemispherical Antenna in a Finite External Medium. (a = 1.1 cm., b = 1.21 cm., c = 5.5 cm., f = 600 MHz,  $\epsilon_{ir} \doteq 3.0$ ) (T = 20°c)

EXTERNAL MEDIUM	PARAMETERS		j X <sub>IN</sub> (OHMS)		
MEDIUM	$\epsilon/\epsilon_0$	σ(mho/m)	THEORY	EXPERIMENT	
AIR	1.0	0.0	-j 20.99	-j 19.5	
DIS. WATER	79.89	0.095	-j 9.057	-j 11.50	
.5N SALINE	70.92	4.52	-j 8.23	-j 10.1	
1.0N SALINE	62.93	7.74	-j 8.07	-j 8.0	
1.5N SALINE	56.94	10.84	-j 8.06	-j 8.8	
2.0N SALINE	50.95	13.84	-j 8.08	-j 9.15	

Table 5.2. Theoretical and Experimental Values of the Input Impedance of a Coated Hemispherical Antenna in a Finite External Medium. (a = 1.1 cm., b = 1.5 cm., c = 5.5 cm., f = 600 MHz,  $\epsilon_{ir} \doteq 3.0$ ) (T = 20°c)

EXTERNAL MEDIUM	PARAM	IETERS	j X <sub>IN</sub> (OHMS)	
	$\epsilon/\epsilon_0$	σ(mho/m)	THEORY	EXPERIMENT
AIR	1.0	0.0	-j 19.34	-j 18.76
DIS. WATER	79.89	0.095	-j 14.89	-j 14.55
0.5N SALINE	70.92	4.52	-j 14.57	-j 14.08
1.0N SALINE	62.93	7.74	-j 14.55	-j 14.03
1.5N SALINE	56.94	10.84	-j 14.55	-j 13.98
2.0N SALINE	50.95	13.84	-j 14.56	-j 14.16

Table 5.1, except that now b = 1.5 cm (b/a = 1.36). Again, the input reactance was measured for different external media. For this case, as shown in the last two columns of the table, there is a smaller variation in  $X_{IN}$  (and hence in  $Z_{IN}$ ) as the external medium is changed. Note that this is the case of a relatively thick coating and the experimental results are in agreement with the theoretical predictions of Chapter 4.

Finally, in Table 5.3, the case of an even thicker cotaing, b = 3.1 cm (b/a = 2.82) is shown. In this case, as shown in the last two columns of the table, there is nearly no variation in the input reactance (and hence in the input impedance) of the spherical antenna as the properties of the external medium are changed. Again, there is a good agreement between theory and experiment.

In consistence with the conclusion made in the last chapter, we have found experimentally that to fabricate a probe which has an input impedance independent of the electrical parameters of the surrounding medium, the thick coating of dielectric materials is needed. Of course, the coating cannot be excessive because small probe dimensions are desired and necessary conditions.

Before closing this section, it is interesting to observe the effects of the relative probe location in a finite conducting body on the antenna input impedance.

Theoretically, when the insulated spherical antenna of

Table 5.3. Theoretical and Experimental VAlues of the Input Impedance of a Dielectrically Coated Hemispherical Antenna in a Finite External Medium. (a = 1.1 cm., b = 3.1 cm., c = 5.5 cm., f = 600 MHz, ε<sub>ir</sub> = 3.0) (T = 20°c)

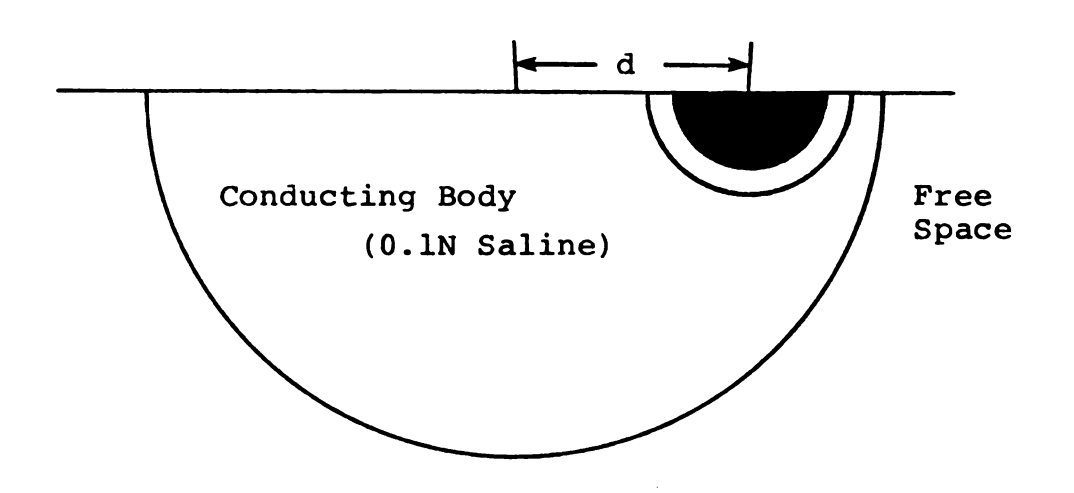
EXTERNAL MEDIUM	PARAMETERS		j X <sub>IN</sub> (OHMS)	
	$\epsilon/\epsilon_0$	σ(mho/m)	THEORY	EXPERIMENT
AIR	1.0	0.0	-j 22.54	-j 21.97
DIS. WATER	79.89128	0.09531	-j 21.59	-j 21.24
0.5N SALINE	70.92058	4.52694	-j 21.77	-j 21.50
1.0N SALINE	62.93319	7.74285	-j 21.75	-j 21.63
1.5N SALINE	56.94402	10.84945	-j 21.75	-j 21.50
2.0N SALINE	50.95491	13.84467	-j 21.75	-j 21.48

Figure 4.1 is not at the center of the spherical conducting body, the problem becomes untractable. However, we can get some idea of the situation by measuring the input impedance of a coated spherical antenna located off-center in a finite conducting body.

In Table 5.4, we show the measured input impedance of an insulated hemisphere as a function of the offcenter distance d. The conducting medium is a 0.1N saline solution and has the parameters of  $\epsilon_r = 77.9$  and  $\sigma = 0.925$  mho/m. The hemisphere has a radius a = 1.1 cm and that of insulating shell is b = 1.2 cm (b/a = 1.09). The conducting body has a radius c = 5.5 cm and the frequency is f = 600 MHz. The relative dielectric constant of the coating is again  $\epsilon_{ir} \doteq$  3.0. As shown in the table, there is some variation in the input impedance as the antenna is moved from the center to the boundary of the conducting body. When d = 0, the antenna is in the center of the body and the theoretical value of the input impedance is shown. As this is the case of thin coating, the variation of the input impedance is expected according to the theory of Chapter 4.

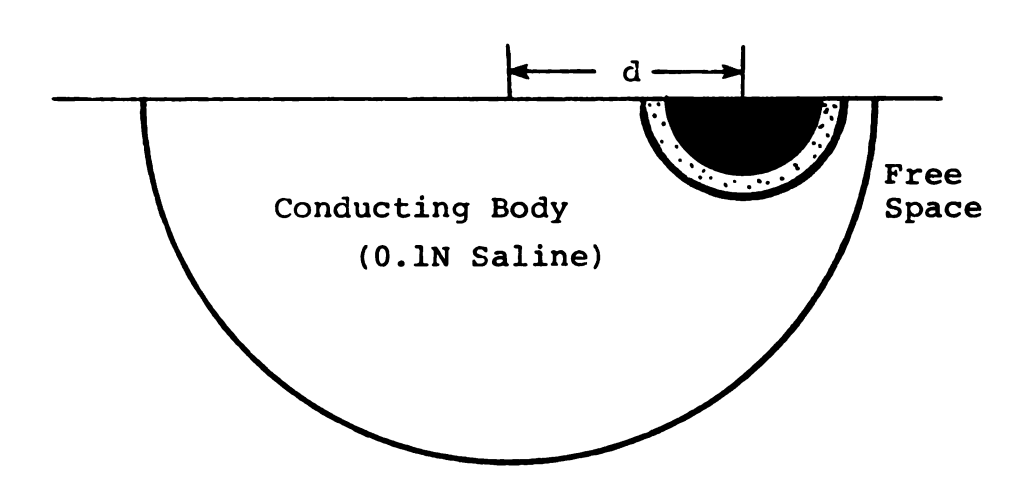
Next, in Table 5.5, we show similar results as in Table 5.4, except that now the coating is increased to b = 1.6 cm (b/a = 1.45). As shown in the table, there is a considerably smaller variation in the input impedance as the antenna is moved off-center.

Table 5.4. Experimental Input Impedance of a Dielectrically Coated Hemispherical Antenna at Different Locations in a Finite Conducting Body (a = 1.1 cm., b = 1.2 cm., c = 5.5 cm.,  $\epsilon_{ir} \doteq 3.0$ ,  $\epsilon_{r} = 77.898$ ,  $\sigma = 0.925$  mho/m, f = 600 MHz; d is the Distance from the Center of the Antenna to the Center of the Conducting Body).



d (cm.)	Z <sub>IN</sub> (ohms)	Z <sub>IN</sub> (ohms)		
0.0	1.0 -j10.5 (Theory:	1.0 -j10.0)		
2.6	1.3 -j14.15			
3.3	1.5 -j15.0			

Table 5.5. Experimental Input Impedance of a Dielectrically Coated Hemispherical Antenna at Different Locations in a Finite Conducting Body (a = 1.1 cm., b = 1.6 cm., c = 5.5 cm.,  $\epsilon_{ir} \doteq 3.0$ ,  $\epsilon_{r} = 77.898$ ,  $\sigma = 0.925$  mho/m, f = 600 MHz; d is the Distance from the Center of the Antenna to the Center of the Conducting Body).



d (cm.)	z <sub>IN</sub> (ohms)	
0.0	0.8 - jl6.0 (Theory:	0.2 - j15.56)
2.6	1.0 - j16.6	
3.3	1.0 - j16.7	

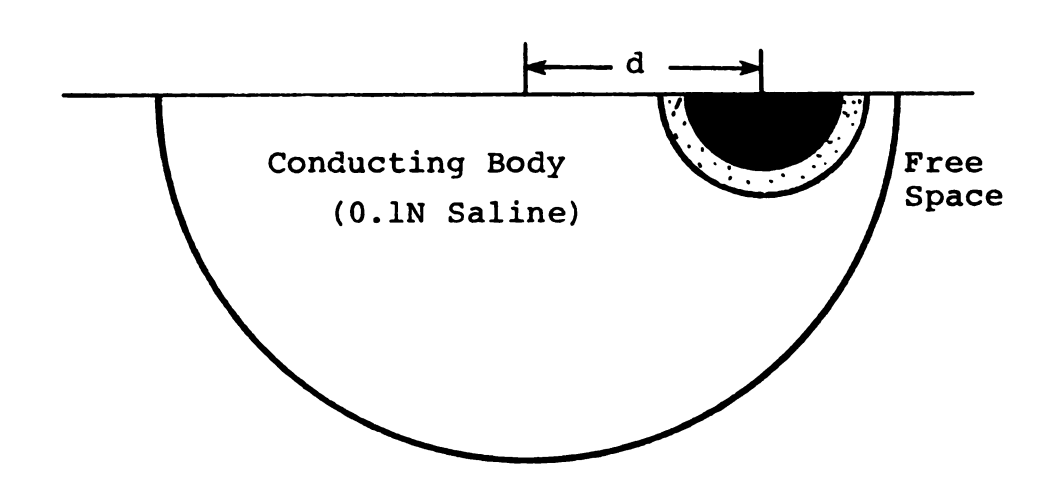
The last table, Table 5.6, shows similar results for the case of an even thicker coating with b = 2.2 cm (b/a = 2.0). We observe in the table that, there is practically no variation in the input impedance of the spherical antenna as it is moved in a conducting body. This implies that a probe with a relatively thick coating has an input impedance almost independent of the relative probe location in a biological (conducting) body. We have reached the similar conclusion theoretically in the last chapter.

# 5.4. Field Measurements using Insulated Spherical Probes

In this section, we discuss some experimental results on the induced electric field in a conducting medium measured with dielectrically coated spherical antennas studied previously. Figure 5.8 shows the schematical configuration of the insulated spherical probe used in the experiments. Two solid metallic hemispheres (made from brass) are separated by a small gap and a microwave diode detector (type HP 5082-2755) is mounted between them as shown in the figure. Two highly resistive thin wires (Nichrome V wires of 2 mil diameter) are attached to the terminals of the diode and led all the way out to the voltage measuring device (a high gain D.C. voltmeter or a SWR meter). The whole structure is coated with a dielectric shell (plexiglas) and a small

		,

Table 5.6. Experimental Input Impedance of a Dielectrically Coated Hemispherical Antenna at Different Locations in a Finite Conducting Body (a = 1.1 cm., b = 2.2 cm., c = 5.5 cm.,  $\epsilon_{ir} \doteq 3.0$ ,  $\epsilon_{r} = 77.898$ ,  $\sigma = 0.925$  %/m, f = 600 MHz; d is the Distance from the Center of the Antenna to the Center of the Conducting Body).



d (cm.)	z <sub>IN</sub> (ohms)	
0.0	0.5 -j19.0 (Theory: 0.13 -j18.	5
2.6	0.56 -j19.0	
3.3	0.65 -j19.0	

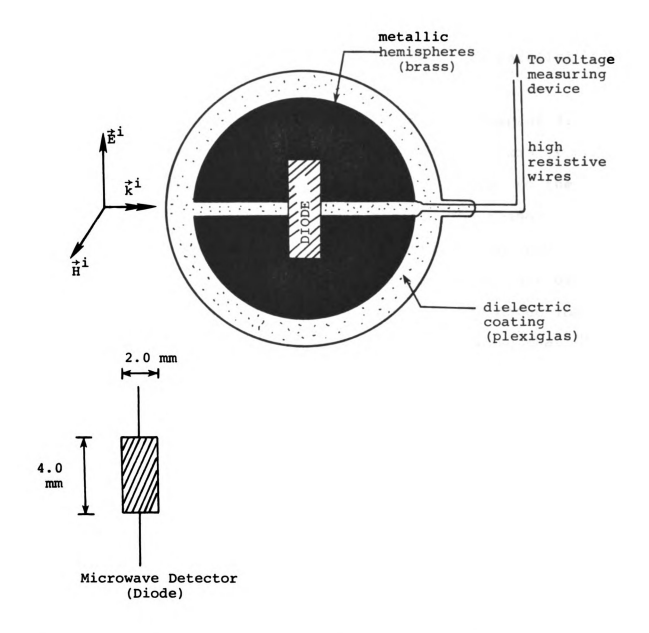


Figure 5.8. Configuration of the Dielectrically Coated Spherical Probe Loaded with a Microwave Detector. (Free Space Incident Plane Wave is also Shown.)

rod (tail) is left for holding the probe to a long plastic stick (not shown in the figure). The microwave detector is a cylindrical diode of diameter 2.0 mm and height 4.0 mm. Note that the diode detector in parallel with the resistive wires and the voltage measuring device constitute the load,  $Z_L$ , as discussed in Chapter 3. The probe can be rotated in such a way that the axis of the diode can be either parallel or perpendicular to the direction of the incident electric field. The reason for using high resistive wires is to minimize the lead wire interference with the incident EM wave. The use of high resistive wires, in turn, necessitates the detection of the probe output to avoid excessive loss due to the lead wires.

As a first series of measurements, we used the spherical probe of Figure 5.8 in a TEM transmission cell [18]. The cross section of the rectangular cell is shown in Figure 5.9 together with the insulated spherical probe. In this experiment, the output leads of the probe were connected to a high gain d.c. voltmeter (a capacitor was also used to filter out the a.c. signal). Before attempting to take any measurements, the output of the spherical probe was calibrated. This was done by monitoring the incident power into the cell from the R.F. generator via a directional coupler. The calibration curve so obtained is also shown in Figure 5.9.

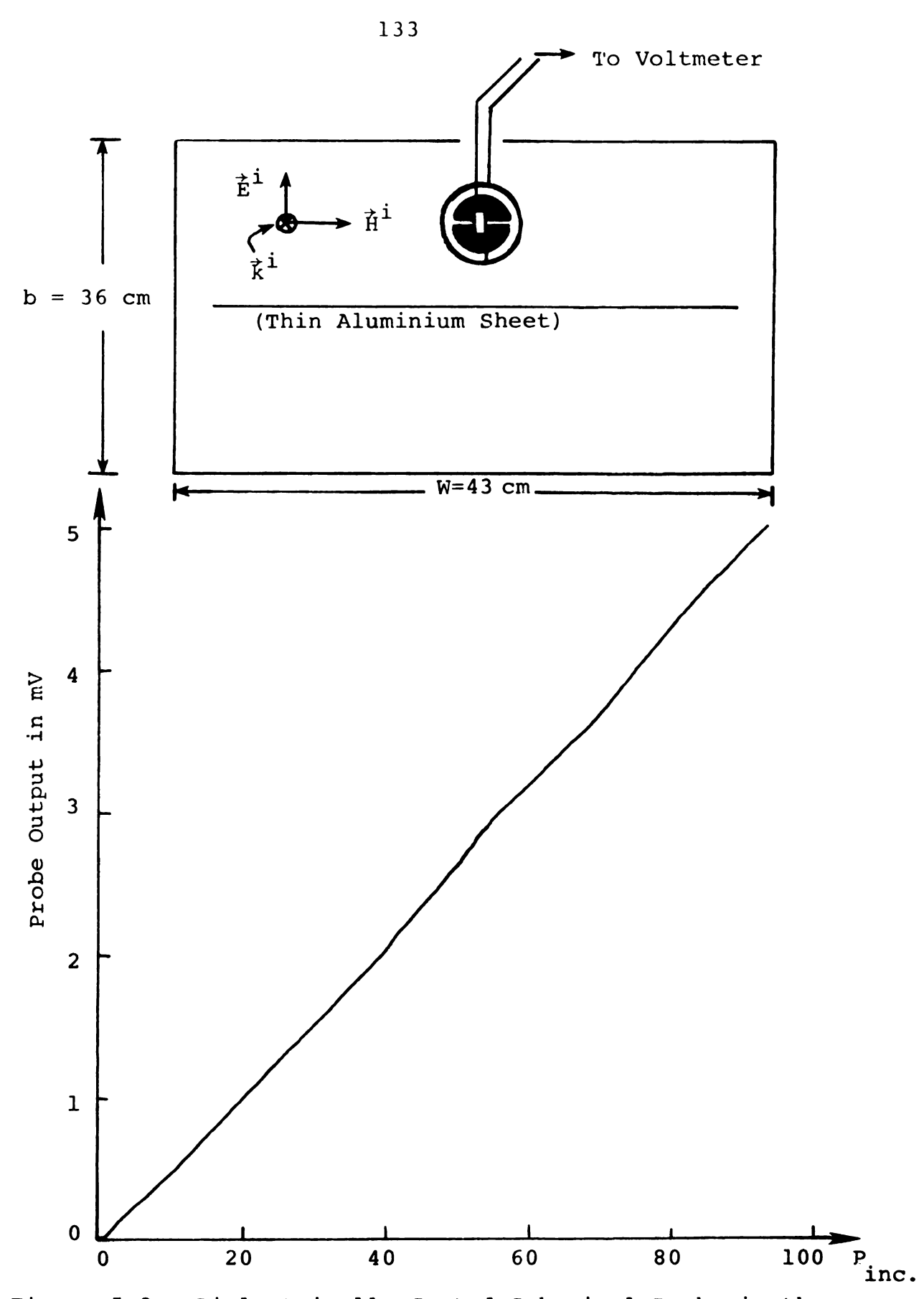
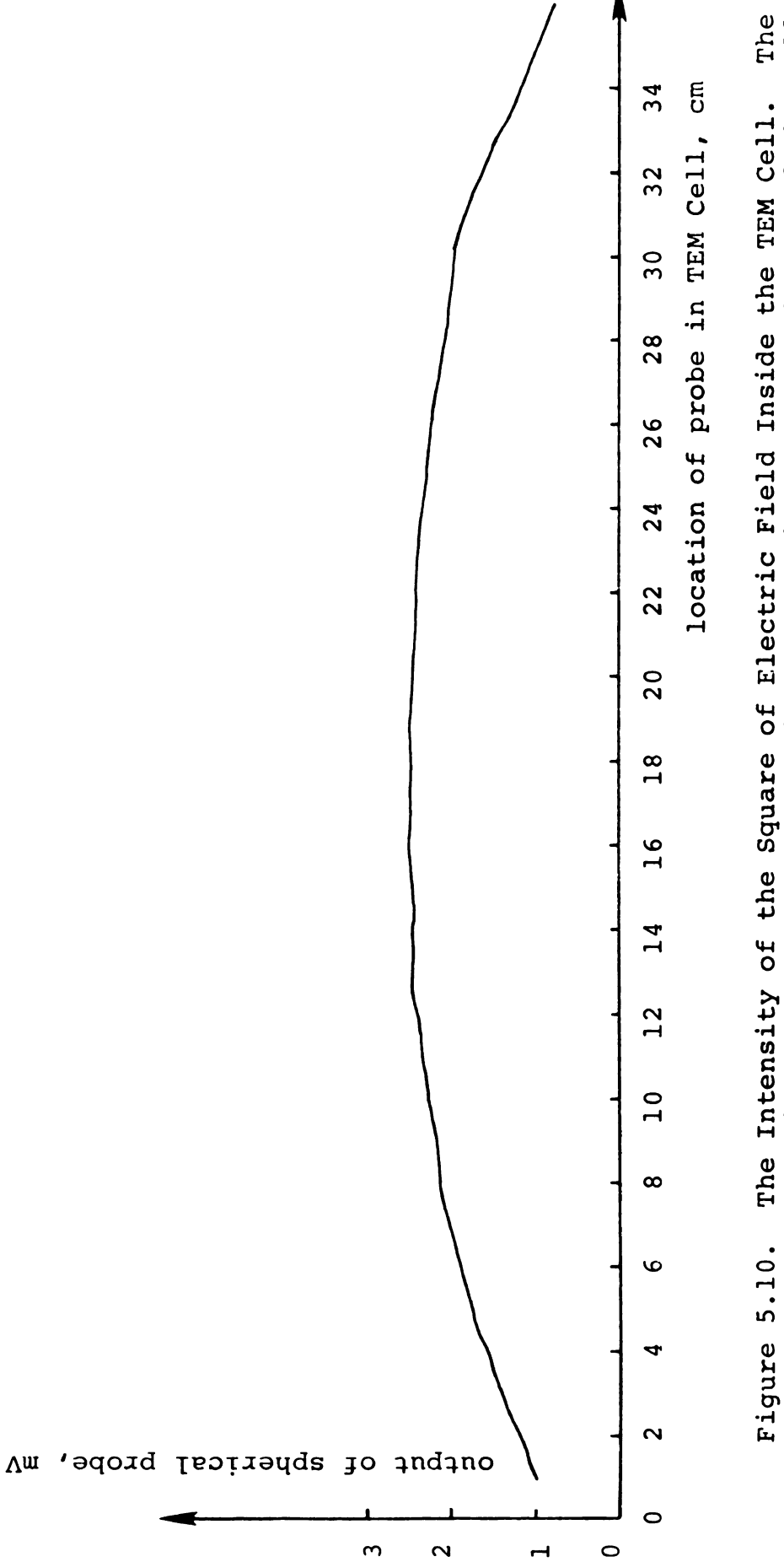


Figure 5.9. Dielectrically Coated Spherical Probe in the Upper Half Side of a TEM Transmission Cell. (Note: not drawn to scale). Calibration Curve of the Probe is also Shown.

As can be seen from the calibration curve, the microwave detector diode of the spherical probe is a Square Law Detector. (This is needed for the optimum operation of the SWR meter used to detect the output of the probes.) The output voltage was measured in millivolts while the incident power from the R.F. generator was in milliwatts. Since power is proportional to the square of the electric field (or the voltage), this means that the probe was actually measuring the square of the electric field at its location. After calibrating the probe, the intensity of the electric field was measured at 6 cm above the center conductor of the TEM cell (the frequency was f = 320 MHz). The result is shown in Figure 5.10. This agrees quite well with the results reported in Reference 18.

We also tried to measure the induced electric fields inside finite conducting structures containing saline solution placed inside the TEM cell. One such measurement is shown in Figure 5.11. Although the measured field was quite symmetric, as one expects theoretically, it was not possible to compare the experimental results with the theoretical induced field calculated by the tensor integral equation method [4] assuming the conducting structures located in free-space. The reason is believed to be due to the fact that when the conducting body is placed in an enclosed metallic chamber,





The Intensity of the Square of Electric Field Inside the TEM Cell. The Spherical Probe was Located 6 cm Above the Center Conductor of the Cell. f = 320 MHz.

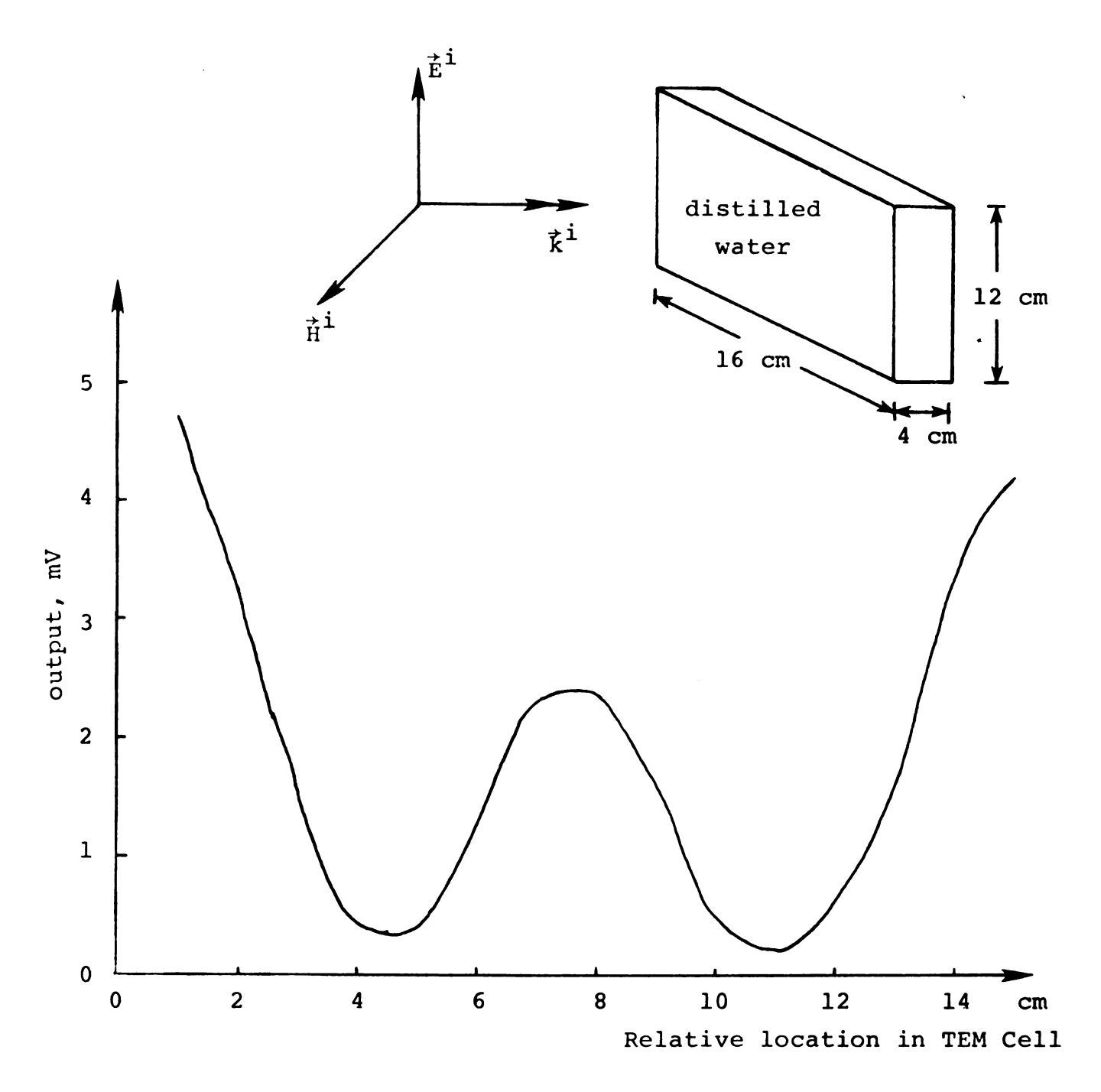


Figure 5.11. The Output of the Dielectrically Coated Spherical Probe Inside a Finite Body Containing the 0.0N Solution. The Frequency is f = 320 MHz.

the wall image effect prevails and, thus, the body can no longer be assumed to be in the free space. The conducting body had the dimensions of 16 cm × 12 cm × 4 cm and the frequency of the incident plane wave was f = 320 MHz. The incident electric field was polarized in the vertical direction (x - axis). In order to study the case of the conducting body in free space, the box containing the saline solution was removed from the TEM cell and placed in a large microwave Anechoic chamber. The construction of this chamber was reported elsewhere [19].

The conducting body was illuminated in the "far zone" of the transmitting antenna within the anechoic chamber and the insulated spherical probe was placed inside the body in such a way that the direction of the incident electric field was perpendicular to the plane of the equatorial gap. On the ceiling of the anechoic chamber in the far field region, a slot was cut, and through which a long plastic stick supporting the probe assembly was connected to the voltage measuring device located outside the A.C. The stick was attached to a shaft driven by a d.c. motor so that the probe can be moved inside the conducting medium by a remote control system. An x - y recorder was used to plot the distribution of the square of the electric field induced in the finite conducting body. A diagram of the anechoic chamber and the configuration of the body is shown in Figure 5.12.

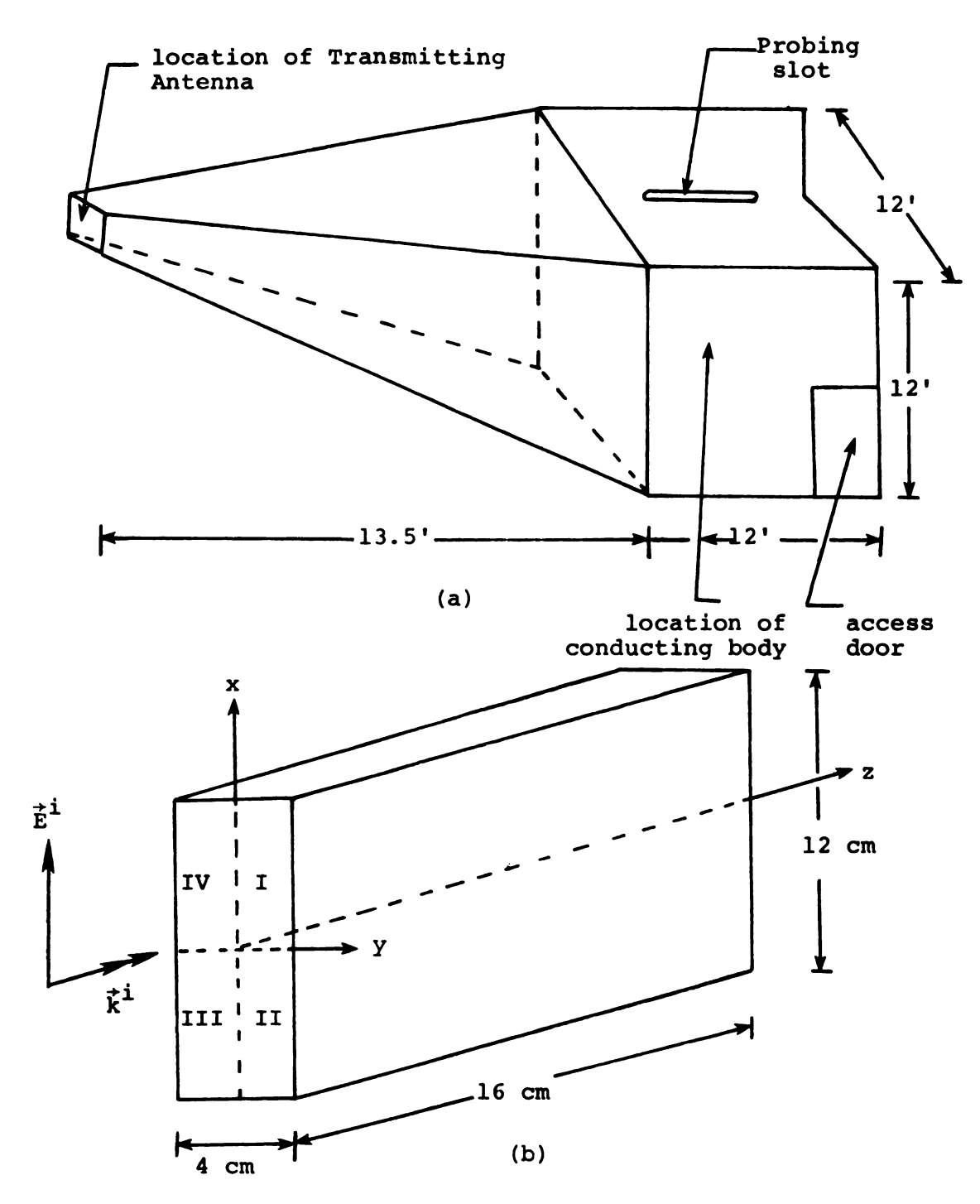
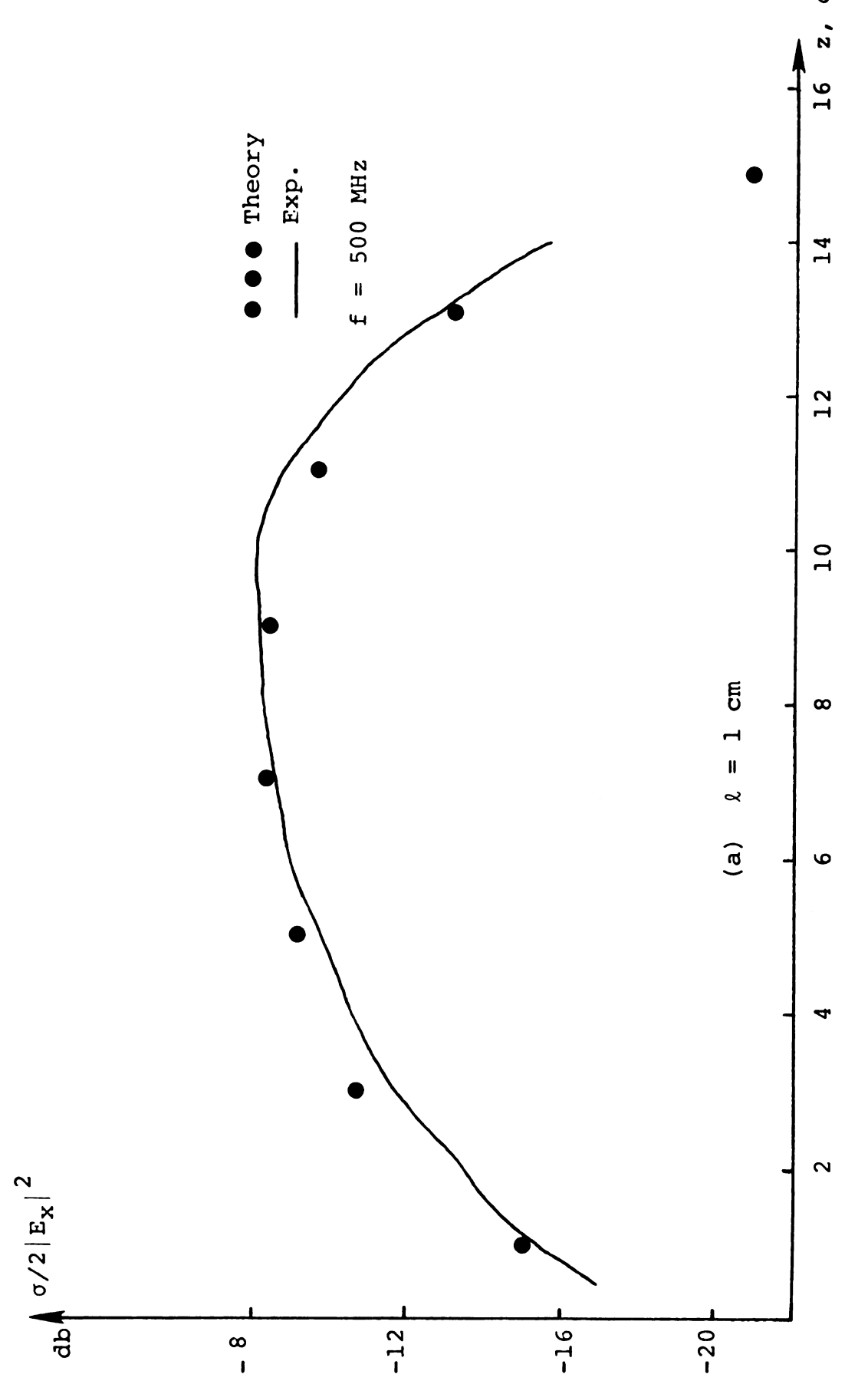


Figure 5.12. (a): Three Dimensional View of Tapered Anechoic Chamber. (b): Conducting Body Illuminated by Incident EM Wave.

The dimensions of the conducting body were 16 cm × 12 cm × 4 cm. The conducting body can now be considered to be located in the free space, and theoretical results for this case are obtainable by the existing theory and an available computer program [20]. To compute the induced electric field, the body was partitioned into 96 of 2 cm<sup>3</sup> cubic cells. A symmetry condition was used to facilitate the numerical calculations.

In the experiment, the medium in the box was the distilled water (0.0N saline solution) and the operating frequency of the transmitting antenna was chosen as f = 500 MHz ( $\lambda_0$  = 60 cm; free space wavelength). At this frequency, the size of the insulated spherical probe as shown in Figure 5.8 was sufficiently small to produce meaningful results. In Figure 5.13 we show some results of the measurements. It is noted that the signal from the R.F. generator was amplified by a power amplifier (Hughes Model 46159H Transistor Amplifier, 500-750 MHz, 20 W) and that the received signal from the spherical probe was monitored on a SWR meter and then fed into x - y recorder (after d.c. filtering). The amplitudes shown in the figure are in db and the theoretical results are for  $\sigma/2|E_v|^2$  where for the distilled water at 500 MHz,  $\epsilon_{\rm r}$  = 79.92 and  $\sigma$  = 0.06 mho/m were assumed.



Along The Distribution of the Square of Electric Field Induced in a 16 cm  $\times$  12 cm  $\times$  4 cm Distilled Water Body as a Function of z Different Depths Indicated by the Parameter "%". Figure 5.13.

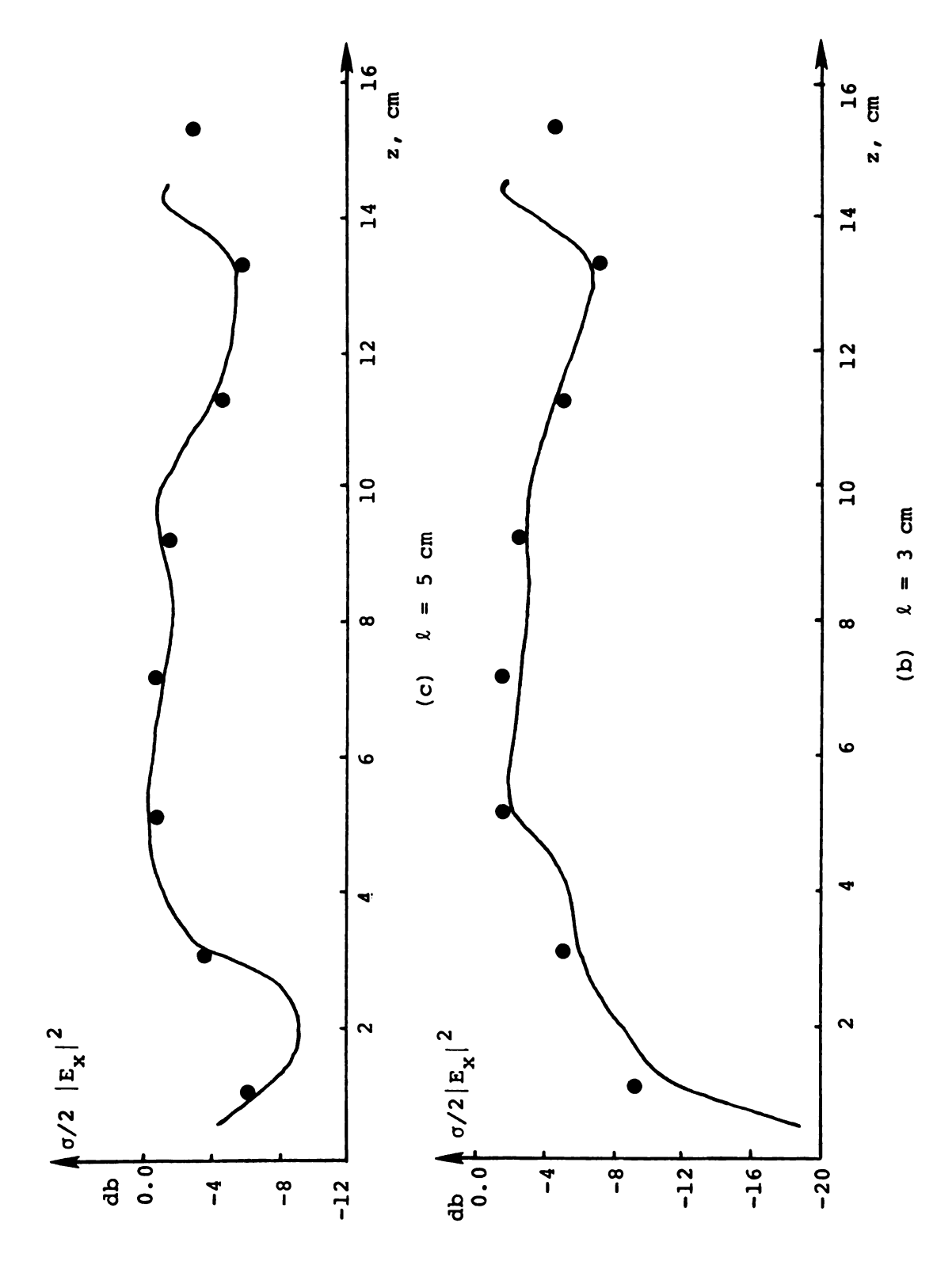
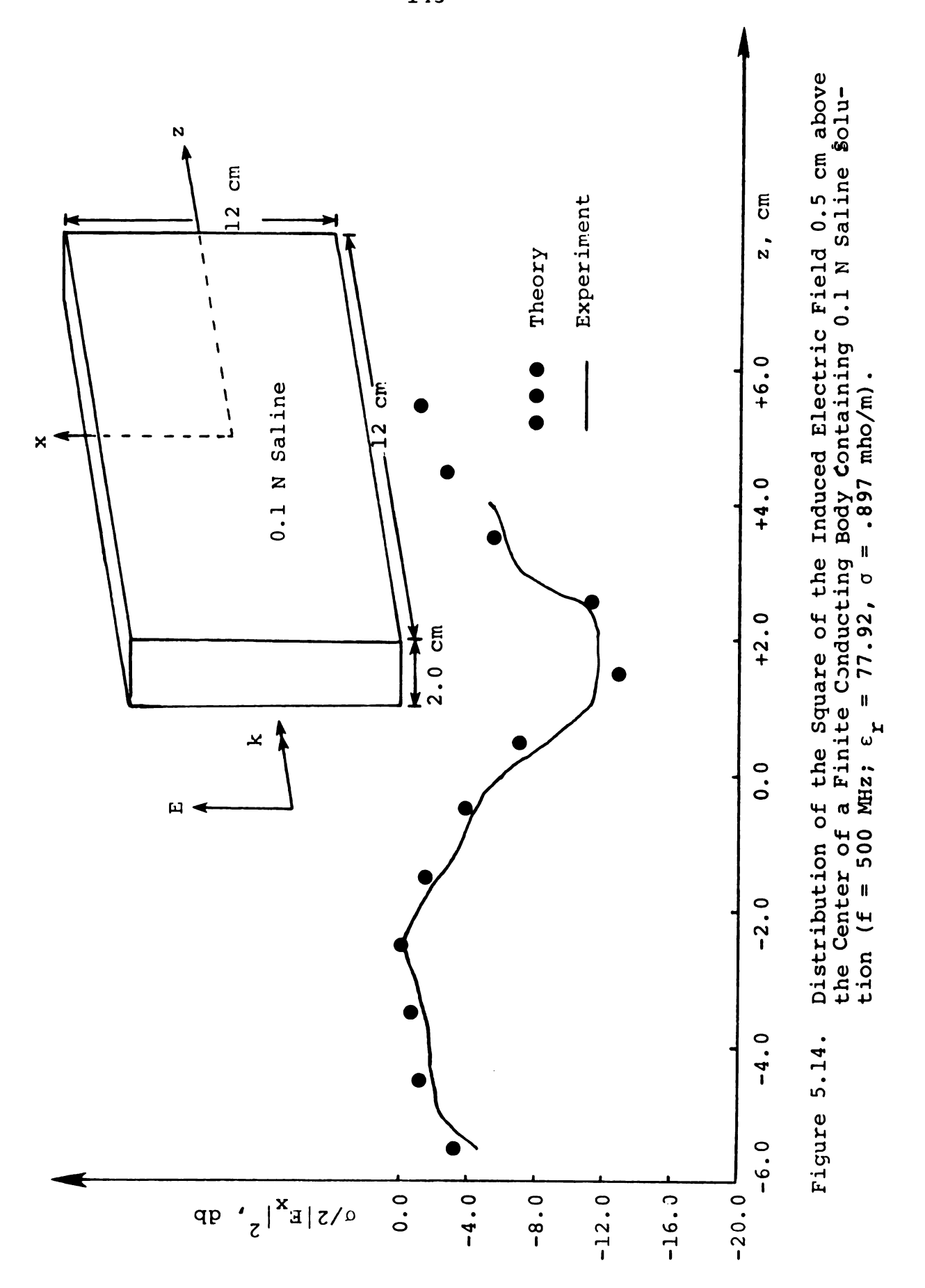


Figure 5.13 (continued)

Theoretical values were computed at the center of each cubic cell. The three plots of Figure 5.13 show the measured values of  $\sigma/2|E_v|^2$  as a function of z along three different depths from the top of the body. The parameter & indicates the distance from the top side of the medium to the center of the spherical probe. can be seen from Figure 5.13, the agreement between the theory and experiment is considered quite good in view of the fact that there exist some numerical errors in the theoretical computation and also some inherent experimental errors caused by lead wires and the container of the conducting medium (made from plexiglas materials). important to mention that, due to the improvement in the construction of the probe (a thicker coating), the experimental error at the body edge as discussed previously in Chapter 4 is now minimized. It is anticipated that if the size of the spherical probe is reduced, better experimental results may be obtained.

Finally, in Figure 5.14 we show similar measurements for a 16 cm  $\times$  12 cm  $\times$  2 cm body containing 0.1N saline solution for which  $\epsilon_{\rm r}=77.92$  and  $\sigma=0.897$  mho/m. The frequency is again 500 MHz and the theoretical results are obtained for cubic cells of 1 cm  $\times$  1 cm  $\times$  1 cm dimensions. Note that now there are more theoretical points for comparison with experiment.



### CHAPTER VI

## SUMMARY AND CONCLUSIONS

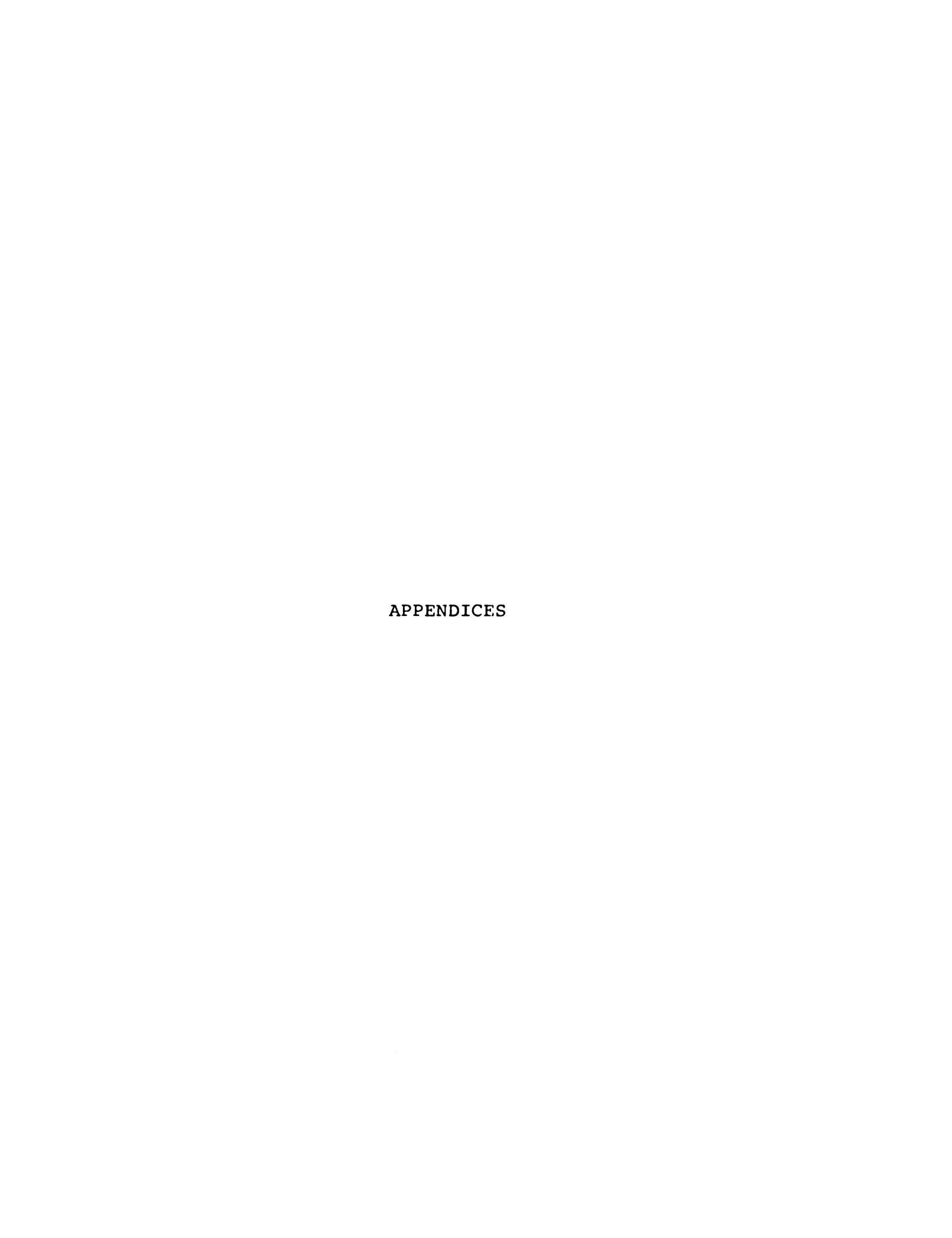
In this thesis we presented some theoretical and experimental results on the study of an electromagnetic spherical field probe in a finite conducting body. The spherical geometry was chosen because an exact, analytical solution can be found to the problem.

After deriving the general relation between the output voltage of a probe and the induced electric field in a volume conductor, the receiving characteristics of an insulated spherical probe immersed in a uniform electric field inside a conducting body were studied. The normalized effective diameter of the probe was shown to be nearly independent of the parameters and dimension of the conducting body when a relatively thick coating of insulating material was used on the probe. After that an expression for the input impedance of a dielectrically coated spherical antenna imbedded in a finite conducting body was derived. The matrix equation formulation was used first, but due to numerical difficulty, an alternative method, based on the transmission line theory, was used to obtain some numerical results. It was

subsequently shown that, for thick coatings with dielectrics of low dielectric constants the input impedance of the spherical probe became nearly independent of the electrical parameters and the dimension of the finite biological body.

Finally, we presented some experimental results on the input impedance of the spherical probe and compared them with the theoretical results. In general, there was a good agreement between theory and experiment. A few examples of actual field intensity measurements inside finite bodies were also reported.

In conclusion, we may say that to fabricate an implantable EM field probe which is insensitive to the properties and dimensions of the conducting body, one should use thick coating of low dielectric constant material to cover (or to insulate) the appropriate probe. Of course, the whole probe structure should be kept electrically small, therefore, as a topic for further research, one may consider the case of two or more thinner layers of different dielectric materials which may achieve the same purpose as a single thick layer of coating does.



### APPENDIX A

# HIGHER ORDER MODES AND THE CONVERGENCE OF THE INPUT ADMITTANCE EXPRESSION

The expression for the input admittance of a dielectrically coated spherical antenna in a finite conducting body, as shown in Figure 4.1, was derived in Equation (4.92) of Chapter 4. Although mathematically this represents the analytical solution to the problem, in a closed form, it is necessary to show that the series converges. Actually a close study of the series shows that its real part converges quickly after a few terms, but its imaginary part does not.

Another point is that, as was shown in Chapter 4, the Hankel functions involved may still cause some difficulty in evaluating very higher order modes. Therefore, it is desirable that to find appropriate forms for the higher order modes or Hankel functions of very high orders that are suitable for the computer computation. In the following, we will give the expressions for the higher order modes and show that the expression for the admittance converges if a finite gap of the antenna is assumed.

As was mentioned in section 4.5, the key quantity of the input admittance expression is  $R_{ln}(b)$ , repeated here for convenience:

$$R_{1n}(b) = \frac{z_{1n}^{+}(b) - z_{2n}^{+}(b) \cdot Q}{z_{1n}^{-}(b) + z_{2n}^{+}(b) \cdot Q}$$
(A.1)

where the complex quantity Q is defined as

$$Q = \frac{1 - K_{2n}(b,c)R_{2n}(c)Z_{2n}^{-}(b)/Z_{2n}^{+}(b)}{1 + K_{2n}(b,c)R_{2n}(c)}$$
(A.2)

other quantities have been defined previously. Actually the dependence of the input admittance of the insulated spherical antenna on the parameters  $(\varepsilon,\sigma)$  and the dimension (c) of the finite conducting body is all given by the complex quantity Q. In the actual computation of the input admittance expression, using a computer, the difficult quantity to compute, for the higher order modes, is this complex quantity Q. However, after few computer programs were run to cover various cases, it was found that for nearly all cases the value of this quantity was equal to unity, accurate to 15 significant figures, for higher order modes. Therefore, we may assume that for higher order modes,

$$Q \doteq 1.0; R_{1n}(b) = \frac{z_{1n}^{+}(b) - z_{2n}^{+}(b)}{z_{1n}^{-}(b) + z_{2n}^{+}(b)}$$
 (A.3)

In other words, the higher order modes of the input admittance depend only on the properties of the medium in the immediate vicinity of the antenna (i.e. the dielectric coating) and are independent of the parameters of the conducting body. Of course, the first few modes depend strongly on the parameters of the conducting body because for those modes, Q depends on the values of these parameters as can be seen from Equation (A.2).

As the index of the summation for the input admittance expression becomes sufficiently large, the following approximations (or asymptotic forms) of the Bessel functions can be used []:

$$\begin{cases} J_{\nu}(z) \doteq \frac{1}{\sqrt{2\pi\nu}} \left(\frac{ez}{2\nu}\right)^{\nu} \\ N_{\nu}(z) \doteq -\sqrt{\frac{2}{\pi\nu}} \left(\frac{ez}{2\nu}\right)^{-\nu} \end{cases}$$
(A.4)

where e=2.718 is the base of natural logarithm. For the case of small spherical antennas, the argument z is small compared to  $\nu$  i.e. we can assume that

$$z \ll v$$
 (A.5)

where  $\nu$  is a large number. For example,  $z = k_1 a = 0.1$  is a typical case while  $\nu = n = 20$ . With the assumption of Equation (A.5) we can write, for the Hankel function of the second kind,

$$H_{\nu}^{(2)}(z) \equiv J_{\nu}(z) - jN_{\nu}(z) \doteq j\sqrt{\frac{2}{\pi\nu}} \left(\frac{2\nu}{ez}\right)^{\nu}$$
 (A.6)

Now, the expression for  $Z_{1n}^+(a)$  as needed in the Equation (4.92) is given by

$$z_{1n}^{+}(a) = j \eta_1 \left[ \frac{H_{n-1/2}^{(2)}(k_i a)}{H_{n+1/2}^{(2)}(k_i a)} - \frac{n}{k_i a} \right]$$
 (A.7)

where  $\eta_1 = \sqrt{\frac{\mu_0}{\epsilon_i}}$ . Using the approximation of Equation (A.6) in Equation (A.7), one gets

$$z_{1n}^{+}(a) = j\eta_{1} \left[ \sqrt{\frac{v+1}{v}} \left( \frac{ez}{2} \right) \left( \frac{v}{v+1} \right)^{v} \left( \frac{1}{v+1} \right) - \frac{v+1/2}{z} \right]$$
 (A.8)

where  $n-1/2=\nu$  and  $k_{\dot{1}}a=z$ . Now since n>>1, we can further simplify the expression in the bracket of Equation (A.8) to get

$$z_{1n}^{+}(a) \doteq j\eta_1(\frac{e}{2} \cdot \frac{z}{v+1} - \frac{v+1/2}{z})$$
 (A.9)

Noting that  $z \ll v$ , Equation (A.9) can be written finally as

$$z_{ln}^{+}(a) \doteq -j\eta_{l} \frac{n}{k_{i}a}$$
 (A.10)

Other higher order wave impedances which appear in the input admittance expression can be written down similarly as,

$$z_{1n}^{-}(a) \doteq j\eta_{1} \frac{n}{k_{i}a}, z_{1n}^{+}(b) \doteq -j\eta_{1} \frac{n}{k_{i}b}, z_{1n}^{-}(b) \doteq j\eta_{1} \frac{n}{k_{i}b}$$
 (A.11)

Note that these impedances are mainly imaginary (reactive) for higher order modes. Returning now to Equation (A.3) for  $R_{ln}(b)$  we can write,

$$R_{1n}(b) \doteq \frac{-j\eta_1 \frac{n}{k_1 b} - z_{2n}^+(b)}{j\eta_1 \frac{n}{k_1 b} + z_{2n}^+(b)} = -1.0$$
 (A.12)

This is a main approximation needed for evaluating the higher order modes of the input admittance series. Note that if the conductivity of the conducting body is high, then Equation (A.12) can be written by inspection. We may now write, for the n-th mode of the input admittance;

$$Y_{IN}(n) \doteq \cos \theta_0 \frac{\pi (2n+1)}{n (n+1)} P_n^1 (\sin \theta_0) P_n^1(0) \frac{1 - K_{1n}(a,b)}{z_{1n}^+(a) + K_{1n}(a,b) z_{1n}^-(a)}$$
(A.13)

where n is a large odd integer. The only remaining quantity to be approximated is  $K_{1n}(a,b)$  which was defined in Chapter 4 to be

$$K_{1n}(a,b) = \frac{H_{n+1/2}^{(1)}(k_i a) H_{n+1/2}^{(2)}(k_i b)}{H_{n+1/2}^{(2)}(k_i a) H_{n+1/2}^{(1)}(k_i b)}$$
(A.14)

Using the approximate values for the Hankel functions, we can show that (note that the real parts of Hankel functions should be retained in the calculation of

Equation (A.14))

$$K_{ln}(a,b) \doteq 1 + \gamma \tag{A.15}$$

where  $\gamma$  is a complex quantity. Substituting this into Equation (A.13), one gets

$$Y_{IN}(n) \doteq \cos \theta_0 \frac{\pi (2n+1)}{n (n+1)} P_n^1 (\sin \theta_0) P_n^1 (0)$$

$$\cdot \frac{-\gamma}{z_{1n}^{+}(a) + z_{1n}^{-}(a) + \gamma z_{1n}^{-}(a)}$$
 (A.16)

which, after using the approximation of Equation (A.10), becomes

$$Y_{IN}(n) \doteq j \cos \theta_0 \frac{\pi (2n+1)}{n^2 (n+1)} P_n^1 (\sin \theta_0) P_n^1(0) \frac{k_i a}{\eta_1}$$
 (A.17)

This is the desired relation for the n-th mode of the input admittance for higher order modes, n >> 1. Note that a similar expression can be derived for the case of spherical antenna in a free space [6].

Equation (A.17) shows that the higher order modes of a small, dielectrically coated spherical antenna depend only on the dielectric coating region and is independent of the parameters of the finite conducting body as stated previously. However, the input admittance will depend on these parameters through the first few terms of its series solution.

Now that a simple form has been found for the higher order modes, we can discuss the problem of convergence (or divergence) of the series. Again we note from Equation (A.17) that the conductance part (or the real part of  $Y_{IN}$ ) of the series converges and we will only show the convergence of the imaginary part, i.e. we write Equation (A.17) as

$$Y_{TN}(n) \doteq jB_{TN}(n)$$
 (A.18)

where,

$$B_{IN}(n) = \cos \theta_0 \frac{\pi (2n+1)}{n^2 (n+1)} P_n^1 (\sin \theta_0) P_n^1(0) \frac{k_i a}{\eta_1}$$
 (A.19)

is a (real) susceptance depending on the large integer n. We will show that  $\Sigma_n B_{IN}(n)$  converges for large n and finite  $\theta_0$ . Before that, the validity of the approximation of Equation (A.18) was checked on the computer. We first used the exact relation [Equation (4.92) of Chapter 4] to compute a few higher order terms of the series, then the computation was repeated using the approximation derived in this appendix. The agreement between the two methods was excellent and appreciable computer time and cost was saved by using the approximation.

The associated Legendre functions are given by

$$P_{n}^{1}(0) = \frac{(-1)^{-(n-1)/2} n!}{2^{n-1} [(\frac{n-1}{2})!]^{2}}$$
 (A.20)

where n is an odd integer. Also from Jahnke and Emde's Tables [21] we have

$$P_n^1(x) \doteq \sqrt{\frac{2n}{\pi}} \sin[n(\pi/2 - x) - x/2]$$
 (A.21)

assuming that  $x \ll 1$ . Equation (A.21) can be written in a product form as  $(x = \sin \theta_0)$ 

$$P_n^1(x) \doteq \sqrt{\frac{2n}{\pi}} \sin n\pi/2 \cos[(n + 1/2)x]$$
 (A.22)

Since n is an odd integer, we can assume

$$n = 2m + 1$$
 (A.23)

where m = 0,1,2,3,4,... Note that n and m will be large numbers. Equation (A.22) can be rewritten as

$$P_{2m+1}^{1}(x) \doteq \sqrt{\frac{2(2m+1)}{\pi}} (-1)^{m} Cos[(2m + 3/2)x]$$
 (A.24)

Substituting Equations (A.20) and (A.24) in Equation (A.19), we have

$$B_{IN}(m) = \cos \theta_0 \frac{\pi (4m+3)}{2(2m+1)^2 (m+1)} \sqrt{\frac{2(2m+1)}{\pi}} \frac{(2m+1)!}{2^{2m} [m!]^2} \cdot \cos[(2m+3/2)\sin \theta_0] \frac{k_i a}{\eta_1}$$
 (A.25)

To simplify Equation (A.25) further, we can use the Stirling's formula for the factorial of large numbers:

$$m! \doteq \sqrt{2\pi m} \left(\frac{m}{e}\right)^m \tag{A.26}$$

where e = 2.718. Using this in Equation (A.25), and simplifying, we have

$$B_{IN}(m) \doteq \cos \theta_0 \frac{2}{m} \cos[2m \sin \theta_0] \frac{k_i a}{\eta_1}$$
 (A.27)

where we have also used the fact that m is a large number i.e. m >> 1.

We have now a very simple form for the higher order modes in Equation (A.27). The summation for the input admittance is

$$Y_{IN} = \sum_{m=0}^{M} Y_{IN}(m) + j \sum_{m=M+1}^{\infty} B_{IN}(m)$$
 (A.28)

where  $Y_{IN}$  (m) represents the first few terms for which exact relation is given by Equation (4.92). The second sum of Equation (A.28) can be replaced by an integral when m is sufficiently large that the approximation of Equation (A.27) is valid, i.e.

$$\Sigma_{m=M+1}^{\infty} B_{1N}(m) \rightarrow \int_{M}^{\infty} \cos \theta_{0} \frac{2}{m} \cos(2m \sin \theta_{0}) \frac{k_{1}a}{\eta_{1}} dm \qquad (A.29)$$

The value for the integral in Equation (A.24) can be found as follows

$$\int_{\mathbf{M}}^{\infty} \frac{1}{m} \cos(2m \sin \theta_0) dm = \int_{\mathbf{M}}^{\infty} \frac{\cos(2m \sin \theta_0)}{2m \sin \theta_0} d(2m \sin \theta_0)$$
(A.30)

letting  $2m \sin \theta_0 = y$ , we have

$$\int_{\mathbf{M}}^{\infty} \frac{1}{m} \cos(2m \sin \theta_0) dm = \int_{2Mx}^{\infty} \frac{\cos y}{y} dy$$
 (A.31)

which is in the form of the Cosine Integral [7]:

$$ci(\alpha) = \int_{\alpha}^{\infty} \frac{\cos u}{u} du$$
 (A.32)

Therefore, the sum in Equation (A.24) can be finally evaluated as

$$\Sigma_{m=M+1}^{\infty} B_{IN}(m) \doteq -j \cos \theta_0 \frac{2k_i a}{\eta_1} \operatorname{ci}(2M \sin \theta_0) \quad (A.33)$$

From Equation (A.33) we observe an important result that as soon as  $\theta_0 \neq 0$ , the sum for the input admittance expression found in Chapter 4 converges because  $\operatorname{ci}(\alpha)$  is always finite if  $\alpha$  is nonzero. However if  $\theta_0 = 0$  (i.e. zero or infinitesimal gap) we see that the series diverges, because  $\operatorname{ci}(0)$  is infinite (actually  $-\infty$ ). In fact, it diverges as  $\ell_7(\sin\theta_0)$  and, therefore, the expression for the input admittance becomes meaningless. Physically this phenomenon is expected since zero gap implies an infinite capacitance connected in parallel at the antenna terminals and it leads to an infinite input admittance.

To close this appendix we show in Table A.1, some computer results illustrating the convergence problem for a particular case in which a dielectrically coated spherical antenna is immersed in a finite conducting body. The radius of the metallic sphere is a = 1.0 cm and the

Table A.1. Illustrating the Convergence of the Input Admittance Series. (a = 1.0 cm., b = 1.5 cm., c = 5.5 cm., f = 600 MHz;  $a/\lambda_0 = 0.02$ ,  $\epsilon_{ir} = 2.1$ ,  $\epsilon_r = 77.9$ ,  $\sigma = 0.925 \text{ V/m}$ ,  $2\theta_0$  is the total angular width, in degrees, of the gap.)

Integer N as in	INPUT SUSCEPTANCE,		·	
$\frac{\sum_{n=1}^{N} Y_{IN}(n)}{\sum_{n=1}^{N} Y_{IN}(n)}$	$\theta^0 = 0$ °	θ <sub>0</sub> = 5°	θ <sub>0</sub> = 10°	
1	5.46	5.41	5.30	
3	6.52	6.43	6.17	
5	7.10	6.94	6.50	
7	7.50	7.26	6.61	
9	7.81	7.48	6.58	
19	8.80	7.73	5.85	
29	9.36	7.41	5.70	
39	9.76	7.02	6.05	
49	10.07	6.81	6.03	
59	10.33	6.83	5.81	
69	10.54	7.01	5.90	
79	10.73	7.18	6.03	
89	10.90	7.25	5.92	
99	11.04	7.18	5.85	
199	12.01	6.99	5.91	
299	12.60	7.12	5.95	
399	12.98	7.06	5.94	
499	13.30	7.06	5.92	
599	13.55	7.09	5.91	
699	13.76	7.05	5.93	
799	13.95	7.09	5.94	
899	14.12	7.07	5.93	
999	14.26	7.06	5.92	

dielectric coating shell has a radius b=1.5 cm with a relative dielectric constant of  $\epsilon_{ir}=2.1$ . The frequency of operation is f=600 MHz (corresponding to  $\lambda_0=50$  cm) and the parameters of the body are  $\epsilon_r=77.9$  and  $\sigma=0.925$  V/m and its radius is c=5.5 cm. Three cases of  $\theta_0=0^\circ$ ,  $5^\circ$  and  $10^\circ$  are considered.

To see how the input admittance series converges, we study the partial sum  $\sum_{n=1}^{N} Y_{TN}(n)$  for different values of N. The real part (or the conductance) of the input admittance was almost unchanged for different N's, as expected, and was equal to 0.160, .156 and .146 millimhos corresponding to  $\theta_0 = 0^{\circ}$ ,  $5^{\circ}$  and  $10^{\circ}$ , respectively. The real part of  $Y_{TN}$  vanished, in general, after the first few terms. On the other hand, for the imaginary part (i.e. the susceptance), as can be seen in Table A.1, the series diverges for the zero gap case ( $\theta_0$  = 0°) while for the case of finite gaps ( $\theta_0$  = 5° and  $\theta_0$  = 10°) the series converges. Usually up to 10 terms or more are needed to get accurate results which agree quite well with the experimental results. Also from this table we can see that increasing the gap width makes the susceptance less capacitive. It is interesting to compare the results obtained here for spherical antennas to that of other kinds of antennas, for example, the circular loop antenna [22].

## APPENDIX B

## COMPUTATION OF HANKEL FUNCTIONS

In this appendix, we first discuss Hankel functions of small arguments as mentioned in section 4.7 in connection with radial transmission lines and then followed with a brief description of the numerical computation of the input admittance expression as derived in Chapter 4. The main purpose of this appendix is to introduce a powerful routine used throughout the computation of the Bessel functions with generally complex arguments.

Hankel functions of the first and second kinds are defined in terms of Bessel and Neumann functions as

$$H_{v}^{(1)}(z) \equiv J_{v}(z) + jN_{v}(z)$$
 (B.1)

and

$$H_{v}^{(2)}(z) \equiv J_{v}(z) - jN_{v}(z)$$
 (B.2)

where  $\nu$ , in general, is a complex number called the "order" of the function involved and z is a complex argument.

Assuming that z = x = a positive real number, we have for the case when x << 1

$$\begin{cases} J_0(\mathbf{x}) \doteq 1.0, N_0(\mathbf{x}) \doteq \frac{2}{\pi} g_n \frac{\gamma \mathbf{x}}{2} \\ J_1(\mathbf{x}) \doteq \frac{\mathbf{x}}{2}, N_1(\mathbf{x}) \doteq -\frac{1}{\pi} g_n (\frac{2}{\mathbf{x}}) \end{cases}$$
(B.3)

which are obtained from the series representations of the Bessel functions and  $\gamma = 1.781$  i the Euler's constant ( $m \gamma = 0.5772$ ). Hankel functions then become

$$\begin{cases} H_0^{(1)}(x) \doteq 1 + j \frac{2}{\pi} n \frac{\gamma x}{2}, H_0^{(2)}(x) \doteq 1 - j \frac{2}{\pi} n \frac{\gamma x}{2} \\ H_1^{(1)}(x) \doteq \frac{x}{2} - j \frac{1}{\pi} n (\frac{2}{x}), H_1^{(2)}(x) \doteq \frac{x}{2} + j \frac{1}{\pi} n (\frac{2}{x}) \end{cases}$$
(B.4)

From Equation (B.4) we can write, for the amplitude and phase functions as introduced in section 4.7 of Chapter 4,

$$\begin{cases} h_0(\mathbf{x}) \doteq \frac{2}{\pi} \left| \mathcal{M} \left( \frac{\mathbf{Y} \mathbf{X}}{2} \right) \right|, & h_1(\mathbf{x}) \doteq \frac{2}{\pi \mathbf{X}} \\ \theta(\mathbf{x}) \doteq \tan^{-1} \left[ \frac{2}{\pi} \mathcal{M} \left( \frac{\mathbf{Y} \mathbf{X}}{2} \right) \right], & \psi(\mathbf{x}) \doteq \tan^{-1} \left( \frac{\pi \mathbf{X}^2}{4} \right) \end{cases}$$
(B.5)

The relations given by Equation (B.5) were used in section 4.7.

Next, as can be seen from Equation (4.92), for the computation of the input admittance (or the input impedance), one needs to generate the associated Legendre functions. For zero argument the relation is simply

$$P_n^1(0) = \frac{(-1)^{-(n-1)/2} n!}{2^{n-1} [(\frac{n-1}{2})!]^2}$$
 (B.6)

for odd integers n. For non-zero arguments, the first three functions are given by

$$P_0^1(\cos \theta) = 0, P_1^1(\cos \theta) = \sin \theta, P_2^1(\cos \theta) = 3/2 \sin 2\theta$$
(B.7)

For other functions we can use the recurrence relation for varying degree [7] as

$$mP_{m+1}^{1}(x) = (2m+1)xP_{m}^{1}(x) - (m+1)P_{m-1}^{1}(x)$$
 (B.8)

where for our case  $x = \sin \theta_0$ .

To compute the various quantities involved in the expression for the input admittance, e.g.  $R_{1n}(b)$ ,  $Z_{1n}^+(a)$ ,... etc., we have to compute Hankel functions of fractional order and complex argument (in general). This can be tedious if one uses the series expansion of the Bessel functions or tries to use tabulated values for these functions. In fact, to compute each term of  $Y_{1N}$  as given in Equation (4.92) one needs approximately 15 different Hankel functions. Fortunately, for this purpose, we had access to a powerful routine for computing cylindrical Bessel functions (including Neumann functions) of complex order and complex argument [23]. The description of the routine and an example of its use follows.

The subroutine to compute the Bessel functions, code-named COMBES, uses the appropriate recursion relationships and normalization factors to compute Bessel functions of the first kind  $J_{_{\rm V}}(z)$  and then uses a summation of  $J_{_{\rm V}}(z)$  to compute the Bessel functions of the second kind (or Neumann functions)  $N_{_{\rm V}}(z)$  [24], where in

general both  $\nu$  and z may be complex, or

$$v = (\alpha + n) + j\beta \tag{B.9}$$

and

$$z = x + jy (B.10)$$

where |n| = 0,1,2,...,N, and  $\alpha$  is positive. Note that the real part of  $\nu$  is written in the form of an integer plus a real number due to the fact that usually we are interested in Bessel functions of integer orders or integer plus half (as in our case). However, the order in general can be any real or complex number. A restriction on the magnitude of the argument is given in the routine as

$$|z| = \sqrt{x^2 + y^2} < 50$$
 (B.11)

In all our problems COMBES was used to calculate the Hankel functions and as we saw earlier, the results were in good agreement with experiments and comparison with existing results.

To "call" the routine in a program, the following statement is used:

CALL COMBES (X,Y, ALPHA, BETA, N, BJR, BJI, BNR, BNI)
(B.12)

where X and Y are the real and imaginary parts of the argument z defined in the program, ALPHA and BETA are as defined in Equation (B.9). |N| + 1 is the number of

values of the functions to be computed. BJR, BJI, BNR and BNI are all one-dimensional arrays. Real part of  $J_{\nu}(z)$  will be stored in BJR while its imaginary part will be stored in BJI. These two arrays (i.e. BJR and BJI) should have a dimension greater than or equal to the maximum of |z|+25 and |N|+15. The real part of  $N_{\nu}(z)$  will be stored in BNR while its imaginary part stored in BNI. Each of these two arrays should have a dimension greater than or equal to the maximum of |N|+1 and 3. In the existing deck these arrays are dimensioned as BJR(100), BJI(100), BNR(50) and BNI(50). In the program of interest it is best that the arrays be dimensioned accordingly, if possible, to avoid errors since the arrays are also used for temporary storage in the routine.

As an example, suppose that we want to compute Hankel functions  $H_{n-1/2}^{(2)}(kr)$  and  $H_{n+1/2}^{(2)}(kr)$  where k is a complex quantity. Then if RK = kr in the program, we can call the routine COMBES as follows:

CALL COMBES (RKR, RKI, 0.5, 0., N, BJR, BJI, BNR, BNI)
(B.13)

assuming that the arrays BJR,...,BNI have been dimensioned properly. RKR, RKI are the real and imaginary parts of kr, respectively. After calling the routine we can construct the Hankel functions as

$$HM = BJR(N) + jBJI(N) - j[BNR(N) + jBNI(N)]$$

$$HP = BJR(N+1) + jBJI(N+1) - j[BNR(N+1) + jBNI(N+1)]$$
(B.14)

where HM is used for  $H_{n-1/2}^{(2)}(kr)$  and HP for  $H_{n+1/2}^{(2)}(kr)$ . Note that since the argument kr was complex, it is necessary to use both real and imaginary parts of Bessel and Neumann functions. Also since the routine will compute the elements of the array from 1 to N+1, in the case where we use Hankel functions in a do-loop, the routine needs to be called only once for the maximum integer number of the do-loop's parameter.

In order to illustrate the accuracy of the numerical results obtained after executing the routine COMBES, we now compute some Spherical Bessel functions. These functions are defined in terms of the ordinary (cylindrical) Bessel functions as

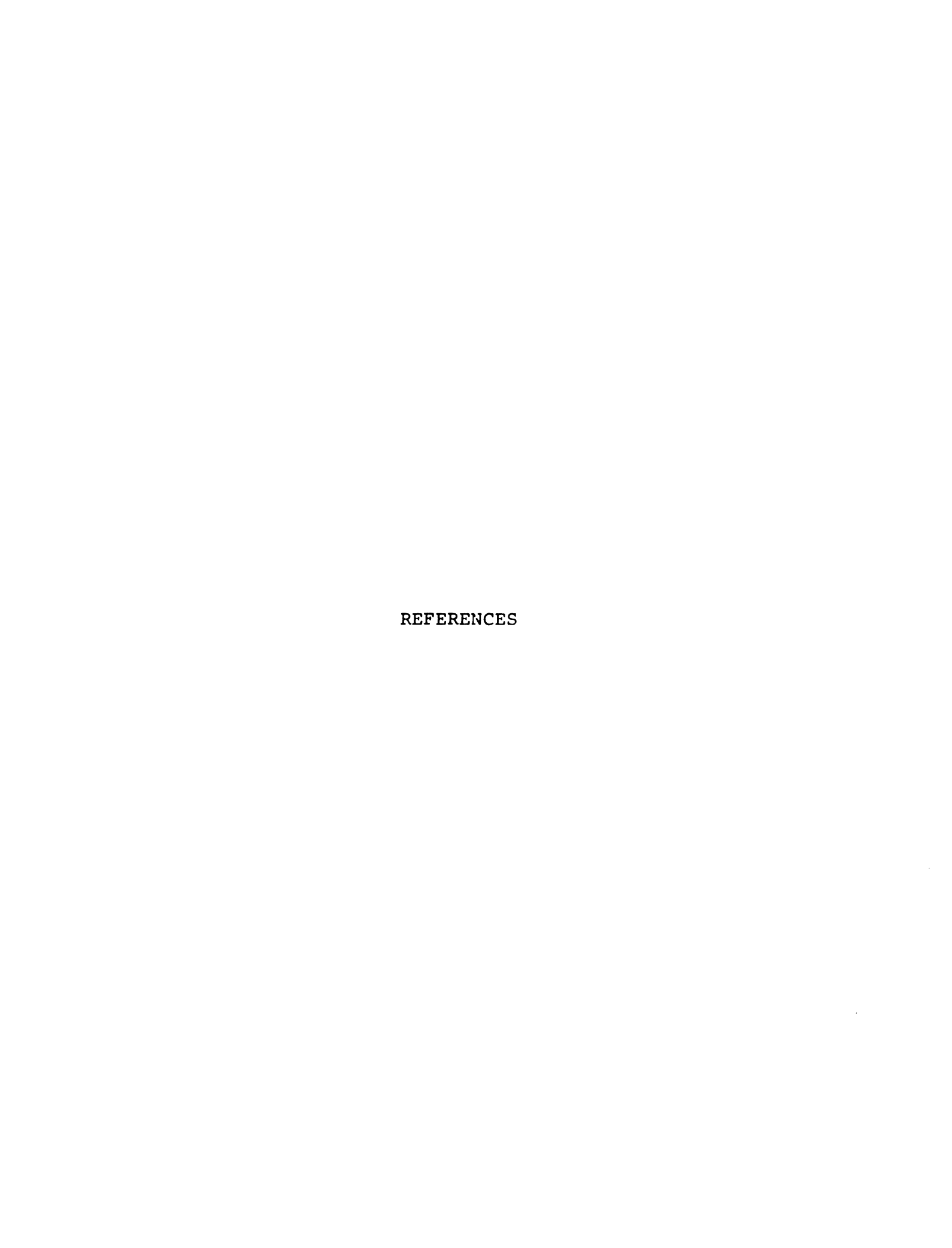
$$j_m(x) = \sqrt{\frac{\pi}{2x}} J_{m+1/2}(x), n_m(x) = \sqrt{\frac{\pi}{2x}} N_{m+1/2}(x)$$
 (B.15)

Table B.1 shows values of the spherical Bessel functions of order m = 0,1 and 2. The real argument x runs from 0.1 to 2.1 (note that x = 0 cannot be computed). These values are computed using the routine described before. A comparison of the values in Table B.1 and that from the National Bureau of Standard's "Tables of Spherical Bessel Functions", which are compiled in Reference [7] shows a very good agreement. Although for all

Table B.1. Spherical Bessel Functions of Order 0, 1 and 2. These Results are Comptued by using the Routine "COMBES".

	÷ (**)	n (m)	÷ (**)	- (m)	÷ (*)	n (w)
<b>x</b>	j <sub>0</sub> (x)	n <sub>0</sub> (x)	j <sub>1</sub> (x)	n <sub>1</sub> (x)	j <sub>2</sub> (x)	n <sub>2</sub> (x)
0.1	.99833	-0.95004	.03330	-100.49875	.00067	-3005.01248
0.2	.99335	-4.90033	.06640	- 25.49501	.00266	-377.52483
0.3	.98507	-3.18445	.09910	-11.59992	.00596	-112.81472
0.4	.97355	-2.30265	.13121	-6.73018	.01055	-48.17368
0.5	.95885	-1.75517	.16254	-4.46918	.01637	-25.05992
0.6	.94107	01.37556	.19289	-3.23367	.02339	-14.79279
0.7	.92031	-1.09263	.22210	-2.48121	.03154	-9.54114
0.8	.89670	87088	.24999	-1.98530	.04075	-6.57399
0.9	.87036	-0.69068	.27639	-1.63778	.03095	-9.76860
1.0	.84147	-0.54030	.30117	-1.38177	.06204	-3.6052
1.1	.81019	41236	.32417	-1.18506	0.7392	-2.81963
1.2	.77670	30196	.34538	-1.02834	.08651	-2.26888
1.3	.74120	20577	.36438	89948	.09969	-1.86996
1.4	.70329	12141	.38138	79061	.11334	-1.57276
1.5	.66500	04716	.39617	69644	.12735	-1.34571
1.6	.62473	.01825	.40871	61333	.14159	-1.16824
1.7	.58333	.07579	.41893	53875	.15595	-1.02653
1.8	.54103	.12622	.42679	47090	.17030	91106
1.9	.49805	.17015	.43229	40850	.18450	81515
2.0	.45465	.20807	.43540	35061	.19845	73399
2.1	.41105	.24040	.43614	29657	.21201	66408

the results encountered in the problem of the input admittance of spherical antennas one had a good accuracy in using the routine COMBES, it is recommended that the reader runs a few examples in special cases first, and then compares it with the values given in standard tables. It is believed that the routine is not very accurate for pure imaginary arguments.



## REFERENCES

- 1. Smith, G.S., "A comparison of electrically short bare and insulated probes for measuring the local radio frequency electric field in biological systems," IEEE Trans. on Biomedical Engineering, Vol. BME-22, No. 6, November 1975.
- 2. Richmond, J.H. and E.H. Newman, "Dielectric coated wire antennas," Radio Science, Vol. 11, No. 1, January 1976.
- 3. Iizuka, K., "An experimental study of the insulated dipole antenna immersed in a conducting medium," IEEE Trans. on Antennas and Propagation, Vol. AP-11, September 1963.
- 4. Livesay, D. and K.M. Chen, "Electromagnetic field induced inside arbitrarily shaped biological bodies," IEEE Trans. on Microwave Theory and Technique, Vol. MTT-22, No. 12, pp. 1273-1280, December 1974.
- 5. King, R.W.P., "The Theory of Linear Antennas," Harvard University Press, 1956.
- 6. Ramo, S., J.R. Whinnery and T. VanDuzer, "Fields and Waves in Communication Electronics," John Wiley & Sons, New York, 1965.
- 7. Abramowitz, M. and I.A. Stegun, "Handbook of Mathematical Functions," Dover Publications, Inc., New York, 1970.
- 8. Stratton, J.A., "Eelectromagnetic Theory," McGraw-Hill Book Company, New York, 1941.
- 9. Infeld, L., "The influence of the width of the gap upon the theory of antennas," Quarterly of Applied Mathematics, Vol. V., No. 2, July 1947.
- Stratton, J.A. and L.J. Chu, "Forced oscillation of a conducting sphere," Journal of Applied Physics, Vol. 12, March 1941.

- 11. Guru, B.S. and K.M. Chen, "Experimental and theoretical studies on electromagnetic fields induced inside finite biological bodies," IEEE Trans. on Microwave Theory and Techniques, Vol. MTT-24, No. 7, July 1976.
- 12. Marcuvitz, N. in Montgomery, Dicke and Parcell, "Principles of Microwave Circuits," McGraw-Hill Book Co., New York, 1947.
- 13. Scott, L.D., "Apparatus for studying the properties of antennas in an effectively infinite dissipative medium," NASA Scientific Report No. 6, Division of Engineering and Applied Physics, Harvard University Press, Cambridge, Massachusetts, December 1969.
- 14. Scott, L.D. and G.S. Smith, "Measurement techniques for antennas in dissipative media," IEEE Trans. on Antennas and Propagation, Vol. AP-21, No. 4, July 1973.
- 15. King, Mack and S.S. Sandler, "Arrays of Cylindrical Dipoles," Cambridge University Press, Cambridge, Massachusetts, 1968.
- 16. Golden, August, Jr., "Radiation from dielectrically coated spherical antennas, a Ph.D. Thesis, Michigan State University, 1969.
- 17. Saxton, J.A. and J.A. Lane, "Electrical properties of sea water," Wireless Engineer, October 1952.
- 18. Crawford, M.L., "Generation of standard EM fields using TEM transmission cells," IEEE Trans. on EM Compatibility, Vol. EMC-15, No. 4, November 1974.
- 19. Kim, O.K., "Surface wave end-fire antenna," A Thesis for Ph.D. degree, Michigan State University, 1973.
- 20. Guru, B.S., "An experimental and theoretical study on the interaction of electromagnetic fields with arbitrarily shaped biological bodies," A Ph.D. Thesis, Michigan State University, 1976.
- 21. Jahnke, F. and E. Emde, "Tables of Functions," 4th edition, Dover Publications, Inc., New York, 1945.
- 22. Short, J.R., "Modification of scattering from thick cylinders and radiation from loops by impedance loading," a Ph.D. Thesis, Michigan State University, 1971.

- 23. AEC Computing and Applied Mathematics Center, Courant Institute of Mathematical Sciences, New York University, New York, N.Y. L0012.
- 24. Goldstein, M. and R. Thaler, "Recurrence techniques for the claculation of Bessel functions," MTAC, Vol. XIII, No. 66, April 1959.

